CHEMISTRY AND BIOLOGY OF TUMOR-ASSOCIATED GANGLIOSIDE GD2

WENYONG TONG

DOCTOR OF PHILOSOPHY

Department of pharmacology and therapeutics

McGill University
Montréal, Québec, Canada

A thesis submitted to the Faculty of Graduate and Postdoctoral Studies in partial fulfillment of the requirements of the degree of Doctor of Philosophy

September 2011

Dedication

This thesis is dedicated to my wife and son.

Abstract

Effective therapies typically target diseased tissues without significantly affecting healthy tissues. A tumor-related glycosphingolipid (GSL), such as ganglioside GD2, distinguishes neuroectoderm tumors from their healthy counterparts and is a validated tumor target. GD2 is clinically targeted for diagnosis and immunotherapy. GD2 plays an important functional role in tumor progression and in chemoresistance. It also plays an important functional role in pain; however, the mechanisms that make GD2 important in such phenomena remain unknown.

Thus, understanding the structure-activity relationship of GD2, a GSL with two sialic acids, would be helpful. However, such studies on glycolipids are challenging. We employed a chemical biology approach to elucidate the structure and function of GD2 and to further direct the rational design of GD2 ligands and vaccines for GD2-related cancer treatment.

The combined use of STD NMR spectroscopy, transferred NOE experiments, and molecular modeling furnished details on the molecular recognition of the ganglioside GD2 by the clinically used anti-GD2 monoclonal antibody 3F8 that can induce apoptosis of GD2 expressing tumours. A binding model that provided the basis for a rational development of GD2 ligands and vaccines was then established. Based on the structural information of GD2-3F8 interactions, small molecule monomeric peptide ligands binding to GD2 were developed. ELISA and NMR experiments demonstrated that peptides selectively bound to GD2 via an induced-fit mechanism. Furthermore, peptidic GD2 ligands, including 3F8, mediated similar biological functions in cell-based assays of activation of NMDA receptor via Src family kinase, calcium fluxe and cAMP. These can explain at least some of the mechanisms associated with tumor progression and pain, where GD2 plays a role. However, current GD2 peptide ligands did not demonstrate any treatment effect *in vivo*.

Hence, we turned to the design of GD2 vaccines as a therapeutic approach. The rigid nature of GD2-oligosaccharides, discovered in our structural study, makes it perfectly suited to drive a structurally convergent immune response. A novel and homogenous tetra-GD2 dendrimer was designed to mimic a clustered GD2 lipid raft. Immunization of mice with tetra-GD2 dendrimer elicited a potent anti-GD2 humoral response. The antibodies (sera or mAbs) thus generated can kill GD2-expressing cells in culture, in the absence of a complement. Tumor growth was significantly delayed *in vivo* in prophylactic and in therapeutic paradigms. Our research strategy may be expanded to other clinically relevant glycolipids.

Résumé

Typiquement, les thérapies efficaces agissent sur les tissus malades sans toutefois nuire considérablement aux tissus en santé. Un glycosphingolipide (GSL) associé à une tumeur, tel que le ganglioside GD2, peut reconnaître selectivement les tumeurs neuroectodermes malignes et est ainsi validé comme une cible tumorale. Sur le plan clinique, on utilise le GD2 à des fins de diagnostic et d'immunothérapie. D'une part, le GD2 joue un rôle fonctionnel important dans la progression tumorale et la chimiorésistance. D'autre part, le GD2 joue un rôle fonctionnel important dans la douleur, mais les mécanismes qui expliqueraient l'importance du GD2 lors de tels phénomènes demeurent encore inconnus.

C'est pourquoi il serait utile de mieux comprendre la relation structure-activité du GD2, un GSL constitué de 2 acides sialiques. Toutefois, entreprendre de telles études sur les glycolipides représente un défi de taille. Nous avons alors utilisé une approche basée sur la biologie chimique pour élucider la structure et la fonction des GD2 et pour mieux concevoir rationnellement des ligands GD2 et des vaccins pour le traitement contre le cancer lié au GD2.

En combinant l'utilisation de la spectroscopie RMN DTS, des expériences NOE transférées et des modèles moléculaires, il est possible d'obtenir plus de détails sur la reconnaissance moléculaire du ganglioside GD2 au moyen du 3F8, un anticorps monoclonal anti-GD2 utilisé médicalement et qui peut induire l'apoptose de cellues cancereuses exprimant GD2. Comme point de départ pour le développement rationnel des ligands GD2 et des vaccins, nous avons établi un modèle contraignant. En nous appuyant sur l'information structurelle des interactions GD2-3F8, nous avons développé des petits ligands monomériques peptidiques liés au GD2. Des expériences RMN et ELISA ont démontré que les peptides se lient sélectivement au GD2 via un mécanisme d'ajustement induit. Par ailleurs, les ligands peptidiques GD2,

dont le 3F8, deviennent médiateurs de fonctions biologiques similaires dans les essais cellulaires de l'activation des récepteurs NMDA via les kinases de la famille Src, les flux de calcium et cAMP. Ces derniers peuvent au moins expliquer certains des mécanismes associés avec la progression tumorale et la douleur, dans lesquels le GD2 jour un rôle prépondérant. Cependant, les ligands peptidiques GD2 actuels n'ont pas démontré les effets désirés au cours des traitements *in vivo*.

C'est pourquoi nous nous sommes tournés vers le développement de nouveaux vaccins GD2 comme une approche thérapeutique. La nature rigide des oligosaccharides GD2, que nous avons découverte par le biais de notre étude structurale, devient une caractéristique parfaitement adaptée pour favoriser une réponse immunitaire structurellement convergente. Un nouveau dendrimère tetra-GD2 homogène a été conçu de manière à reproduire un radeau lipidique GD2 regroupé. L'immunisation des souris par le dendrimère tetra-GD2 a engendré une puissante réponse humorale anti-GD2. En l'absence d'un complément, les anticorps (sera ou mAbs) ainsi générés peuvent tuer les cellules exprimant le GD2 en culture. La croissance tumorale a été considérablement retardée *in vivo* dans les paradigmes thérapeutiques et prophylactiques. Notre stratégie de recherche pourrait ainsi être élargie pour inclure d'autres glycolipides pertinents sur le plan clinique.

Table of contents

Acknowledgements

Working on such a multidisciplinary project, I have obtained a lot of help from many people. Without them, this thesis would not be possible. Here, I would like to sincerely express my gratitude to everyone who has supported me.

I am grateful to my supervisor Dr. Horacio Uri Saragovi who guided me into the wonderful world of chemistry and biology. Dr. Saragovi is always available for discussions and technical help. His mentorship has been crucial to the completion of my study and research.

My advisory committee, including Dr. Terry Hébert, Dr. Kalle Gehring and Dr. Greg Miller, has also been very helpful in providing useful scientific feedback and career advice throughout my study and research.

I would like to thank our collaborators Dr. Michel Gilbert (Institute for Biological Sciences), Dr. Karl Hansford (Mimetogen Pharmaceuticals), Dr. William D. Lubell (University of Montreal), Dr. John W. Blankenship (University of Montreal) and my colleague Dr. Hinyu Nedev for their excellent support for my chemistry research.

For my NMR study, I must thank Dr. Tara Sprules. She ensured a high quality of NMR data and my NMR assignments. More importantly, she helped to solve some key problems and provided valuable discussions for both my experiments and manuscripts.

For my molecular modeling study, Dr. Shafinaz Chowdhury did an excellent molecular docking. Dr. Jinming Zhou gave me helpful suggestions on molecular dynamic simulations. I wish to thank many unknown people who provided discussions and answered my questions in the Internet forums of ARIA, AMBER, SPARKY, NMRPipe, and FINK. I wish them to keep continuing this worldwide communication.

For my biological study, I would like to thank my colleague Dr. Alba Galan, Dr. Fouad Brahimi, Michael Perron, Pooja Jane, Dr. Ljubica Ivanisevic, Dr. Karen Meerovitch (Mimetogen Pharmaceuticals) and my summer students Gloria To and Yogesh Bramhecha. Another important

aspect is that a harmonious relationship with my lab members provided me a stimulating working environment.

I am very grateful for the doctoral scholarships from the Montreal Center for Experimental Therapeutics in Cancer (1 year) and FRSQ (3 years).

I am deeply thankful to a close friend of my family, Miss Barbara Bessis, for help with the preparation of this thesis.

Finally, I would like to thank my wife Dr. Wei Lin, parents and parents-in-law and my son. Especially, Wei Lin supported me in both my life and study during these 5 years. As a wife, she spent much more time than me on taking care of our son and family affairs. As a medicinal chemist, she always discussed my experimental problems with me and provided good suggestions. Even now, she is reading my thesis. I never forget my both of parents for the encouragement and love. I would thank my son for bringing me a lot of life's pleasures.

List of figures

List of tables

Contributions of authors

This thesis is written in a manuscript-based format in accordance with the regulations of the Faculty of Graduate studies and Research from McGill University. The thesis is composed of:

Chapter 2 is a published article and its supplemental information is presented as **Appendix I**, together with one published book chapter for methods presented as **Appendix II**.

Chapter 3 is unpublished data as an extensional study for **Chapter 2.**

Chapter 4 is an article submitted with supplemental information presented as **Appendix III**.

Chapter 5 is an article submitted.

The manuscripts were prepared by W. Tong and Dr. H. Uri Saragovi and they were edited by co-authors. I am the first author for all the manuscripts.

The chapter 2 entitled “Small Molecule Ligands of GD2 Ganglioside, Designed from NMR Studies, Exhibit Induced-Fit Binding and Bioactivity” was a published paper from the journal ***Chemistry and Biology*** in 2010***.*** Detailed methods for the structure-based design (**Appendix II**) were written in a book chapter of ***Methods in Molecular biology*** (in press) entitled “Rational design of peptide ligands against a glycolipid by NMR studies”.

Figure 2.1A	Dr. Meerovitch performed ELISA experiments and prepared figure 1A. I repeated the ELISA results.
Figure 2.2,2.3,2.5 & 2.6	I prepared samples. Dr. Sprules (manager of NMR facility) and I set up parameters for NMR experiments. I performed the 3D-structure calculations of two types of GD2 and

	peptides as well as all the data analysis and prepared all figures.
Figure 2.4	Dr. Chowdhury performed the docking experiments, and then we built up the binding model together with use of the GD2 structures I calculated and she prepared the figures. And then I ran the CORCEMA-ST program to do quality check of the binding model and to calculate Rf-factor.
Figure 2.7	Dr. Meerovitch performed ELISA experiments and prepared figure 7A and 7B. Dr. Gagnon performed experiments and prepared figure 7C and 7D. I repeated the experiments presented as figure 7A, 7B and 7D.
Figure S1-4, & Table S1-7	I prepared samples. Dr. Sprules and I set up parameters for NMR experiments. I performed all the experiments and prepared all figures and assignment tables. Dr. Sprules did quality check of my assignments of peptides.
Figure S5 -S7	Dr. Chowdhury performed all the data analysis and prepared all figures. Dr. Saragovi and Dr. Cheung provided the sequence of 3F8.
Appendix II	I prepared figure 1. Other figures are copied with permission from the Chem. Biol. journal.

The chapter 3 entitled “GD2 peptide ligands” is unpublished data. All the peptide sequences were designed by me and synthesized by Dr. Nedev. I performed all the experiments and prepared the table and figures. The in vivo experiments were done by Dr. Karen Meerovitch, and are referred to with permission.

The chapter 4 entitled “Immunization with GD2 ganglioside carbohydrate dendrimers elicits tumor-killing antibodies, as an efficient therapeutic cancer vaccine” is a manuscript submitted. I did the analyses and prepared all the figures and the table. Dr. Saragovi did most of the

injections, and the LDI animal facility helped me with bleeding. I did tumor measurements that were recorded by Gloria To and Yogesh Bramhecha. I performed all competitive ELISA experiments.

Figure 4.1	Dr. Gilbert and Anna-Maria Cunningham synthesized the AP-GD2 designed by me. I performed the synthesis of tetra-GD2 dendrimer.
Figure 4.2 & 4.3	I performed the experiments.
Figure 4.4	I performed the experiments for figure A and B, which were repeated by Yogesh Bramhecha. I developed the hybridomas with the help of Dr. Saragovi, Anne Marcil and Gloria To. Yogesh Bramhecha performed the experiments for figure C and antibody isotyping under my supervision.
Table 4.1	Gloria To performed ELISA under my supervision. I performed FACS.

The chapter 5 entitled “Ligands of ganglioside GD2 activate the Src kinase and NMDA receptors and regulate cell biology in neuronal cell lines” is a manuscript submitted. I performed all experiments and analyses and prepared all the figures except the figure 3F and 4 done by Dr. Lezcano and Dr. Gagnon respectively.

Contributions to original knowledge

1. The two water-soluble phenylthio-GD2 and amino-phenyl ether-analog of GD2 were designed and chemoenzymatically synthesized.

2. Complete assignments for GD2s were accomplished through 1D and 2D NMR (COSY, TOCSY, HMQC, HMBC, and NOESY/ROESY).

3. Three dimensional (3D) structures of GD2-oligosaccharides were calculated by molecular modeling software (AMBER) based on NMR constrains.

4. GD2 structures are relatively rigid.

5. Dynamic interactions between GD2 and its monoclonal antibody 3F8 in aqueous solution were revealed by STD-NMR. The major residue interacting with 3F8 is the middle neuraminic acid.

6. A reasonable 3D binding model of GD2 and its monoclonal antibody was proposed and validated by CORCEMA-ST program based on STD NMR signals.

7. NMR structure-based design of ligands and vaccines targeting glycolipids was proposed, which can be applied to other functional glycans.

8. Three dimensional structures of unbound and bound GD2 peptide ligands were calculated by molecular modeling software (ARIA) based on NMR constraints.

9. Both anti-GD2 antibody 3F8 and GD2 peptide ligands binding to GD2 might be regulated by an induce-fit mechanism.

10. A practical synthetic method of well-defined GD2 and GD3 dendrimers was developed.

11. *In vitro* and *in vivo* showed that the immunogenic tetra-GD2 and GD3 dendrimer might be a potential homogenous prophylactic and therapeutic cancer vaccine.

12. Two monoclonal antibodies 4A3.4 and 8H3.4 (mouse IgG2 types) against both GD2 and GD3 developed from mouse splenocytes immunized with a well-define chemical, tetra-GD3 dendrimer.

13. Phosphorylation of the NMDAR NR2B unit via activation of Src family kinase was induced in neuroblastoma cells by anti-GD2 antibody 3F8 and by peptide ligands of GD2. The signal could be blocked by Src kinase inhibitor PP2 and the NMDAR antagonist ketamine.

14. Calcium influx via the NMDAR was induced by anti-GD2 antibody 3F8 in neuroblastoma cells, which could be blocked by Src kinase inhibitor PP2 and NMDAR antagonist ketamine.

15. Anti-GD2 antibody 3F8 or GD2 direct binding peptide ligands, not like BDNF, selectively induced the sequential phosphorylation of NR2B-containing NMDA and Src family kinase, which might be a molecular mechanism for anti-GD2 antibody induced pain.

List of abbreviations

APC	antigen-present cells
ADCC	antibody-dependent cell-mediated cytotoxicity
ax	axial
BDNF	Brain-derived neurotrophic factor
CDC	complement-dependent cytotoxicity
CDR	complementarity determining region
COSY	correlation spectroscopy
cAMP	cyclic AMP
CTB	cholera toxin-B
CMC	critical micelle concentration
DC	dendritic cells
DPC	dodecylphosphocholine
DMF	dimethylformamide
FAB	fragment antigen-binding
FGFR	fibroblast growth factor receptors
eq	equatorial
HAMA	human anti-mouse antibodies
HMBC	heteronuclear multiple bond correlation
HMQC	heteronuclear multiple quantum correlation
HSQC	heteronuclear single quantum coherence
Gal	galactose
GalNAc	N-acetyl galactosamine
Glc	glucose
GEM	group epitope mapping
GM-CSF	ganulocyte-macrophage colony-stimulating factor
GSL	glycosphingolipid
HGF	hepatocyte growth factor
IFN	interferon
IgG	immunoglobulin

IL	interleukin
IRAK-M	IL-1 receptor associated kinase
KLH	keyhole limpet haemocyanin
mAb	monoclonal antibody
MD	molecular Dynamic
NeuAc	N-acetylneuraminic acid or Neu5Ac
NeuGc	N- glycolylneuraminic acid
NMR	nuclear magnetic Resonance
NMDA	N-Methyl-D-aspartic acid receptors
NOESY	nuclear Overhauser enhancement spectroscopy
NF-κB	nuclear factor kappa-light-chain-enhancer of activated B cells
PPM	parts per million
RMSD	root-mean-square deviation
ROESY	rotating frame Overhauser effect spectroscopy
SFK	Src-family tyrosine kinases
STD-NMR	saturation transfer difference-NMR
SCLC	small-cell lung cancer
1/2/3-D	One or two or three dimensional
SPR	surface plasmon resonance
TrNOE	transferred nuclear Overhauser enhancement (trNOE)
TN-R	tenascin-R
TNF-α	tumor necrosis factor- α
TOCSY	Total correlation spectroscopy
VEGF	vascular endothelial cell growth factor
VL	variable domain light chain
VH	variable domain heavy chain

Chapter 1 General Introduction

Chemistry and biology of tumor-associated gangliosides

Background

Gangliosides are neuraminic acid-containing glycosphingolipids that are found on the plasma membrane of cells in all types of tissues. A common core structure for gangliosides is lactose that is connected to a ceramide lipid tail (Figure 1.1**)**. The sugar head of ganglioside protrudes from the cell surface, while the ceramide lipid tail is embedded in the outer leaflet of the plasma cell membrane.

Not all kinds of gangliosides are ubiquitously expressed. Some gangliosides, such as GM2, GD2 and GD3, are expressed in the developing embryo and are rare in post-birth normal tissues (*1-3*). Nevertheless they are highly expressed in particular neuroectodermal tumors of origin (*4*), such as lymphoma, melanoma, neuroblastoma, and small-cell lung cancer (SCLC). These are called tumor-associated gangliosides and have been validated as tumor markers (*5-8*).

Gangliosides are also biologically active glycolipids and can act as receptors (*9*). There is accumulating evidence that gangliosides play an important role in normal physiological functions (e.g., embryogenesis (*10*) and neuroprotection (*11, 12*)), as well as in pathological conditions (e.g., tumorigenesis, metastasis, angiogenesis and immunosuppression (*13*)). The underlying molecular mechanisms of functional gangliosides are assumed to operate by means of an ensemble of GD2 interacting with

various functional membrane proteins in lipid rafts that are detergent-resistant microdomains of the cytoplasmic membrane (*14*).

Because of the unique distribution of gangliosides on malignant cells and their functional roles in tumor progression, tumor-associated gangliosides are attractive targets for passive and active immunotherapy. Several anti-ganglioside monoclonal antibodies (mAb) and vaccines that are based on ganglioside structures have been developed for clinical use during the last twenty years. However, there are still some issues about current antibody treatments (e.g., side effects) and vaccine therapies (e.g., heterogeneousness and low immunogenicity).

An understanding of the structure and function of gangliosides may help to improve the current cancer immunotherapies that target these glycolipids. This general introduction will focus on the recent reports of the chemistry and biology of tumor-associated gangliosides, since the study of gangliosides presents unique challenges that may require a chemical biology approach.

First, there is little structural information about gangliosides. Gangliosides are difficult to use for structural studies because of their tendency to form micelles in water due to their amphiphilic properties. Underivatized gangliosides are hard to crystalize. Therefore, nuclear magnetic resonance (NMR) is an important experimental technique for the structural biology study of gangliosides. Chemistry definitely plays an

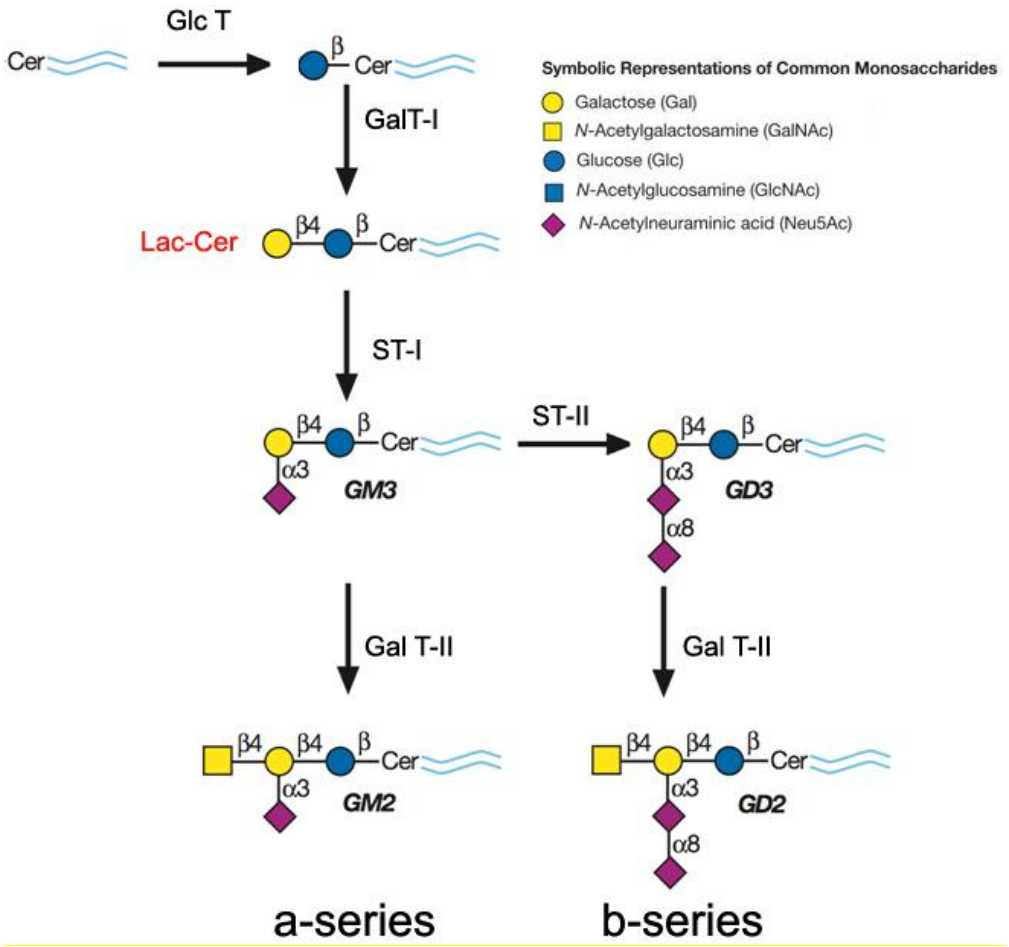

Figure 1.1 Biosynthesis pathway of some types of gangliosides associated with cancer. Gangliosides have a common core structure of lactose connected to a ceramide lipid tail. Cer, ceramide, *N*-acylsphingosine; Lac-Cer, lactosyl ceramide; ST, sialyltransferase; Gal T, galactosyltransferase; GalNAc T, *N*-acetyl-galactosaminyltransferase; Glc T, glucosyltransferase. Picture is adopted from Essentials of Glycobiology (2nd edition), Varki A, Cummings RD, Esko JD, et al., editors.

important role in obtaining appropriate ganglioside analogues for structural studies.

Second, gangliosides can be receptors that induce intra- and extra-cellular signaling-transduction by controlling lipid rafts. However, the functional investigation has been complicated by genetic approaches because gangliosides are not under direct genetic control. Knockout or over-expression glycosyltransferases (Figure 1.1) that are involved in the biosynthesis of gangliosides typically leads to heterogeneous glycolipids. The development of selective, direct-binding, small, molecule ligands for glycolipids might help to clarify individual ganglioside functions.

Third, an understanding of how gangliosides interact with signaling proteins or antibodies will benefit the structure base-design of ganglioside direct-binding ligands and ganglio-oligosaccharides vaccines to be better potential therapies.

Chemistry and structural biology studies

It is necessary to obtain large quantities of well-defined oligosaccharides and their analogues for biochemical, biophysical and biological studies. However, the extraction of significant amounts of gangliosides from natural sources is very difficult and not practical because such glycolipids that are composed of diverse congeners (e.g., GD2 and GD3) (Figure 1.1) are extremely minor constituents in living organisms. Much effort has been invested in synthesizing these gangliosides for structural and functional studies.

Synthesis

Gangliosides are distinct from other glycolipids by the fact that they contain one or more neuraminic acid (sialic acid) residues. According to how many neuraminic acids are possessed by the gangliosides, the gangliosides are simply defined by Svennerholm nomenclature in which M, D, T and Q refer to mono-, di-, tri- and tetrasialogangliosides, respectively (*15*) . According to the biosynthetic pathway, gangliosides are grouped into a, b c and o-series.

Neuraminic acids structurally are distinguished from other monosaccharides and are not easily incorporated into glycoconjugates (*16*). Hence, the synthesis of gangliosides (sialo-glycoconjugates) requires an understanding of the chemistry of neuraminic acid. It is a daunting task to synthesize these glycolipids in a traditional way, especially as tumor-associated gangliosides usually have complex structures with branch carbohydrate sequences (e.g., GD2 and GD3).

Despite these challenges, there have been some examples of elegant syntheses of tumor-related gangliosides. Both a-series gangliosides, like GM3, GM2, GD1a and GT1a (*17, 18*), and b-series gangliosides, like GD3, GD2, GT1b and GQ1b (*19-21*), have been synthesized. However, the procedures were very complex, and the yields were not high. These yields may be sufficient for functional studies, but they are not practical for therapeutic purposes.

Several glycosyltransferase and sialyltransferases regulate the biosynthesis of gangliosides in a Golgi apparatus (Figure 1.1) (*22*). Recent advances in molecular biology and the characterization of various pathogens have identified several bacterial glycosyltransferases and sialyltransferases that have the same activity as mammalian enzymes (*23*). Since these enzymes can be cloned and expressed in *E. coli*, it has been possible to produce large-scale quantities of well-defined gangliosides or analogues of ganglio-oligosaccharides (*24, 25*). All major tumor-associated gangliosides and their mimics have been efficiently synthesized in recent years. For instance, analogues of GM2, GM3, GD2 and GD3 have been chemoenzymatically synthesized using glycosyltransferases and sialyltransferases (*26-29*). These chemoenzymatic assembly methods have simplified the synthesis of complex ganglio-oligosaccharides. In these studies, all sugar head structures have been linked to a convenient functional group that can be conjugated to proteins, lipids, solid supports and other functional groups. These conjugates make it possible to easily study conformations of gangliosides and further develop homogenous cancer vaccines.

Structural and conformational studies

To date, there have not been many structural studies of tumor-associated gangliosides due to their complex structures and unique chemical properties. The majority of structural and conformational studies of gangliosides have been undertaken by high-resolution NMR

experiments and molecular modeling. Most three-dimensional (3-D) structural and interaction studies have focused on GM1 (*30-33*), which is ubiquitous for most eukaryotic cells and is involved in viral entry and important neurobiological events, such as neurodifferentiation, synaptogenesis and synaptic transmission. This information has been quite helpful for studies on tumor-related gangliosides. GM3 structures in an organic solution were based on NOE-based distance and molecular mechanics and dynamics programs (*34*). Although the above studies have provided very valuable structure data, such conformations may need to be investigated further, since new and improved molecular modeling software is now available and may provide further insights.

A recent study by our collaborators has demonstrated the molecular recognition characteristics of antibodies against GD1a and GD3 by saturation transfer difference (STD) NMR (*35*). Several carbohydrate residues are involved in the binding between GD1a and its mAb. In contrast, only the terminal neuraminic acid residue of GD3 interacts with its antibody. Furthermore, a binding model of the anti-GD2 mAb 3F8 to GD2 that is based on STD-NMR and NOE experiments has been proposed by our group (*36*). Our results have also confirmed the previous molecular dynamic (MD) studies (*37, 38*) on GD2 modeling. In fact, these MD simulations have investigated the conformations of all a- and b-series of ganglioside head-groups. Overall, these studies have indicated that ganglioside sugar heads are less flexible, especially the core lactose

structures, than previously thought. The terminal mono- or disaccharide (neuraminic acids) moieties define ligand specificity, since the conformational preferences of these sugar units are independent of the rest of the molecules.

In summary, the structural data of antibody-gangliosides have provided valuable insights into the appropriate presentation of gangliosides as antigens (**See Chapter 5**).

Molecular roles of gangliosides in cancer

Lipid rafts that are small and highly dynamic microdomains on the cell membrane are specifically enriched in particular lipids (e.g., gangliosides and cholesterol) and in various proteins, depending on different cell types (e.g., receptor and non-receptor tyrosine kinases, small G-coupled proteins, PKC isozyme, GPI-anchored proteins, integrins and teraspanins (TSPs)) (*14, 39*).

Ganglioside-mediated signaling transductions are generally regulated by two different mechanisms. Within lipid rafts, clustered endogenous gangliosides can induce cellular signaling pathways through multivalent interaction with signaling molecules. On the other hand, gangliosides are often actively shed from the tumor to their micro-environment in the form of micelles. Shed gangliosides are able to be incorporated into cell membranes to modulate other cells' signaling transduction.

Gangliosides in tumorigenesis

Several *in vitro* studies have demonstrated that the enrichment of the cell membranes of normal fibroblasts with the complex ganglioside GD1a enhanced epidermal growth-factor receptor signaling and Src kinase activation, which led to cell proliferation (*40-42*). The simple ganglioside GM3 modulates the tumor suppressor, PTEN-mediated, cell cycle progression in colon cancer cells, which provides one mechanism of anti-proliferative effects of GM3 (*43*).

Some very recent *in vivo* studies also link gangliosides with tumor formation. For example, GD3 synthase expression enhanced breast cancer cell proliferation in the absence of growth factors and promoted tumor growth in SCID mice by the constitutive activation of c-Met kinase (*44, 45*). The GM3 synthase/GM2 synthase double knockout in murine oncogene-transformed fibroblasts completely depleted gangliosides and impaired tumor growth (*46*). However, current research is still an extension of previous approaches (*13*). Adding exogenous gangliosides may lead to inconsistent results and may not address the physiological roles of endogenous gangliosides. Blocking their biosynthesis through the knockout of related glycosyltransferases may cause a complex pattern of interferences (e.g., the cell proliferation effects of GD3 and GD2 vs. the anti-proliferation effects of GM3) and cannot clarify the roles of individual ganglioside.

Another approach to elucidation of the biological functions of gangliosides is to utilize specific monoclonal antibodies (mAbs). For instance, anti-GM2 mAb has been shown to inhibit the growth of GM2-expressing glioma cells (*47*) and SCLC cells (*48*). Anti-GD3 mAb has been shown to suppress the growth of human melanoma (*49-51*) and glioma cells (*52*). Anti-GD2 mAb has been shown to induce apoptosis in SCLC (*53, 54*) and neuroblastoma cells (*55, 56*). In addition, our lab demonstrated that the anti-GD2 mAb 3F8 induced Src-kinase-dependent-calcium-influx and promoted cell death through apoptosis in lymphoma cells. The fact that the anti-GD2 mAb 3F8 is functional is the fundamental basis for rational development of GD2 direct-binding ligands in our study (**See Chapters 2, 3 and 5**).

In summary, these studies indicate that tumor-related gangliosides are involved in cell proliferation.

Gangliosides in cell adhesion and metastasis

Several gangliosides have been shown to be adhesion molecules that promote tumor metastasis. For instance, b-serials of gangliosides, such as GD2, GD3 and GT1b, have been shown to interact with the extracellular domain of N-terminal domain of integrin through carbohydrate-carbohydrate interactions (*57*). They are also involved in binding to E-selectin (*58, 59*) and Siglec 7 (*60*) that is related to metastasis. Tenascin-R (TN-R), a matrix protein and adhesive protein, has been reported to be a putative endogenous ligand for GD2 (*61*). TN-R is

highly expressed in the extracellular environment of small cell lung cancer (SCLC) (*61*). However, it is interesting to note that some gangliosides, such as GM2 and GM3, inhibit cell motility and proliferation by the modulation of integrin and the function of fibroblast growth factor receptors (FGFR) or hepatocyte growth factor (HGF) operate by GM3/TSP CD9 complex (*62-65*) or GM2/GM3/CD8 (*66, 67*). Consequently, GM2 and GM3 inhibit Src kinase and Met kinase respectively. The overexpression of a ganglioside-specific α -2, 6-sialyltransferase ST6GalNAcV increased the expression of GM2α and GM3 gangliosides, which inhibited glioma growth *in vitro and in vivo*. However, this overexpression of ST6GalNAcV also decreased the expression of GM1b and other glycolipids, such as Gb3, and Gb4 (*68*).

Taken together, these results suggest that gangliosides play an important role in cell adhesion and invasion. Gangliosides may induce different signaling pathways depending on cell types. However, this needs to be further elucidated.

Gangliosides in angiogenesis and immunosuppression

It is known that gangliosides are actively shed by tumor cells to form micelles that are inserted into normal cells in microenvironments. This leads to angiogenesis and the suppression of anti-tumor immune response.

Adding exogenous gangliosides GD1a and GD3 to endothelial cells, strongly amplified vascular endothelial cell growth factor (VEGF) induced

signaling, which indicated that certain gangliosides are important for angiogenesis (*42, 69*). These results were consistent with other studies that used genetic deletion of GD3-related biosynthesis enzymes (*70-72*). However, as previously discussed, both methods have their drawbacks, namely that they cannot clearly determine which ganglioside modulates the signaling pathway that is related to tumor angiogenesis. In other words, down-regulating one ganglioside can up-regulate another one that may have the reverse effects. For instance, GM3 inhibits angiogenesis by the inactivation of VEGF-induced signaling by direct interaction with VEGF and associated receptors (*73-75*).

The immune silencing of gangliosides has been known for a long time. Tumor-shed or exogenous gangliosides can inhibit the function of several immune cells, such as helper T-cells (*76-78*), natural killer cells (*79-81*), antigen-stimulated T/B-cells and dendritic cells (DC) (*82-84*). It has been reported that the length of ceramide lipid tails can affect the immunosuppression of tumor gangliosides (*85*). Ganglioside GD2 containing the shorter fatty acyl chain is more immunosuppressive than the one that has a longer chain.

Several mechanisms have been proposed: a) it was postulated that gangliosides are involved in a CD95/Fas-mediated apoptotic pathway in lymphocytic cells (*39, 86, 87*); b) apoptosis may be induced by the cytoplasmic movement of gangliosides like GD3 towards the mitochondria membrane in lymphocytic cells (*39*); c) glioblastoma cells cocultured with

T cells may induce T-cell apoptosis via CD70 and gangliosides, such as GM2 and GD1a, in contrast to glioblastoma cells that do not express those gangliosides (*88*); d) various gangliosides, including GD3, GD2, and GT1B, may decrease IFN-α production and enhance the IL-4-dependent differentiation of $CD4^+$ T cells, which suggests that these gangliosides may modulate the balance of type-1/type-2 T cell responses acting at multiple regulatory levels (*89*); e) significant inhibition of nuclear localization of NF-κB proteins in activated dendrite cells (DC) by gangliosides may inhibit the antigen-present cells (APC) function and the cytokine secretion, In turn, this may diminish the antitumor immune responses (*90*); and f) the inactivation of toll-like receptors through up-regulation of IL-1 receptor associated kinase M(IRAK-M) by exogenous GM2, GD3, and GD1a/1b, instead of GM3, may indicate that the innate immune response is also compromised (*91*).

In conclusion, many observational studies clearly suggest that gangliosides are involved in tumorigenesis, metastasis, angiogenesis and immunosuppression. In addition, different gangliosides exhibit various roles in tumor progression.

Cancer therapy targeting gangliosides

As tumor markers, gangliosides are attractive targets for passive (antibody treatment) and active immunotherapy (cancer vaccine). There are several anti-ganglioside antibodies and ganglioside-based vaccines that have been investigated in clinical trials over the last 20 years. They

Table 1.1 Clinical trials of anti-GD2 antibody combined with cytokines

mAb	Trial design	Disease	Cytokines	Response	Toxicities	Refs
14G2a (mIgG2a)	Phase I N=33 patients	neuroblastoma	IL-2	1 partial 1 complete	pain, allergic fever	(*92*)
3F8 (mIgG3)	Phase II N=34 patients	Neuroblastoma	GM-CSF	12 of 15 had complete remission (CR) of bone marrow (BM) disease	**Pain**, rash	(*93*)
Ch14.18 Human-Mouse Chimeric IgG1	Phase I N=24 patients	melanoma	IL-2	1 complete response, 1 partial response, 8 patients with stable disease	allergic weakness, **pain** peripheral neuropathy.	(*94*)
	Phase I N=24 patients	Neuroblastoma	GM-CSF IL-2	tolerable	**pain**, fever, nausea, emesis, diarrhea, urticaria, capillary leak hypotension	(*95*)
	Phase II N=39 patients	refractory neuroblastoma	IL-2 fused with CH14.18	21.7% complete response	capillary leak, hypoxia, **pain**, rash, allergic, elevated transaminases, and hyperbilirubinemia	(*96*)
	Phase III N=226 patients	high-risk neuroblastoma	GM-CSF IL-2	event-free survival (66+/-5% vs. 46+/-5% standard-therapy at 2 years) and overall survival (86+/-4% vs. 75+/-5% standard-therapy at 2 years)	**pain** of grade 3, 4, or 5, capillary leak and hypersensitivity	(*97*)

IL-2: interleukin-2; GM-CSF: granulocyte-macrophage colony-stimulating factor.

are used to treat minimal residue diseases of neuroectodermal cancer, such as neuroblastoma, melanoma and SCLC, after chemotherapy and radiation.

The main mechanism of immunotherapy is the utilization of antibodies or vaccine-induced antibody-dependent cell-mediated cytotoxicity (ADCC) and complement-dependent cytotoxicity (CDCC) (*98*). There are also some non-immune, system-mediated effects, as gangliosides are functional in tumor formation and progression. It has been seen that anti-ganglioside antibodies may induce the apoptosis of tumor cells. They may also block the tumor cell adhesion, metastasis and angiogenesis or may augment the immune system by binding and clearing free immunosuppressive shed-tumor-gangliosides in blood.

Passive cancer immunotherapy

Disialoganglioside GD2

GD2 is highly expressed in some tumor tissues such as neuroblasotoma (*99*), meleanoma (*4*) (*100*), sarcoma (*101*), small-cell lung cancer (*5*) and brain tumors (*102, 103*), while it has a very restricted distribution in normal adult tissues, such as the central nervous system and peripheral nerves (*1, 3*). GD2 is a very “hot” target for cancer therapy. Several mAbs (Table 1.1) have already been developed for clinical uses (*104*).

Mouse IgG monoclonal anti-GD2 antibodies 14G2a (*99*) and 3F8 (*105*) have been extensively tested in clinical trials. The results from the

three clinical trials for 14G2a (*106-108*) and four clinical trials for 3F8 (*109-112*) that respectively evaluated them as a single agent indicated that they were not very effective in treating melanoma and the refractory minimal residue neuroblastoma.

In order to augment the immune system and enhance the anti-tumor effects of these antibodies, 14G2a and 3F8 combined with IL-2 (*113*) and/or ganulocyte-macrophage colony-stimulating factor (GM-SF) (*114, 115*) were examined *in vitro*. Subsequently, a better outcome has been demonstrated for 14G2a (*92*) and 3F8 (*93, 116*) in several clinical trials (Table 1.1) because more patients showed an anti-tumor response than before. However, the antitumor effects of 14G2a and 3F8 were quickly compromised by human anti-mouse antibodies (HAMA) since the human immune system recognizes mouse antibodies as foreign. Hence, human-mouse chimeric anti-GD2 antibody CH14.18 as a second generation has been developed to avoid HAMA.

Ch14.18 is the variable regions of mouse mAb14G2a that are fused with the constant regions of a human IgG1-κ (*117*). There was almost no effect when using this antibody alone against adult metastatic melanoma or neuroblastoma in the three early clinical trials of phase I (*104)* (*118*). The anti-isotype or idiotype-antibodies detected in patients may contribute to the low efficacy of CH14.18. However, CH14.18 treatment has improved the overall survival of patients when it was administered to a

subset of young patients who had been diagnosed with metastatic neuroblastoma.

Similarly, CH14.18 combined with IL-2 and GM-SF has been evaluated for the treatment of patients with high-risk neuroblastoma in three clinical trials of phase I (*94, 95, 119*) and in one clinical trial of phase II (*96*) (Table 1.1). Promising results were obtained. This led to a very recent phase III clinical trial (*97*). The results of this phase III study have shown that CH14.18 combined with IL-2 and GM-SF increased the event-free survival of high-risk neuroblastoma patients by 20%. This immunotherapy regimen has now become standard for the care of young neuroblastoma patients.

Although the humanized antibody CH14.18 has avoided some issues, such as low efficacy and HAMA, there are still some side effects for all anti-GD2 antibodies. These may be caused by added cytokines, such as IL-2 and GM-SF. However, there is one major side effect that is induced by anti-GD2 antibodies - severe abdominal/pelvic pain (*104*). Inflammatory effects by complement activation may be one of the mechanisms attributed to pain (*120*) (*121*).

Taken together, passive immunotherapy targeting GD2 has shown promising anti-tumor activity in patients who have GD2-expressing tumors, especially neuroblastoma.

Disialoganglioside GD3

Most cancer therapies that target GD3 are applied to melanoma because GD3 is expressed in most human melanoma tissues, while the normal counterparts scarcely express GD3 (*122, 123*). R24, an IgG3 mouse mAb against GD3, was found to be cytotoxic *in vitro* (*124*). However, the results of several clinical trials that evaluated R24 alone (*125, 126*), and the antibody combined with some cytokines like IL-2 (*127*), tumor necrosis factor-α (TNF-α) (*128*) or GMSF (*129*), were not promising. A preliminary trial (phase I) reported that a chimeric anti-GD3 mAb KM871 may have potential for metastatic melanoma patients (*130*).

In summary, passive cancer therapy that targets gangliosides, especially GD2, is promising. However, antibody therapy has some limitations. First, anti-ganglioside antibodies may cause some side effects (Table 1.1). Second, most anti-ganglioside antibodies, due to their murine origin, are immunogenic and induce neutralizing HAMA or anti-idiotypic antibodies (as described), which ultimately causes the therapy to be ineffective. Third, the production of antibodies is expensive and they are limited in supply. Hence, the development of ganglioside vaccines has been proposed and developed (*131-135*).

Active cancer immunotherapy

The cancer vaccine, one type of active cancer immunotherapies, utilizes antigens to boost the immune system to protect itself against malignant cells.

The ganglioside vaccines may be a good approach to the treatment of related cancers. However, some challenges to the development of gangliosde-based cancer vaccines remain. First, gangliosides are difficult to use because of their poor water solubility and their tendency to form micelles in water due to their amphiphilic properties. Second, carbohydrates or glycolipids have low immunogenicity and generally induce T-cell independent antibodies such as IgM types (*136*). Third, carbohydrates are always conjugated to an immunostimulant protein carrier, such as the keyhole limpet haemocyanin (KLH), to overcome the low immunogenicity. However, those kinds of glycoconjugates are heterogeneous (*8*), and their quality cannot be guaranteed. Fourth, natural sources of tumor-associated gangliosides are limited (*8, 137, 138*). Fifth, due to their complex structures, it is extremely difficult to synthesize them in a conventional way. Finally, there is little ganglioside structure information available (*8*).

Despite the limitations, several types of ganglioside vaccines have been investigated in animals and humans (Table 1.2). One major type is ganglioside-KLH vaccines. Alternatives are anti-idiotype antibody vaccines, DNA vaccines and liposomes.

Ganglioside-KLH vaccines.

Not all gangliosides are equally immunogenic. More immunogenic gangliosides include fucosyl GM1, GM2, N-glycolyl (NeuGc) GM3 and GD2, which are markers for SCLC (*139*), (*140, 141*), melanoma (*142-144*),

neruobastoma (*99*) and breast cancer (*145*). Low immunogenic gangliosides include GD3 (*122, 123*) and GM3 (*146, 147*). Various ganglioside-KLH vaccines have produced different effects.

Table 1.2 Ganglioside vaccines

Antigen	Type of vaccine	Type of cancer	Status	Refs
Fuc-GM1	Fuc-GM1-KLH	SCLC	Clinical benefit need to be determined	(*148, 149*)
GD2	GD2 lactone-KLH	Melanoma	No clinical benefit	(*150*)
GD3	GD3 lactone-KLH	Melanoma	No benefits	(*151*)
GM2	GM2-KLH	Melanoma	No benefits, clinical trials Phase III failed	(*152*)
GD2 or GD3	anti-idiotype antibodies (Ab3 and Ab3')	Melanoma	Low efficacy in clinical trials	(*153, 154*)
GD2	GD2-peptide mimotopes DNA vaccine	Neuroblastoma	Pre-clinical	(*155, 156*)
GD2	GD2 mimotope DNA vaccines	Neuroblastoma	Preclinical	(*157*)
NeuGcGM3	proteoliposome	Breast cancer	good immunogenicity in phase I	(*158, 159*)

SCLC: small-cell lung cancer.

SCLC patients have exhibited a good immune response to the Fuc-GM1-KLH conjugate vaccine. Fuc-GM1-KLH elicited antibodies had a good binding to and killing effect on tumor cells (*148, 149*). However, their clinical benefits have not yet been determined.

GD2 and GD3 lactone-KLH have been developed as cancer vaccines to overcome the low immunogenity of GD2 or GD3-KLH (*150, 151, 160, 161*). The improved GD2 or GD3 lactone KLH vaccination could induce CDC in most melanoma patients, but the anti-GD2 or GD3 antibody response was transient with a low titer, and the long-term effects have not been examined. One possible reason for the low immunogenicity of these KLH-conjugated vaccines is that antibody response to these gangliosides is independent of natural killer cells (*162*). Overall, a great deal of effort is needed to develop immunotherapy that targets GD2 or

GD3. More recent studies have been focused on the development of new adjuvants to increase the immunogenicity of the GD3 vaccine (*163, 164*). However, the use of strong adjuvants may induce toxicities.

The GM2-KLH vaccine (*165, 166*), which is referred to as the GMK vaccine (Progenics Pharmaceuticals, Inc, Tarrytown, NY), has been shown to induce high titers of both IgM and IgG antibodies in melanoma patients and to mediate CDC and ADCC of melanoma cell lines *in vitro* (*165, 166*). Although a phase II study has shown that a high dose of interferon α-2b (IFN-α-2b) does not diminish an antibody response to GM2 (*167*), a randomized, phase III study was terminated because the treatment benefits of IFN-α-2b plus GMK were no better than IFN-α-2b in relapse-free survival and overall survival in melanoma patients (*152*). This result was also confirmed by a recent clinical trial (the European Organization for Research and Treatment of Cancer 18961).

Although the clinical trials for the GM2 vaccine alone were terminated, it may be incorporated into multivalent vaccines or applied to other types of cancers. For instance, the “tetravalent” vaccine combination of GM2, fucosyl GM1, globo H and polysialic acid was designed for use against SCLC as SCLC tumors express these four glycolipids (*168, 169*). Plans have been made to investigate this tetravalent vaccine by tests in SCLC patients.

In summary, no ganglioside-KLH vaccine with adjuvants was effective for melanoma in patients, although there were antibody responses.

An anti-idiotype antibody vaccine

An anti-idiotype antibody mimicking GD2 and GD3 may induce immune responses in melanoma patients (*170, 171*). However, its efficacy was very low (*153, 154, 172-177*). In fact, anti-idiotype antibodies (Ab3 and Ab3') induction was correlated with long-term survival after anti-ganglioside antibody therapy of neuroblastoma (*178, 179*).

An anti-idiotype mAb (Ab2) 1E10 that specifically reacts with NeuGc-GM3 has been developed and investigated in melanoma (*180*), breast cancer (*181, 182*) and small-cell lung cancer (*141*). The phase I clinical trials have demonstrated that most patients have developed a specific and strong immune response to NeuGc-GM3 and that the vaccine was safe. Although these initial clinical trials have shown good immune responses with low toxicities induced by the NeuGc-GM3 vaccines, further investigations remain to be done to determine whether there is a correlation between the immune response and a clinical benefit for patients.

DNA vaccines

GD2-peptide mimotopes and GD2 mimotope DNA vaccines have been shown to inhibit tumor growth in mice. Peptide vaccines are derived from phage display peptide libraries by panning with GD2-specific mAb

(*183-186*). GD2 mimotope DNA vaccines encoded anti-idiotype antibodies (*157*) or GD2-mimicking peptides (*155, 156*). Although cross-reactive immunity was induced by mimotopes, humoral responses were limited and were not very effective in protecting the host when challenged with ganglioside-expressing tumors (*184*).

Liposomes

A heterophilic ganglioside cancer vaccine composed of NeuGc-GM3 in a very small size proteoliposome has shown good immunogenicity and low adverse effects in patients (*158, 159*).

Taken together, it is still worth testing current ganglioside-based vaccines for other cancers, although they were not effective in treating melanoma and it is known that even anti-ganglioside antibody treatments have shown much more clinical benefit on neuroblastoma than melanoma.

Conclusions and future directions

A better strategy may be to study gangliosides from the perspective of chemical biology.

For the chemistry of gangliosides, the important breakthrough is the chemoenzymic synthesis of complex structures of ganglio-carbohydrates. It is feasible to design and synthesize sufficient different ganglioside analogues for structural (**Chapter 2**), functional and therapeutic studies.

Due to the limitation of current research technologies, the molecule mechanisms implicated by means of gangliosides themselves within the lipid rafts have remained elusive. The development of selective

ganglioside direct-binding ligands, including mAbs and small molecules, will help to dissect the signaling pathway related to gangliosides (**Chapters 2, 3 and 5**). Studies of the molecular mechanism modulated by these glycolipids will absolutely benefit the current ganglioside-targeted cancer therapy.

In respect to cancer therapy that targets gangliosides, it is time to design and develop a homogenous mono- or multivalent cancer vaccine in order to avoid the side effects of antibody treatment (**Chapter 4**). The combination of antibodies/conjugated antibodies, vaccines or selective small molecules may improve the efficiency and efficacy of cancer treatment.

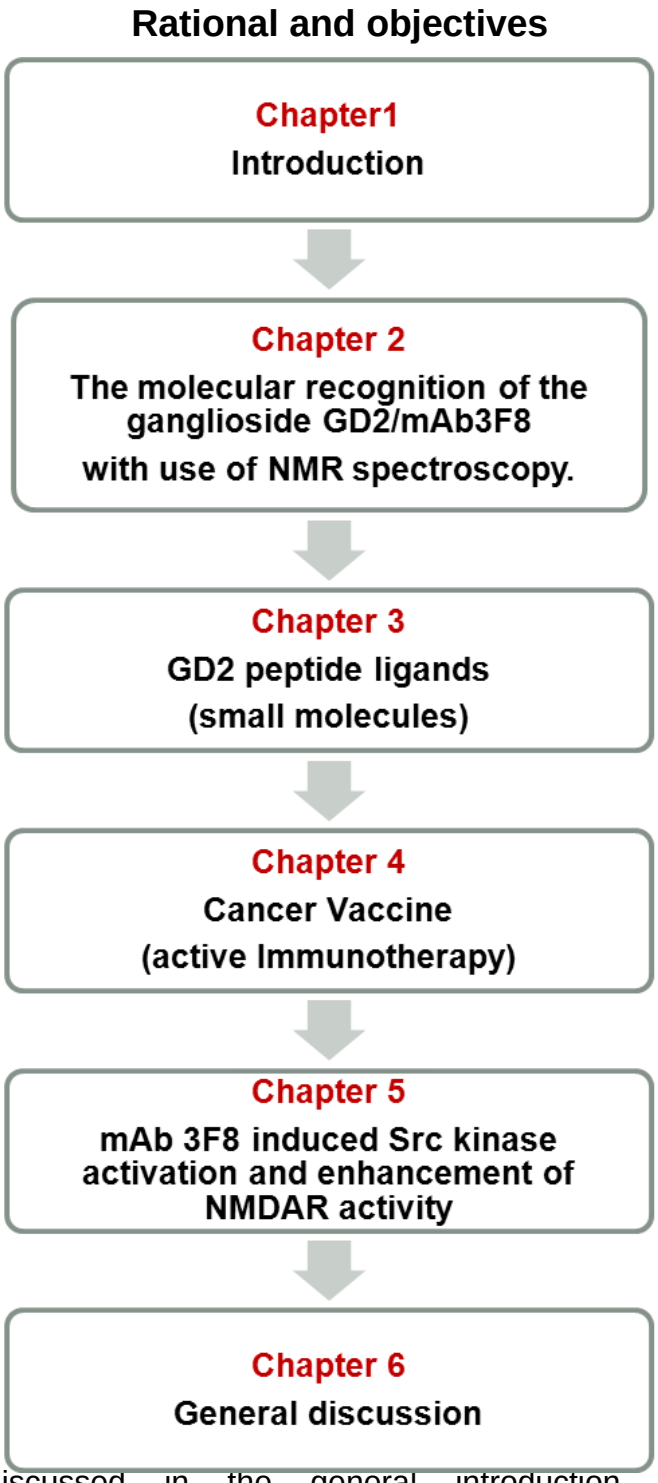

As discussed in the general introduction (**Chapter 1**), chemoenzymatic synthesis of water-soluble GD2 analogues makes it possible to study the structure and function of ganglioside GD2. This

project goal is to improve the therapeutic treatment for GD2-postive cancer. Chemical biology is used as an approach for this project.

An outline of the thesis is presented in the figure above. First, the conformations of GD2 in the free state and bound state (interactions with an anti-GD2 monoclonal antibody) were studied with use of NMR (**Chapter 2**). From this work, GD2 peptide ligands were rationally designed based on a binding model that is consistent with the NMR data. These GD2 ligands can specifically bind to GD2 and are functional in that they activate signal transduction in cellular assays. However, these peptide ligands did not demonstrate any treatment effect *in vivo* (**Chapter 3**).

As a clinically validated tumor marker, GD2 is an attractive target for cancer immunotherapy. A novel type of soluble GD2 analog that is highly immunogenic (tetra-GD2 dendrimer) was designed. *In vivo* vaccination with tetra-GD2 dendrimer induces antibody responses and inhibits tumor growth. So, it might be a potential cancer vaccine (**Chapter 4**).

Ligands of GD2, including antibodies, were utilized to dissect the cellular signaling transduction via binding to GD2 in order to explain a possible molecular mechanism of anti-GD2 antibody-induced pain in clinical trials (**Chapter 5**). Finally, the results and future directions are discussed **(Chapter 6).**

Chapter 2

Small Molecule Ligands of GD2 Ganglioside, Designed from NMR Studies, Exhibit Induced-Fit Binding and Bioactivity.

Wenyong Tong[1,2], Martin Gagnon[1,2,ζ], Tara Sprules[5], Michel Gilbert[6], Shafinaz Chowdhury[1], Karen Meerovitch[3, 7], Karl Hansford[7], Enrico O. Purisima[8], John W. Blankenship[10,ξ], Nai-Kong V. Cheung[9], Kalle Gehring[3, 5], William D. Lubell[10], H. Uri Saragovi [1, 2, 4, *]

[1]Lady Davis Institute-Jewish General Hospital, Montréal, Quebec, Canada, H3T 1E2.

Departments of [2]Pharmacology and Therapeutics, [3]Biochemistry, [4]Oncology and the Cancer Center, McGill University, Montréal, Quebec, Canada H3G 1Y6.

[5]Quebec/Eastern Canada High Field NMR Facility, McGill University, Montréal, Quebec, Canada, H3A 2A7.

[6] Institute for Biological Sciences, National Research Council Canada, Ottawa, K1A 0R6.

[7] Mimetogen Pharmaceuticals, Montreal, Quebec, Canada, H3T 1E2.

[8] Biotechnology Research Institute, National Research Council Canada, Montreal, Quebec, H4P 2R2.

[9]Department of Pediatrics, Memorial Sloan Kettering Cancer Center, New York 10065, USA.

[10]Department of Chemistry, Université de Montréal, Montréal, Québec, Canada, H3T 1N8.

[ζ] Present address: Chlorion Pharmaceuticals, Montreal, Quebec, Canada.

[ξ] Present address: Trubion Pharmaceuticals, Seattle, Washington, USA.

Summary

Ganglioside GD2 is a cell surface glycosphingolipid. Targeting of GD2, i.e., by anti-GD2 mAb 3F8, is used clinically for cancer diagnosis, prognosis and therapy. Here, the conformations of free GD2, and of GD2 bound to mAb 3F8 were resolved by saturation transfer difference NMR and molecular modeling. Then, three small molecule cyclic peptide ligands that bind to GD2 selectively were designed. Transferred Nuclear Overhauser Enhancement of the GD2-bound conformation of the peptide ligands showed an induced-fit binding mechanism. The mAb 3F8 and the peptidic GD2 ligands mediate similar biological functions in cell-based assays of calcium fluxe and Src-activation. Thus, small molecules can selectively and functionally interact with a sugar head group. This work furthers the concept of rationally designing ligands for carbohydrate targets; and may be expanded to other clinically relevant gangliosides.

Introduction

The structures of the glycans protruding from eukaryotic plasma membranes change with the onset of cancer (*187*) and other pathologies. For example, ganglioside GD2 is expressed during embryonic development, and in the adult it is normally expressed at very low levels in the peripheral nervous system and the cerebellum (*188, 189*) but it is over-expressed in neuroblastomas, small-cell lung carcinomas, and melanomas (*4, 5, 190, 191*). GD2 is thus targeted clinically for diagnosis and immunotherapy (*192*) using anti-GD2 monoclonal antibodies (mAb), such as IgG3 mAb 3F8. The importance of gangliosides in tumorigenesis, tumor progression and tumor metastasis may be due to their biological functions (*13, 193*) which include cell recognition, cell matrix attachment, cell growth or differentiation; including the induction of Ca^{++} fluxe and the activation of the *src* family kinases (*13, 194, 195*).

Previously, the interactions of mAbs directed against ganglioside GT1a and GD3 were studied by saturation transfer difference (STD) Nuclear Magnetic Resonance (NMR) spectroscopy and surface plasmon resonance (SPR) measurements (*35*). Also, binding epitopes and conformations were obtained by STD and 2D NMR in the presence of GM1 micelles for natural peptides that interact with ganglioside GM1 (enkephalin (*196*), amyloid peptide (*197*) and bradykinin (*198*)). However, GD2 has not been studied in this manner; and more importantly generally the structural data obtained for carbohydrates have been impervious to

the design of selective ligands with biological activity.

Here we studied whether NMR-based approaches can generate GD2-selective ligands with biological activity. We report the use of STD NMR spectroscopy (*199*) to study the binding characteristics of anti-GD2 mAb 3F8 to two forms of GD2; (i) intact ganglioside GD2 in dodecylphosphocholine (DPC, that form micelles as a plasma membrane mimic), and (ii) the "GD2 carbohydrate head" as a water soluble phenylthioether-analog of GD2 that lacks ceramide and lipids.

Then we synthesized three GD2-selective peptidic ligands which mimic mAb 3F8; using mAb mimicry design (*200*). Their structures and their binding to GD2 micelles mimicking lipid rafts were studied by NMR. The conformation of the peptidic GD2 ligands bound to the head group of GD2 was characterized by transferred nuclear Overhauser enhancement (trNOE) experiments that demonstrated their conformational change on ganglioside binding, and a likely induced-fit mechanism. The peptides have biological activity similar to the original ligand mAb 3F8, in cell-based assays of calcium fluxe and *src*-activation. This report demonstrates that a small molecule peptide, designed from experimental binding data, can be a ligand that selectively and functionally interacts with a ganglioside sugar head group.

Results and discussion

Generation of a soluble GD2 analog for structural studies.

Ganglioside GD2/3F8 interactions can be inhibited by soluble thiophenyl GD2 (Figure 2.1, panel A) in a dose-dependent manner (Figure 2.1, panel B). The IC_{50} of this water-soluble thiophenyl GD2 is ~10 μM. Competition is considered to be specific because thiophenyl GD3 does not affect the binding of ganglioside GD2 to 3F8. Thus, soluble thiophenyl GD2 can be considered a structural analogue of ganglioside GD2.

Resonance assignments of ganglioside GD2 in DPC, thiophenyl GD2 and structure calculations.

The complete proton and carbon chemical shift assignments for ganglioside GD2 in DPC micelles and thiophenyl GD2 in aqueous solution are provided in Appendix I supplemental Tables S1 and S2, respectively. 51 distance restraints, including one between glucose and the lipid tail ceramide, were obtained from 2D-ROESY for ganglioside GD2 in DPC micelles. The 2D-NOESY spectra that were obtained on thiophenyl GD2 with a mixing time of 200 ms detected 48 NOEs, which were used to construct conformations of thiophenyl GD2 (Figure 2.2). The RMSD within each group of conformers was ~0.7 Å excluding the two terminal residues. The structure of thiophenyl GD2 in water differed from that of ganglioside GD2 in DPC micelles (RMSD=3.0 Å) primarily in the glycosidic dihedral

angles $\phi_4\varphi_4\omega_4\chi_4$ (Figure 2.1 panel A; and Appendix I supplemental Table S3), which means the terminal neuraminic acid residue can dynamically adopt different conformations in different chemical environments. The average value of $\phi_2\varphi_2$ is very similar to those reported by a molecular dynamics study, indicating that the conformation of the linkage between galactose and glucose is not influenced by the presence of other residues in the ganglioside (*38*). These structures demonstrated that the ceramide moiety interacted with the carbohydrate in a way that altered its conformation, which indicates that the conformations of head group and ceramide with lipid tail are inter-related and influenced by the micelle membrane (*201*).

The NMR conformers show a well-structured carbohydrate, which in a 10 ns MD simulation study was stable (data not shown). Next we studied how this stable structure behaves in the presence of ligands, such as mAb 3F8.

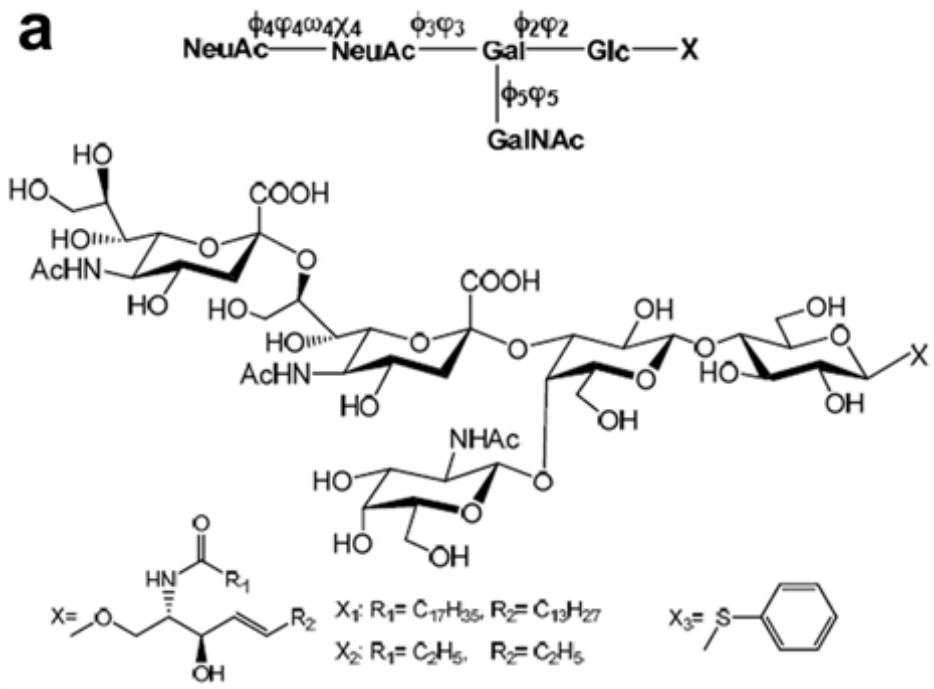
a
NeuAc
NeuAc
Gal
Glc
X
GalNAc
COOH
AcHN
NHAc
OH
HO
X1: R1= C17H35, R2= C13H27
X2: R1= C2H5, R2= C2H5
X3= S

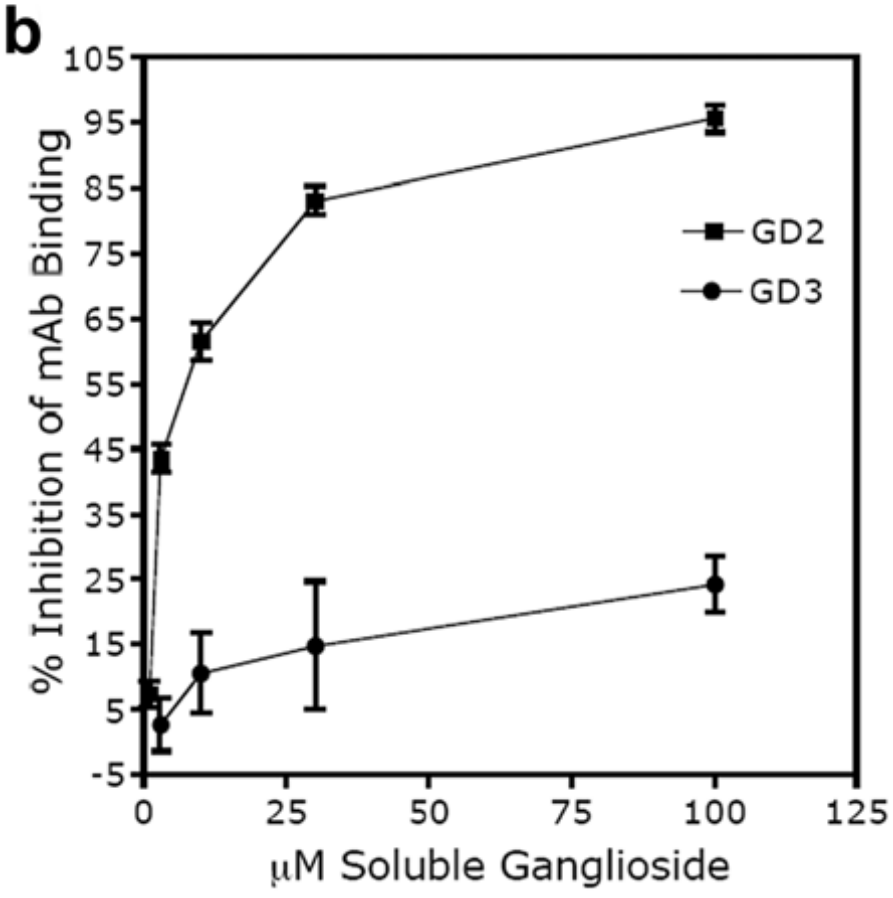
b
% Inhibition of mAb Binding
μM Soluble Ganglioside
GD2
GD3
105
95
85
75
65
55
45
35
25
15
5
-5
0
25
50
75
100
125

Figure 2.1 Structures and antibody binding of ganglioside GD2 and its derivatives. (**A**) The carbohydrate "head" of GD2 is shown, to which can be attached either a ceramide or lipid tail (X1), this is herein referred to as ganglioside GD2. The ceramide tail of ganglioside GD2 can be truncated (X2) for the purpose of modeling. X3 is a synthetic water-soluble thiophenyl GD2, lacking the ceramide and lipid tail, as an analog of ganglioside GD2. Residues and torsion angels are shown (also see Supplemental Table S3). The glycosidic angles are defined as follows: φ=O5-C1-O-CX' (C1-C2-O-C3' in Neu5Ac-α2-3-Gal) and ψ=C1-O-CX'-C(X-1)'. For the Neu5Ac-α2-8-Neu5Ac, φ=C1-C2-O-C8', ψ=C2-O-C8'-C7', ω=C6-C7-C8-C9 and X=C5-C6-C7-C8.

(**B**) Soluble thiophenyl GD2 binds to anti-GD2 mAb 3F8 and therefore competes 3F8 binding to immobilized ganglioside GD2 in competitive ELISA. Soluble thiophenyl GD2 inhibited the binding of mAb 3F8 (5 ng/well) to immobilized GD2 (10 ng/well) in a dose-dependent manner with an IC_{50} of 10 μM. Shown is the average ± SEM from 3 independent assays. As control, soluble thiophenyl GD3 did not inhibit 3F8-ganglioside GD2 interactions; but did inhibit the binding of anti-GD3 mAb R24 to ganglioside GD3 (data not shown).

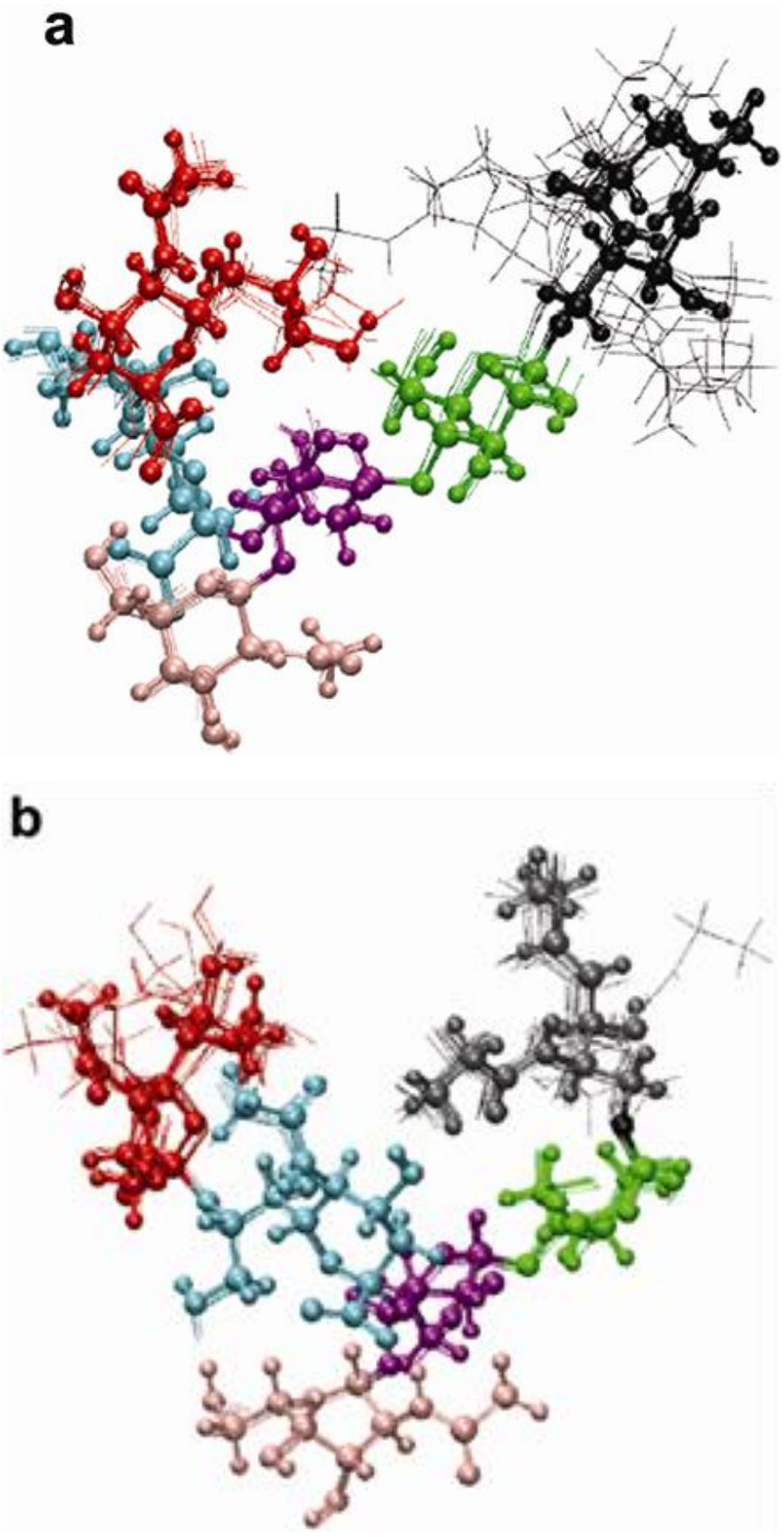
a
b

Figure 2.2 Superimposition of GD2 structures as determined from annealing simulation with refinement of NMR.

(**A**) Ensemble of thiophenyl GD2 structures (14 conformers).

(**B**) Ensemble of GD2 ganglioside structures with truncated lipid tails (16 conformers). Glucose = green, galactose = purple, N-Acetyl galactosamine = pink. Two N-acetyl neuraminic acids are in blue (NeuAc (2-3)) and red NeuAc (2-8). For modeling, both ceramide and thiophenyl groups were replaced by a truncated ceramide (black) with a shorter sphingosine and fatty acid. The reference structure is in ball and stick representation, and the others are in Line representation.

Group Epitope Mapping (GEM)-The binding interactions of thiophenyl GD2 and Ganglioside GD2 with mAb 3F8.

STD signals show that the binding of soluble thiophenyl-GD2 to 3F8 can be resolved (Figure 2.3A and 2.3B, Figure S2). The most prominent peaks in the STD spectra arise from the resonances of the neuraminic acids **(**NeuAc) (2-3) residue connected to galactose (Gal). The H3 equatorial (eq) proton of NeuAc (2-3) experiences the largest STD amplification factor (Figure 2.3C). Integral values from the reference and STD spectrum show that if the largest signal, H3eq, is set to 100% (T_{sat}= 5 s), the H2 proton of β-glucose (Glc) and the N-acetyl methyl resonances reach about 38% and 25% respectively (Figure 2.3D). Small contributions are also observed for protons at 3.8-3.9 ppm, and 3.6-3.7 ppm, which could arise from β-glucose, NeuAc (2-3) and NeuAc (2-8). However, the signal is not strong enough to distinguish individual contributions. For the anomeric protons of glucose and N-acetyl galactosamine (GalNAc), no obvious STD response was observed, which may be due to their close proximity to the HDO resonance.

The intensities of the observed STDs are primarily dependent upon the longitudinal relaxation rate of the free ligand proton at long saturation times (*202*). This is seen at the long saturation times (1-5s) employed in our experiments (Appendix I Table S4). The methyl groups and Glc/Gal H2 protons have the longest T1s, and in the STD spectra give more

significant signals than other sugar protons falling between 3.6 and 3.9 ppm.

The proton of NeuAc (2-3) H3 eq, which has a short T1 (0.7s), showed the largest amplification factor at different saturation times (data not shown). This indicates that the side of sugar rings with the N-acetyl group and carboxylic acid is directed towards the antibody. Additional STD experiments with increasing concentrations of thiophenyl-GD2 shows that a maximum amplification is reached for the more weakly interacting protons at 1 mM (Figure 2.3C). The more strongly interacting proton did not reach maximum amplification under the experimental conditions. Any possible non-specific contribution to this binding cannot be excluded at this time (*203*), as there is no high affinity inhibitor to saturate the specific binding site.

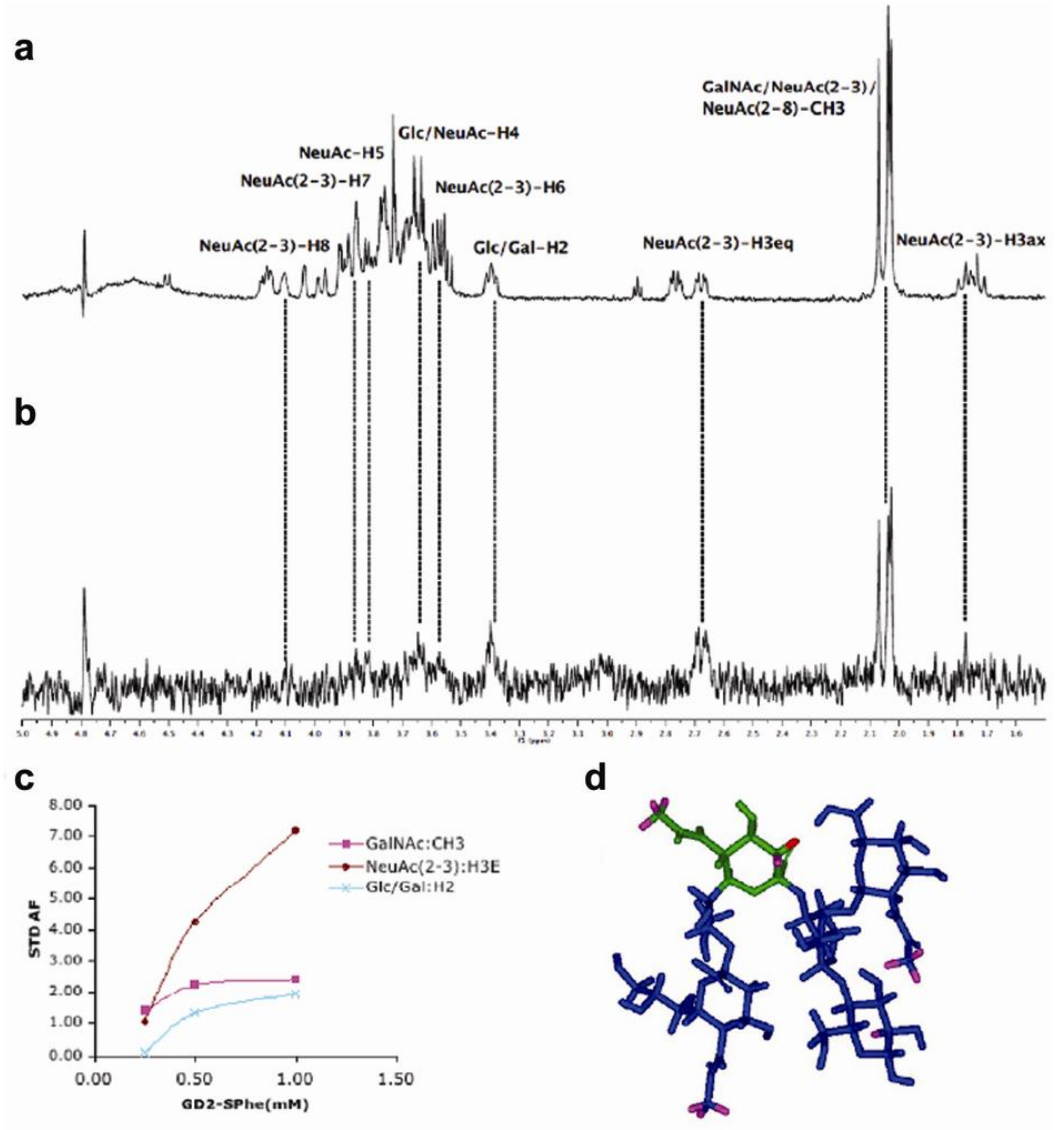

Figure 2.3. STD NMR spectra, STD amplification factor and structure model of thiophenyl GD2 binding to mAb 3F8. (**A**) Reference spectrum of a mixture of thiophenyl GD2 (500 µM) and 3F8 (10 µM binding sites) at a 50:1 ratio. (**B**) STD NMR spectrum of the same sample (T_{sat}= 5 s). (**C)** Observed STD amplification factors of several resonances of thiophenyl GD2 plotted against the ligand concentrations (T_{sat}= 3 s). (**D**) The most prominent peaks in the STD spectra arise from the resonances of the residue NeuAc (2-3) in green. Atoms in red correspond to the strongest STD signal, which is assigned a value 100%. Magenta coloring corresponds to residues that are about 20-40% saturated.

The STD NMR profile of ganglioside GD2 embedded in DPC micelles showed that the water–exposed sugar head groups could also interact with the antibody. The STD spectrum of GD2 ganglioside in DPC micelles interacting with mAb 3F8 showed that additional peaks of sugar and ceramide are observed at 3.8-3.9ppm, the peaks from the acetyl methyl resonances are enhanced, and a new DPC peak at 3.28ppm appears (Appendix I supplemental Figure S2).

The control STD spectrum of GD2 ganglioside in DPC micelles with no mAb 3F8 shows signals arising from the methyl groups of neuraminic acid and N-acetyl galactose, and from DPC, caused by irradiation of the DPC micelle or by non-specific interaction of these methyl groups with the DPC micelle.

To confirm whether signals in the STD spectrum in the presence of mAb 3F8 arise from saturation transfer from the mAb, the on resonance saturation frequency was shifted from -2 to 9 ppm. This resulted in a very similar STD spectrum, indicating that the GD2 head group did interact with mAb 3F8 in this membrane-like environment. The low signal to noise in the STD spectra of the GD2/mAb spectra made it difficult to obtain definitive binding epitope information, however it is clear that some parts of the carbohydrate are more important than others for the binding interaction.

Next, we further studied the interaction by computer docking, to determine whether conformational changes occur in the complex.

Docking studies of GD2 with mAb 3F8.

In the absence of a crystal structure for mAb 3F8, a model was generated for the binding of GD2 in the antigen-binding site of 3F8 antibody based on homology modeling with other mAbs. Intermolecular interactions (both electrostatic and hydrophobic) were observed between the GD2 molecule and 3F8 (Figure 2.4). At the antigen-binding surface, GD2 interacts mainly with residues of light chain 3 (L3), heavy chain 2 and 3 (H2 and H3) of complementarity determining region (CDR), as well as with framework residues.

Both the glucose and galactose residues of GD2 bound in the shallow groove in mAb 3F8 between the variable domain light (VL) and variable domain heavy (VH) chains and interact with residues of CDRs. The N-acetylgalactosamine residue occupies the lower part of the groove and the N-acetyl group makes good hydrophobic interactions with framework residue Ile2. Both NeuAcs bind into a relatively flat area of the antigen-binding surface formed mainly by the residues of the H2 CDR and few residues of the H3 CDR (Figure 2.4A and 2.4B). Four residues in the antigen binding site hydrogen bond with the GD2 molecule (Figure 2.4C).

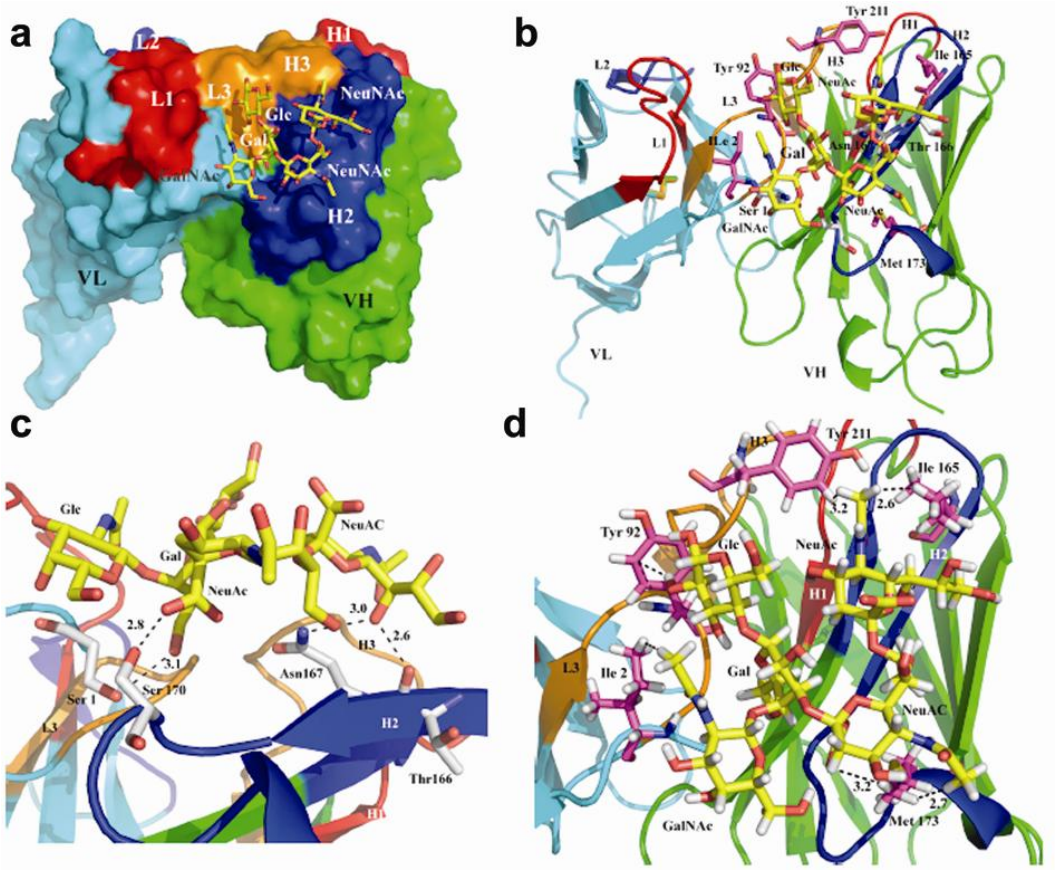

Figure 2.4. The predicted binding mode of GD2 in the antigen binding surface of a Fab fragment of 3F8 antibody.

(**A**) The Fab fragment is displayed as a molecular surface. Color coding is as follows: VL (cyan), VH (green), L1 (red), L2 (blue), L3 (orange), H1 (red), H2 (blue), and H3 (orange). GD2 is depicted as capped sticks with carbon, nitrogen and oxygen in yellow, blue and red, respectively.

(**B**) The Fab of 3F8 VL and VH is displayed as a ribbon structure. Selected residues of 3F8 are represented as thick-capped sticks with carbon, nitrogen and oxygen in pink, blue and red, respectively. GD2 is shown as capped sticks, color-coded as in panel A. Significant nonpolar interactions with GD2 are observed for Ile2 (framework), Tyr 92 (L3), Ile 165, Met 173 (H2) and Tyr 211 (H3). Electrostatic interactions with the GD2 molecule are observed for Ser1 (framework), Thr 166, Asn 167 and Ser170 (H2).

(**C**) Detailed view of polar interactions between the 3F8 antibody and the GD2 molecule. The Fab of 3F8 VL and VH is displayed as a ribbon

structure. Selected residues of 3F8 are represented as thick capped sticks with carbon, nitrogen and oxygen in gray, blue and red, respectively. GD2 is shown as capped sticks, color-coded as in panel A. Black dashed lines are H-bonds. Distances are measured between the heavy atoms. Ser1 (framework), Thr 166, Asn 167 and Ser170 (H2) form H-bonds with the GD2 molecule.

(**D**) Hydrophobic interactions between GD2 with the residues of 3F8. These residues are Ile2 (framework), Tyr 92 (L3), Ile 165, Met 173 (H2) and Tyr 211 (H3) are represented as thick-capped sticks with the carbon, nitrogen, oxygen and hydrogen atoms in pink, blue, red and white, respectively. Distances are measured between hydrogen atoms.

The middle NeuAc shows hydrogen-bond interactions with Ser170 on the H2 CDR, whereas the terminal one is largely solvent exposed. The hydroxyl group on the seventh carbon of the terminal NeuAc forms a hydrogen bond with the H2 CDR of 3F8 by way of the backbone carbonyl of Thr166 and the side chain of Asn167. The N-acetyl groups of both Neu5Ac residues make non-polar contacts with Tyr211, Ile165 and Met173 (Figure 2.4D). The calculated binding energy of the 3F8 and GD2 complex was -8.2 kcal/mol (Ki = 0.95 µM).

The bound conformation of GD2 in our docking model is different from the unbound one determined by NMR (RMSD=~3.0 Å excluding the two terminal residues). The GD2/3F8 binding model showed that both NeuNAcs bound into a relatively flat and shallow surface area formed mainly by the residues of H2 CDR loop and a few residues of the H3 CDR loop (Figure 2.4A and 2.4B). This may explain why the middle NeuAc (2-3), instead of the terminal one, is the most prominent residue interacting with 3F8 (Figure 2.3A and 2.3B).

In order to validate the docking binding model, the theoretical STD effect upon some protons was calculated with the CORCEMA-ST program at different saturation times (Appendix I supplemental Table S4 and Methods). Taking into account an estimated experimental error of 10-20% for the STD data, the R-factor (0.42) is indicative of a reasonable fit between the experimental and calculated values. Hence, our binding model is compatible with the experimental STD data.

Together, the STD-NMR epitope mapping of thiophenyl GD2 and ganglioside GD2 with mAb 3F8 and the docking studies of GD2 with 3F8 are consistent, and provide a starting point for designing small molecule ligands of GD2.

Design of peptidic ligands.

Further support for the predicted region of mAb 3F8 that binds to GD2 comes from the fact that peptide ligands could be designed from this region to mimic the antibody binding surface and yield peptides that interact with GD2 micelles. Small peptidic GD2 ligands M1, M50 and SS58 were designed based on models of the monoclonal antibody 3F8/GD2 complex, mainly mimicking the H2 CDR that curiously also corresponds to a sequence in Tenascin-R (accession number NP_003276), which is reported to be a putative GD2 ligand (*61*). A comparison of anti-GD2 mAbs and TN-R sequences showed high sequence homology between the mAb CDRs and the N-terminal portion of TN-R, which is thought to be the GD2-binding site. It is intriguing that this sequence, ASN-TYR-ASN, is very restricted in the mammalian genome and appears in very few proteins.

Core sequences were flanked by cysteine residues, which, once oxidized, form an intra-molecular S-S bond forcing the peptides to adopt the cyclic, β-turn-like conformation seen in CDRs. All peptides were synthesized and tested as control linear analogs devoid of terminal cysteines, to verify the effect of structure on binding. In addition, several

control cyclic peptides of related sequences were inactive. To validate the docking binding model and investigate how these peptide ligands bind to GD2, their interactions were studied by NMR and *in vitro* assays.

Assignments of peptide ligand resonances and structure calculations.

The sequences and complete proton chemical shift assignments for the eleven-residue peptides M50 and SS58 and the ten-residue peptide M1 are provided in Appendix I supplemental Tables 5, and 6. Three-dimensional structures were calculated for M50 and M1 from NMR data. The conformations of these two peptides are relatively flexible in the free state (Appendix I supplemental Table 7). The data show that a random coil is the main secondary structure for M50 (Figure 2.6) and for M1 (Appendix I supplemental Figure S3), with a β-turn as a minor conformation.

Group Epitope Mapping (GEM)-The binding interactions of peptide ligands M50, M1 and SS58 with GD2 micelles.

The ganglioside GD2 concentration (200 μM) in STD NMR experiments exceeded the reported Critical Micelle Concentration (CMC) (*204*), and 1D-^{1}H NMR spectra showed that it formed micelles in water (data not shown). The STD spectrum indicates that the M50 peptide ligand binds to ganglioside GD2 micelles (Figure 2.5A and 2.5B). All of the protons in the M50 peptide experienced some degree of saturation on binding to GD2. Calculation of the STD effects for each resolved proton

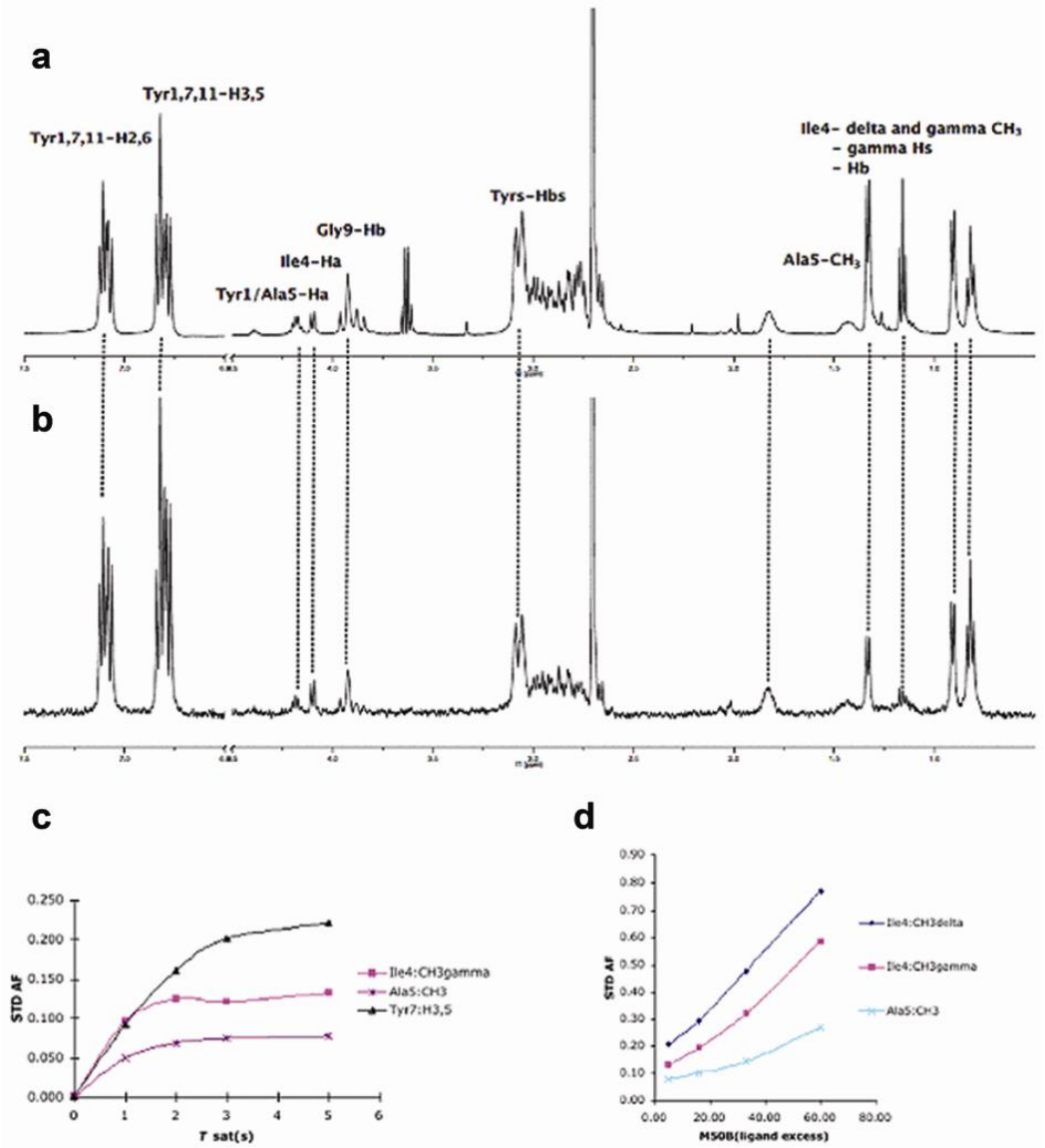

Figure 2.5. STD NMR spectra and STD amplification factor for a mixture of ganglioside GD2 micelles and M50B. (A) Reference spectrum of a mixture of ganglioside GD2 micelles (200 μM) and peptide ligand M50B (1 mM) in a ratio of 1:5. (**B**) STD NMR spectrum of the same sample at 298 K (T_{sat}= 5 s). (**C**) Observed STD amplification factors of several resonances of peptide ligand M50B plotted against the saturation time in a ratio of 1:5 (ligand excess). (**D**) Observed STD amplification factors of several resonances of thiophenyl-GD2 plotted against the ligand concentrations (T_{sat}= 5 s).

signal indicated that the tyrosines and Ile4 made the most important contacts with GD2. The aromatic resonances of Tyr1, 6 and 11 could not be resolved to itemize individual effects; however, the overlapping multiplet structure was very similar in the reference and STD spectra, indicating that each aromatic ring contributed equally to the intensity.

STD experiments were recorded at saturation times varying from 1 to 5s for a five-fold ligand excess, demonstrating that the maximal amplification factor is reached by 3s of saturation for residues with weaker interactions such as alanine (Figure 2.5C). The T1s for the resolved protons in the free peptide were measured using an inversion-recovery pulse sequence, and indicated that at longer relaxation times (> 2s) the STD intensities were dominated by T1 effects. Protons with the longest T1s, such as those in the tyrosine aromatic rings, display the largest STD effect. The initial slope of this plot gives a more accurate reflection of the binding epitope (*202*). Although very short (<1s) saturation time were not employed in this study the relevance of Tyrosines and Isoleucine is indicated from their steeper initial slope in comparison with the resolved glycine or alanine protons. A series of STD titration experiments delivered STD amplifications as a function of ligand excess (Figure 2.5D). This shows that the maximal effect was not reached under the experimental conditions, which were limited by the necessity to maintain a minimum concentration of GD2 ganglioside to ensure micelle formation.

The interactions of two other peptide ligands (M1 and SS58) with ganglioside GD2 micelles were also investigated by STD experiments (see Appendix I supplemental Figure 4 for STD NMR spectra). STD signals of M1 and SS58 show that the ligands bind to the GD2 micelles. As was observed for M50 (Figure 2.5), the tyrosines and the methyl resonances of threonine and isoleucine gave the largest STD effects suggesting that the protein-glycan interactions are dominated by hydrophobic side chains of methyl groups and aromatic rings.

In order to study the conformation of bound ligand, and to complement the STD NMR results, NOESY experiments were recorded for a mixture of M50 and GD2 ganglioside micelles. Many more cross peaks were observed in the NOESY spectrum of the mixture in comparison to NOESY or ROESY spectra of the free peptide (Figure 2.6A). For instance, several cross-peaks between Hα and amide (Gly3 -Ala5, Ile4-Asn6, Ile4-Tyr7, Ala5-Tyr7 and Gly9-Try11) were observed. These transferred NOEs showed that the major conformation of the ligand becomes a β-turn ("W" shape) in the bound state as compared to a more flexible β-coil ("U" shape) in the free state (Figure 2.6B and 2.6C, and Appendix I supplemental Table S7).

Analysis of the average secondary structure of M50 by the software DSSP (*205*) shows that in the bound state there are multiple β-turns with three hydrogen bonds formed, while no hydrogen bonded turns exist in the free state. In the bound state the turns are formed by Cys2 to Ala5, Asn6

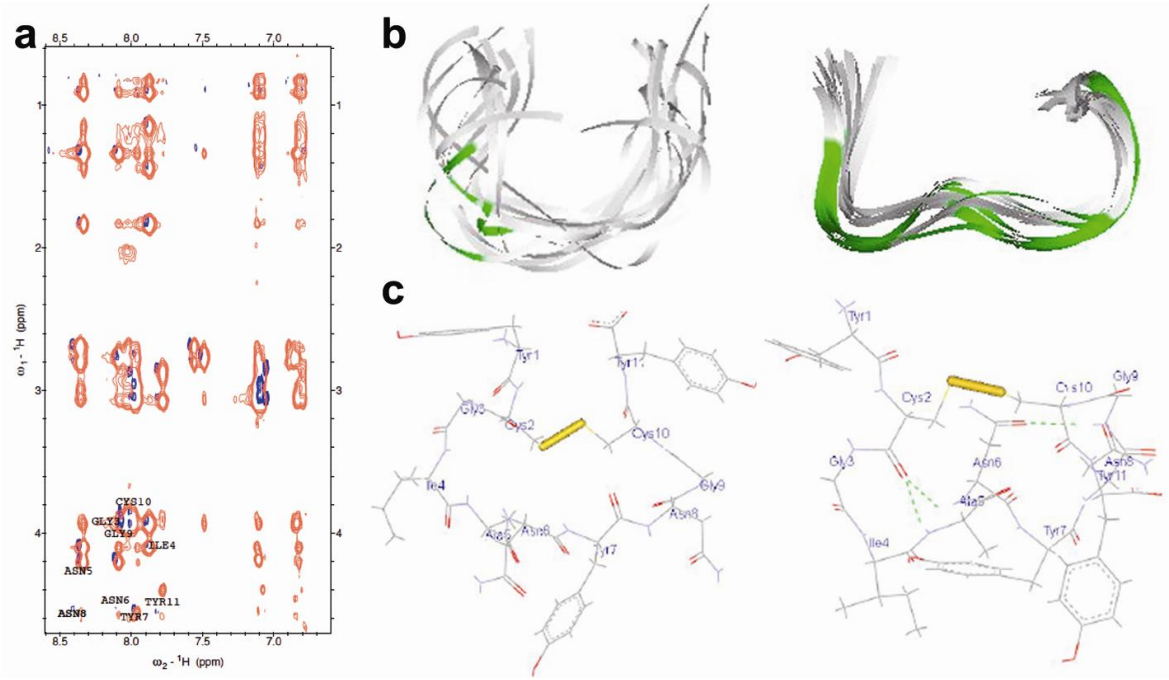

Figure 2.6. Ensemble of 12 and 19 lowest-energy structures calculated for the M50B in the free and bound state in water respectively.

(**A**) Overlay of ROESY spectrum (black) of M50B in the free state and trans-NOESY spectrum (red) of M50B in the bound state. The mixing times used to record these spectra are 200 and 100ms respectively.

(**B**) The ensembles of structures are in flat ribbon representation and the β turn is in green.

(**C**) The average structure is in line representation (water molecules are removed). The disulfide bond is in yellow. Three hydrogen bonds between carbonyl group and amide of Cys2 and Ala5, Cys2 and Asn6 and Asn6 and Gly9 are in green.

to Gly9, and Cys2 to Asn6. In contrast, in the free state the sequence Gly3 to Asn8 forms a more flexible U-shaped β-coil (Figure 2.6B). The RMSD between these different states is 2.7 Å (calculated for residues 2 to 10).

It appears that the STD spectra were influenced by T1 effects at the longer saturation times used in this study, however, the trNOE results for the peptide that show that it adopts a conformation in the presence of GD2 where aromatic and Ile residue side-chains are on the same face of the molecule, directed towards the carbohydrate. Although transferred NOE data was not obtained for the other peptidic ligands M1 and SS58, we anticipate that they might also form a similar β-turn upon binding to GD2 because of their high degree of sequence homology to M50.

Together, these data suggest an induced-fit model in which cyclic peptidic ligands adopt a new β-turn conformation upon interacting with GD2. Such β-turn conformation resembles those adopted by antibody CDRs (*200*).

Assessment of ligand interactions with gangliosides by competitive ELISA.

The binding specificity of M50, M1, and SS58 was evaluated by competitive ELISA using immobilized gangliosides GD2, GD3, or GM1.

M1 inhibits the binding of mAb 3F8 to GD2 in a dose-dependent manner, with an IC_{50} between 100 and 200 μM. M50 inhibits binding of mAb 3F8 to GD2 by 66% at 200 μM (Figure 2.7A).

SS58 inhibits the binding of mAb 3F8 to GD2 by 50% at 350 μM. In control assays, SS58 does not prevent cholera toxin B from binding GM1. The peptide also shows weak inhibition of anti-GD3 antibody binding to GD3 (Figure 2.7B). Thus the SS58 peptide has excellent selectivity for GD2 over GM1, and good selectivity for GD2 over GD3.

It is possible that SS58 binds to both GD2 and GD3. Whether or not SS58 binds specifically to GD3 is a difficult issue to resolve as the peptide has lower affinity and lower avidity than 3F8. As well, the peptide represents only a selected part of the pharmacophore of 3F8 and some of the 3F8 specificity may have been compromised. GD2 and GD3 have very similar chemical structures; the only difference being that GD2 has an N-acetyl-galactose connecting to the galactose (Appendix I Figure S2). For these three reasons, especially the closeness of the epitopes of GD2 and GD3, it is not surprising that the peptide could bind to GD3 with low efficacy in the ELISA competition assays.

More than 50 control peptides were tested in parallel, including linear analogs of the active cyclic peptides, and several inactive cyclic peptides of related sequences. For example, control peptide 57 (a linear and unstructured analog, see Methods) did not block GD2-3F8 interactions (data not shown), suggesting that a constraint to induce a β-turn is required; and cyclic peptide NB1.HC1.7 (YCTNYGVCY) derived from a different domain of 3F8 did not inhibit the binding in the ELISA.

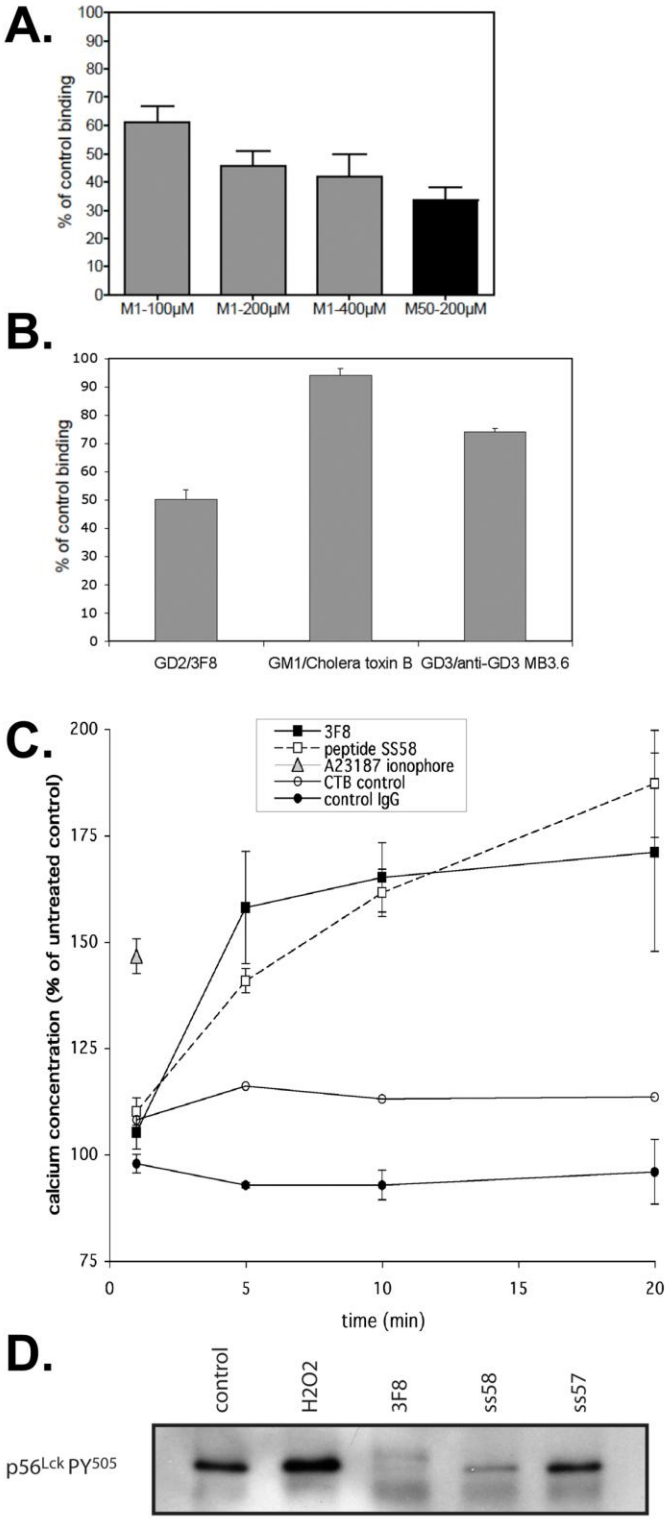
A.
% of control binding
M1-100μM
M1-200μM
M1-400μM
M50-200μM
B.
% of control binding
GD2/3F8
GM1/Cholera toxin B
GD3/anti-GD3 MB3.6
C.
3F8
peptide SS58
A23187 ionophore
CTB control
control IgG
calcium concentration (% of untreated control)
time (min)
D.
control
H2O2
3F8
ss58
ss57
p56Lck PY505

Figure 2.7. Peptide ligands M1, M50 and SS58 selectively bind to ganglioside GD2.

(**A**) Binding of peptides M1 and M50 to GD2 was evaluated by their ability to compete anti-GD2 mAb 3F8 binding to immobilized GD2. M1 and M50 strongly inhibit GD2/3F8 interaction. Shown are the averages ± SEM of 4-6 independent assays, n=3 per assay. (**B)** The selective binding of peptide SS58 to GD2 ganglioside was evaluated by its ability to compete anti-GD2 mAb 3F8, but not anti-GD3 mAb MB3.6 binding to immobilized GD3, or cholera toxin B binding to immobilized GM1. Shown are averages ± SEM of 2 independent assays, n= 4 per assay.

(**C**) Peptide SS58 increases intracellular calcium. Live EL4 cells (expressing GD2 and GM1) were treated with mAb 3F8 (13 nM), control mouse IgG (mIg), peptide SS58 (20 μM), the GM1 ligand CTB or the calcium ionophore A23187; and intracellular calcium concentrations were evaluated over time by flow cytometry using the calcium-sensitive fluorophore Rhod-2 AM. Shown are averages of 4 independent assays ± SEM. (**D**) EL4 cells were treated with control mIgG (13 nM, lane 1), hydrogen peroxide (H_2O_2, 20 mM, lane 2), anti GD2 mAb 3F8 (13 nM, lane 3) or peptides SS58 (3.3 μM, lane 4) or peptide SS57 (3.3 μM, lane 5) for 20 minutes at 37˚C. The $p56^{Lck}$ immunoprecipitated samples were probed for Tyr^{505} $p56^{Lck}$ using a specific anti-pY^{505} antibody. The blot shown is representative of 4 independent experiments.

Overall the data are consistent with the binding detected by NMR, and with the interpretation that the peptide ligands bind the carbohydrate of GD2.

Functional mimicry of mAb 3F8.

Binding of ganglioside ligands (such as antibodies) to cell surface gangliosides induces Ca^{++} fluxe (*194, 195*) measurable by the calcium sensitive fluorophore Rhod-2 AM. The Ca^{++} fluxe involve the activation of the Src family kinases (*13, 193, 195*).

We studied intracellular Ca^{++} levels and activation of the Src family kinase $p56^{LCK}$ in the EL4 thymoma cell line, which expresses GD2 and GM1, but does not express GD3 on the plasma membrane. Exposure of EL4 cells to positive control mAb 3F8 (13 nM) increased intracellular Ca^{++}. Negative controls (untreated cells or cells treated with non-binding mouse IgG) do not affect Ca^{++} levels, and the positive control ionophore increases intracellular Ca^{++} levels rapidly. This is consistent with the literature (*195*). Test treatment with SS58 (20 μM) strongly increases the intracellular Ca^{++}, although the effect is slower than that of mAb 3F8 (Figure 2.7C). The increased intracellular Ca^{++} caused by both mAb 3F8 and SS58 can be blocked by a Src -inhibitor PP1 (data not shown).

In biochemical assays, exposure of EL4 cells to positive control mAb 3F8 or to test SS58 peptide reduced the phosphorylated state of $p56^{LCK}$-$pTyr^{505}$. The negative control linear analog SS57 does not induce $p56^{LCK}$-$pTyr^{505}$ de-phosphorylation; whereas the positive control phosphatase

inhibitor H_2O_2 increases the phosphorylated state of $p56^{LCK}$-$pTyr^{505}$ (Figure 2.7D). These results are consistent with the above studies of Ca^{++} fluxe. The $p56^{LCK}$-$pTyr^{505}$ is an inhibitory phosphotyrosine, and its de-phosphorylation is required for activation of the kinase enzymatic activity of $p56^{LCK}$, leading to Ca^{++} fluxe (*206*). In further control assays, treatment of a GD2-negative subclone of EL4 cells with peptide SS58 did not activate $p56^{Lck}$, even though these cells express the same levels of $p56^{Lck}$ as the parental GD2 cells (data not shown).

Together the data show that functionally these small peptidic ligands of GD2 activate signalling pathways in live cells in a manner similar to mAb 3F8.

Significance

In this study, the combined use of STD NMR spectroscopy, transferred NOE experiments, and molecular modeling furnished details on the molecular recognition of the ganglioside GD2 by the monoclonal antibody 3F8; specifically details of conformational changes in the antibody CDR loops. Moreover, similar NMR experiments were performed on complexes between GD2 and three small peptide ligands, which were designed using the structural information and which were validated in binding and functional studies.

The present work reveals the key pharmacophoric groups that are required for the recognition of the cell surface carbohydrate epitope recognized by the mAb 3F8 and suggests an induced-fit mechanism

through which unstructured antibody CDRs may adopt a -turn conformation upon interacting with GD2.

Our work furthers the concept that it is possible to develop small molecule ligands of highly flexible targets such as ganglioside carbohydrates, and rationalizes that gangliosides may be druggable targets. The structural information gleaned from studying the protein/ and peptide/carbohydrate interactions has enhanced understanding of ganglioside-ligand interactions and may facilitate design of improved GD2 ligands, and ligands for other gangliosides.

Experimental procedures

Synthesis of thiophenyl GD2.

Thiophenyl GD3 was synthesized from thiophenyl Lac as described (*35*). Thiophenyl GD2 (Figure 2.1A) was synthesized from thiophenyl GD3 using a recombinant β-1,4-*N*-acetylgalactosaminyltransferase (CgtA, construct CJL-30) and an UDP-GlcNAc 4-epimerase (Gne, construct CPG-13) originally cloned from *Campylobacter jejuni* (*26, 207*). The sample was purified (>98%) by HPLC (Waters 600) using a C-18 semipreparative column (Phenomenex), and was verified by mass spectrometry (ESI-MS) and NMR. The measured molecular weight of thiophenyl GD2 corresponded to expected values.

Peptide ligand synthesis.

Peptides were designed based on the structures of mAb 3F8 and Tenascin-R. Peptide ss58 is YCGGIANYNCY, peptide M1 is YCGTNYNGCY, and peptide M50 is YCGIANYNGCY. Peptide SS57 is a linear analog which can not cyclize, with sequence GGIANYNTS. Peptides were synthesized with an Advanced Chemtech automatic synthesizer using solid-phase Fmoc chemistry. After cleavage from resin and side-chain deprotection, peptides were subjected to cyclization by oxidation (which caused disulfide-bond formation) at 4°C under O_2 in 50 mM ammonium bicarbonate, pH 8.5. Cyclic peptides were re-purified (>95%) by HPLC (Varian) using a C-18 preparative column (Phenomenex), and were characterized by mass spectrometry and NMR spectroscopy. The measured molecular weight of linear and cyclic peptides corresponded to expected values.

Quantification of thiophenyl GD2–3F8 mAb interactions by competitive ELISA.

Gangliosides GD2 or GD3 (Advanced ImmunoChemical Inc.)(10 ng/well, in ethanol) were immobilized onto polystyrene Corning Strip Well 96-well plates (Fisher Scientific) by evaporation in a fume hood for 2 hours. The wells were then filled with phosphate buffered saline containing 0.5% bovine serum albumin (PBS-0.5% BSA) for one hour. In competition assays, increasing concentrations of soluble ganglioside, dissolved in PBS, were added to the plates for 30 minutes before adding the mAbs. Then,

anti-GD2 monoclonal antibody 3F8 (5 ng/well) (prepared and characterized in house (*208*)) or anti-GD3 monoclonal antibody R24 (15 ng/well) (Abcam) was added for 15 min. The plates were washed three times with PBS-0.5% BSA and incubated 20 minutes with 1/1000 dilution of horseradish peroxidase (HRP)-conjugated anti-mouse antibody (Sigma). After three washes with PBS-0.5% BSA and two with PBS, the colorimetric substrate TMB One Solution (Promega) was added, and the reaction stopped with 0.5 N H_2SO_4 and the plates were read at 450 nm (Benchmark Plus, Bio-Rad). Wells with no mAb added were treated as background and standardized as 0% binding. Wells with no competitor ganglioside added were standardized as 100% binding.

NMR spectroscopy.

All NMR experiments were carried out on a 500 MHz Varian INOVA NMR spectrometer equipped with a triple resonance H {CN} cold probe and z-axis pulsed field gradients. 2D NMR spectra were processed by NMRPipe (*209*) and assigned by SPARKY 3 (T. D. Goddard and D. G. Kneller, University of California, San Francisco).

NMR spectroscopy of ganglioside GD2 and thiophenyl GD2. Mixed micelles were prepared by dissolving ganglioside GD2 (1 mM) and the detergent dodecylphosphocholine-d38 (DPC, molar ratio 1:40) in deuterated 50 mM phosphate buffer (pD 6.6) (*33*). Thiophenyl GD2 was dissolved in deuterated 50 mM phosphate buffer. Spectra were obtained at 308 K or 298 K, respectively. ^{1}H-^{1}H gradient-selected COSY spectra,

DQF-COSY, TOCSY, ROESY with 200 ms, NOESY spectra with mixing times of 50-200 ms, ^{13}C HMBC and HSQC spectra were recorded. ^{1}H chemical shifts were referred to an internal sodium 2,2-dimethyl-2-silapentane-5-sulfonate standard (DSS) at 0.00 ppm. ^{13}C chemical shifts were indirectly referenced to the proton frequency (see additional details in the Supplemental Methods).

NMR spectroscopy of peptide ligands. Samples contained M1, M50 or SS58 in 10% D_2O/90% H_2O (v/v) or 100% D_2O at pH 6.0 or 3.0, at 298 K. Standard experimental protocols were used for TOCSY, phase-sensitive double quantum filtered-COSY, COSY-30, NOESY and ROESY spectra.

STD NMR spectroscopy.

A 1D saturation transfer difference pulse sequence with internal subtraction via phase cycling was employed to record difference spectra (*210*). On-resonance irradiation of GD2 gangliosides and mAb 3F8 was performed at 0 ppm, except in the case of GD2-DPC micelles, where on resonance irradiation of the antibody was at -2 ppm. Off-resonance irradiation was at 34.8 ppm. Reference spectra were recorded using the same pulse sequence with saturation pulses applied at 34.8 ppm, and no internal subtraction. Experiments were recorded with saturation times of 5 s, 3 s, 2 s and 1 s. Spectra were recorded with 32000 points, a sweep width of 16 ppm, and 1024 to 2048 transients (see additional details in the Supplemental Methods). STD spectra were processed by MestReNova-

Lite v5.2.1-3586 (Mestrelab Research SL). To test the shaped pulse selectivity, STD experiments on thiophenyl-GD2, M50B, M1 and GD2 in DPC micelles alone without antibody were acquired. No ligand signals were present in the STD spectra for thiophenyl-GD2, M50B, and M1. However, there is a non-specific signal of methyl groups for GD2 in DPC micelles. Inversion-recovery experiments to measure longitudinal relaxation times (T1) for free thiophenyl-GD2 and M50 were acquired. For the titration and saturation experiments, we used the STD amplification factor (*210*) for a better assessment of the absolute magnitude of the STD effect. After the STD NMR experiments, transient transferred NOE experiments employing different mixing times were performed.

Sample preparation for thiophenyl GD2 and mAb 3F8/Ganglioside GD2 in DPC and mAb 3F8 interactions. 3F8 was concentrated using Amicon centrifugal filters (10 kDa cutoff, Millipore) and exchanged several times with a deuterated 50 mM phosphate buffer (pH 6.0). The mAb preparations were combined with freeze-dried thiophenyl GD2 or ganglioside GD2 in DPC (CDN Isotopes) micelles at molar ratios ranging from 1:25 to 1:200; the final oligosaccharide concentrations were between 0.125 and 1 mM. Difference spectra were recorded for ligand in the absence of binding partner to confirm that the ligand was not excited by the saturation pulses at 0 ppm.

Sample preparation for peptide ligands bound to ganglioside GD2 micelles. The ganglioside GD2 was subjected to three cycles of freeze-

drying with D_2O to remove traces of water and to prepare a stock solution with a final concentration of 3 mM in deuterated 50 mM phosphate buffer, pH 6.2. Dilution effects from addition of this GD2 stock solution to peptide ligands solution to make different ratios were minimal. Stock solutions of peptide ligands, 2 to 3 mM each, were prepared by dissolving them in deuterated 50 mM phosphate buffer. The concentrations of the peptides were determined by UV (Nano-drop 1000, Wilmington) at 280 nM. 1D STD NMR spectra were acquired at 298 K for a variety of peptide to GD2 ratios.

Structure calculations.

Different mixing times of NOESY spectra were used to evaluate the linear build-up of NOEs. Molecular dynamics simulations with NMR refinement in the AMBER 9 GB Model (*211*) with the force field (Glycam_04.dat (*212*) and GAFF (*213*)) were employed to determine the energetically favorable conformations of the two types of unbound ganglioside. The topology file of truncated ceramide was produced by ANTECHAMBER (*214*). 3D structures of peptide ligands were calculated by the software ARIA 2.2/CNS 1.2 with the network anchoring approach (*215*). From the 200 structures calculated for each peptide, the 20 lowest energy ones were chosen and clustered by MMTSB (*216*). Structures were visualized using Discovery Studio 1.7 (Accelrys), PyMOL and VMD-Xplor on Mac OS X (see additional details in the Supplemental Methods).

Docking studies.

Structure prediction, model building and refinement. The crystal structure of malaria antigen AMA1 antibody Fab (pdb code 2q8a) (*217*) and 13G5 antibody Fab (pdb code 2gjz) (*218*) were selected as templates for the light chain (84%) and heavy chain (84%) of 3F8 respectively. The homology modeling was carried out using the program COMPOSER in SYBYL 7.3 (Tripos). Structural refinement of the complex was done by stepwise energy minimization in Sybyl using the AMBER all atom force field to a gradient of 0.05 kcal/mol/Å. This energy-minimized model was then used as starting point for MD simulation in explicit water, using the AMBER ff03 force field in the AMBER 9. The MD average structure was obtained from the most stable part of the trajectory for docking study (see additional details in Supplemental Methods and Supplemental Figures S5 and S6).

Molecular docking of GD2 and CORCEMA-ST calculations. The GD2 docking in the putative binding site of Fab fragment of 3F8 was performed with in-house docking software (manuscript in preparation). A box around the 6 CDRs of the heavy and light chain of 3F8 was constructed and defined the binding region to be searched. In order to sample various conformations, 12000 conformers of GD2 were generated from snapshots taken from an MD simulation (12-ns) in explicit water using AMBER ff03 and GAFF force fields starting from the NMR structures. Partial charges of the conformers were calculated by the AM1-BCC

method (*219*). Each of the docked conformers of GD2 was exhaustively docked into the 3F8 Fab and scored. The top-scoring 100 poses were clustered. The most populated cluster was taken to be representative of the true GD2 binding mode in the Fab of 3F8 antibody. The best-scored pose from this cluster was selected to represent the binding model. This pose was subjected to minimization followed by a 5-ns MD simulation. The MD trajectory was used to calculate a predicted binding free energy of the complex using a Solvated Interaction Energy (SIE) approach (*220*). Then, CORCEMA-ST (*221*) program was used to calculate theoretical STD effects (see additional details in the Supplemental Methods).

Detection of peptide-ganglioside interaction by competitive ELISA.

ELISAs were as described above, except that cyclic or linear peptides (50 µg/well, in PBS) were added to the wells as putative competitors for 1 hour before anti-ganglioside antibodies or anti-GM1 cholera toxin-B (CTB). Selectivity of competitive inhibition of GD2-3F8 interactions was determined by monitoring the effect upon GM1-CTB and GD3-anti-GD3 interactions. Wells with no peptide added or control irrelevant peptide added were standardized as 100% binding. Wells with no 3F8 added and also wells where 3F8 was replaced with mouse IgG were standardized as 0% binding.

Intracellular calcium studies.

GD2-expressing EL4 thymoma cells (1 x 10^6 per sample) were washed with Ringer's solution (155 mM NaCl, 4.5 mM KCl, 2 mM $CaCl_2$, 1 mM

$MgCl_2$, 10 mM D-glucose, 5 mM HEPES) and resuspended in 1 ml Ringer's for 15 minutes at 37°C. Then 5 μM Rhod-2AM (Molecular Probes) was then added to the cells and incubated for 30 minutes at room temperature with mild agitation. Cells were washed, and resuspended in 1 ml Ringer's and incubated for 30 minutes, after which cells were stimulated with the indicated ganglioside ligands (or calcium ionophore A23187 as control) and analyzed over a 30-minute period for intracellular Ca2+ using a flow cytometer (Becton-Dickinson).

Ex vivo T-cell receptor activation.

EL4 thymoma cells (5×10^6 per sample) in culture media were treated with control mouse IgG (13 nM), mAb 3F8 (13 nM), peptides 57 and 58 (3.3 μM) or hydrogen peroxide (20 mM) for 20 minutes at 37°C. After lysis in mild lysis buffer (10 mM CHAPS, 0.15 M NaCl, 0.01 M sodium phosphate pH 7.2, 2 mM EDTA, 50 mM sodium fluoride, EDTA-free protease inhibitor cocktail (Roche)) p56Lck protein was immunoprecipitated with protein A-agarose beads (Upstate Biotechnology) coated with anti-$p56^{Lck}$ mAb 3A5 (Santa Cruz) and samples were probed in Western blots for Tyr505 $p56^{Lck}$ using rabbit anti-PY505 antibody (Abcam).

Supporting data

Appendix I includes 7 Figures, 7 Tables, and extended Methods and references.

Acknowledgements

Supported by the Canadian Institutes of Health Research (MOP77577 to WDL; MOP192060 to HUS; and MOP-81277 to KG). NMR experiments were recorded at the Québec/Eastern Canada High Field NMR Facility, supported by grants from the Canada Foundation for Innovation, the Natural Sciences and Engineering Research Council of Canada, and the Fonds de la recherché en santé du Québec (FRSQ). WYT received a scholarship from the FRSQ and from the Montreal Center for Experimental Therapeutics in Cancer. We thank Dr. Warren Wakarchouk (IBS-NRCC) and Marie-France Karwaski (IBS-NRCC) for the synthesis of thiophenyl-GD3 and thiophenyl-GD2, and Dr. Teresa Lama (Mimetogen Pharmaceuticals) for peptide synthesis.

Connecting text between Chapter 2 and Chapter 3

In the last chapter, the conformations of GD2 and interactions between GD2 and its monoclonal antibody were studied by 2D and STD NMR experiments for the first time (Figure 2.2 and 2.3). A 3D binding (Figure 2.4) model was built up based on this structural information. GD2 peptides were designed to validate the binding model. ELISA and STD NMR experiments showed that these peptides specifically bind to GD2 (Figure 2.7), and when a GD2 peptide binds to GD2, its conformation is via an induced-fit mechanism (Figure 2.6). Further, these ligands also demonstrate the similar biological functions with the mAb 3F8 in cell-based assays of calcium fluxe and Src-activation in EL4 lymphomas cells (Figure 2.7). Therefore, our binding model is reasonable.

In fact, chapter 2 already includes the background and most results about peptides ligands for chapter 3, such as the first generation ligand SS58 developed by Dr. Gagnon and the second generation of ligand M1 and M50 developed by Mimetogen Pharmaceuticals. In chapter 3, we wonder whether we can improve the affinity, stability and solubility of current ligands since the binding model is available.

Chapter 3

GD2 peptide ligands

Abstract

The peptides binding to GD2, reported in Chapter 2, were redesigned to make improvements to their binding and/or physicochemical properties. While the affinity of these ligands was improved ~2-fold, the solubility was reduced. Moreover, although the parental peptides (*36*) and the new peptides can induce calcium influx after binding to cell surface GD2, they do not kill GD2 expressing tumor cells *in vitro* (Dr. Martin Gagnon, unpublished data) or *in vivo* (Dr. Karen Meerovitch, unpublished data). Therefore, GD2-binding peptides do not have therapeutic effects. These peptides were, therefore, abandoned as a lead.

Introduction

The first generation of GD2-binding peptide ligand SS58 is not very soluble in water (128 μg/mL). The solubility of the second generation, M1 and M50, are improved (1100 μg/mL in water), but the affinity is similar to SS58. Here, structure-based design was done to further improve the binding of peptides to ganglioside GD2.

Result

The second generation of GD2 peptide ligand design.

It is known that the heavy chains 2 and 3 (H2 and H3) of the CDR is the main part of antibody interaction with the sugar head of ganglioside GD2 (Figure 2.4, Chapter 2). Based on the binding site of 3F8/GD2 as well as the sequence of Tenascin-R and peptide ligands, fourteen peptides (Table 3.1) were designed to keep the core sequence of ASN-TYR-ASN (NYN). Compared with SS58, M1 and M50, most sequence changes involved changing or adding various amino acids C-terminal to the core sequence of NYN.

Assessment of ligand interactions with gangliosides by competitive ELISA.

The binding specificity of 14 peptides was evaluated by competitive ELISA using immobilized ganglioside GD2 (Figure 3.1). As can be seen, the cyclic peptide WT_4 have a similar binding profile to SS58 (Figure 3.1A), but its solubility is much more improved (1350 μg/mL in water) since the newly designed peptide can be dissolved in an aqueous buffer for assays. One linear peptide, WT_1, demonstrated higher affinity than SS58, but it is not soluble in water (Figure 3.1B). Moreover, WT_1, like SS58, is hydrophobic and needs to be dissolved in DMSO as a stock solution.

GD2 Peptide ligands increase intracellular calcium.

The kinetics of Ca^{++} fluxe was studied in SH-SY5Y-TrkB cells. WT_4, like mAb 3F8, and SS58, can significantly increase the intracellular calcium concentration in SY5Y-trkB neuroblastom cells (Figure 3.2, also see chapter 2 figure 2.7 and chapter 5 figures 2.3).

Table 3.1. Sequences of peptide ligands

Peptides	**Sequence**					
Cyclic						
SS58	YC	GG	IA	NYN		CY
M1	YC	G	T	NYN	**G**	CY
M50	YC	G	IA	NYN	**G**	CY
Linear						
WT_1		GG	IT	NYN	**SAFM**	S
WT_2		GG	T	NYN	**QKFK**	K
WT_3		GG	IA	NYN	**TSSK**	E
Cyclic						
WT_4	YC	GG	IT	NYN	**S**	CY
WT_5	YC	G	IA	NYN	**TSSK**	CY
WT_6	YC	G	T	NYN	**SAFMS**	CY
WT_7	YC	G	T	NYN	**SAFA**	CY
WT_8	YC	G	T	NYN	**SAFL**	CY
WT_9	YC	G	T	NYN	**SMS**	CY
WT_10	YC	GG	IA	NYN	**SMS**	CY
WT_11	YC	G	T	NYN	**SA**	CF
WT_12	YC	G	T	NYN	**SL**	CF
WT_13			IT	NYN	**CSAFM**	CS
WT_14			IT	NYN	**CTSSK**	CE

In bold are major modifications to SS58.

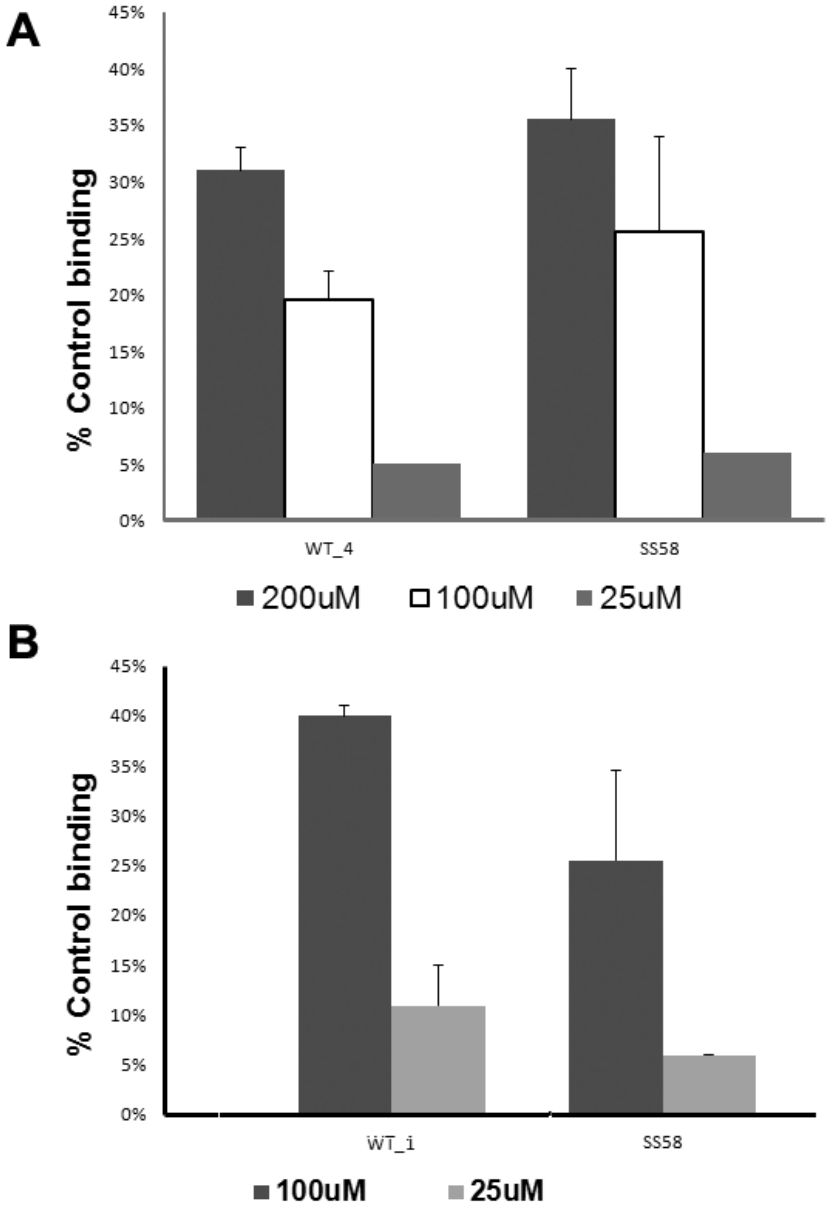

Figure 3.1. Peptide ligands WT_4 and WT_1 selectively bind to ganglioside GD2. Binding of peptides WT_1 and WT_4 was evaluated by their ability to compete anti-GD2 mAb 3F8 binding to immobilized GD2. Shown are the averages ± SEM of 3-4 independent assays, n=3 per assay.

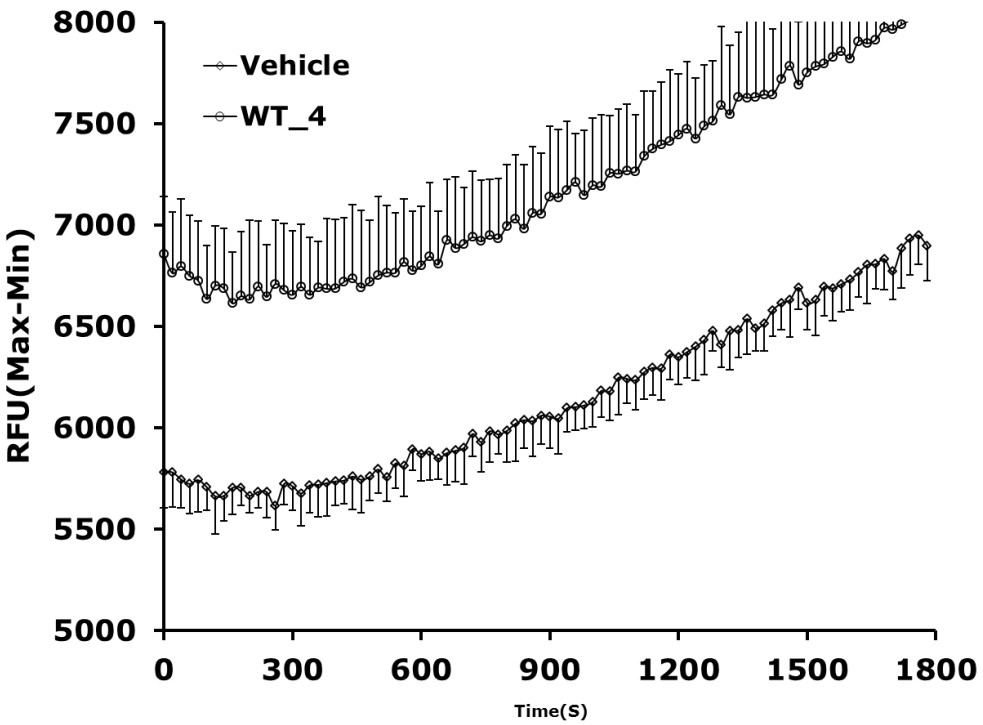

Figure 3.2. Calcium fluxe induced by WT_4. SH-SY5Y-TrkB cells were loaded with Fluo-8NW dye solution, and were then treated with WT_4 (25 μM). A negative control was also tested. For Ca++ assays, the data are a representative result of two independent experiments each done in quadruplicate ± SD.

***In vitro* and *in vivo* studies on GD2 peptide ligands.**

The cell killing efficacy of GD2 peptide ligands was further evaluated in vitro by MTT assays. SS58, M1 and M50 did not show any significant cytotoxic effect on EL4-GD2 lymphomas cells (Dr. Martin Gangon, unpublished data). Moreover, these ligands could not inhibit growth of GD2-expressing tumors in mice (Dr. Karen Meerovitch, unpublished data by Mimetogen Pharmaceuticals).

Discussion and conclusion

Fourteen redesigned peptides were produced with the aim to improve binding to GD2, and cytotoxic activity. Although these GD2 ligands can affect some cell functions such as calcium influx, they did not show cytotoxic effects.

The modification of the sequence of the C-terminal part of peptide seems to be helpful to increase the solubility or binding respectively. However, there might be a balance between affinity and solubility. The increase of hydrophobicity of a peptide ligand results in more binding to ganglioside GD2 (WT_1 *vs*. WT_4).

Peptide WT_4, like SS58, can bind to ganglioside GD2 with similar affinity and further induce calcium influx. Since SS58, M1 and M50 did not work in vivo, evaluation of the redesigned peptides in vivo was not done. However, these peptides are first artificial ligands to show direct

interacting with glycolipid; they might still be valuable for studying the glycolipid-modulated signaling transduction (See chapter 5).

Methods

Peptide syntheses, competitive ELISA and Calcium assay are described in the Chapter 2 and Chapter 5 respectively.

Connecting text between Chapter 2, 3 and Chapter 4

As was shown in chapter 3, the first generation and second-generation peptide ligands of GD2 have problems such as solubility and lack of efficacy in vivo. However, the target GD2 is clearly valid; therefore we decided to develop a GD2-based cancer vaccine. For that purpose, we used the chemical biology information from Chapter 2. We also worked out a set of criteria that would circumvent the problems of other ganglioside vaccines, such as GD2-KLH vaccine, mentioned in the Introduction (Chapter 1).

It has been known that the GD2s are clustered in the lipid raft as a functional molecule. So we think that multivalent carbohydrate clusters might be more effective for stimulating an active immune response. Scaffolds such as “tree-like” branched structures called dendrimes are used for the multivalent presentation of carbohydrates (*222, 223*). Multiagency would better mimic the rafted carbohydrate aggregated on the tumor cell.

Three findings from Chapter 2 helped us to develop a novel GD2 carbohydrate cluster that resembles the GD2 clusters in a lipid raft. First, the synthetic method of GD2 analogue like thiophenyl GD2 for NMR studies makes it possible to design a homogenous and immunogenic GD2. Second, the presentation of the correct ganglioside structure to the immune system might result in humoral responses with the desired

selectivity. The NMR studies on the conformations of GD2 and interactions between GD2 and its monoclonal antibody demonstrated that GD2 conformation is relatively rigid and adopts the similar conformations in different chemical environments, even when it binds to the mAb 3F8. The middle neuraminic acid is the major residue interacting with the antibody (Figure 2.3). The clinically relevant mAb 3F8 bound ganglioside GD2 and thiophenyl-GD2 these structures in very similar ways. Thus, these kinds of GD2 analogues are suitable for recognition by the humoral immune system. The analogues mimic the carbohydrate with ceramide mimics, but do not contain lipid tails. Third, it has been observed that GD2 peptide ligands interact with GD2 micelles in STD-NMR experiments. In the following chapter, design, synthesis and validation of the immunogenic and the anti-tumoral properties of a tetra-GD2 dendrimer were investigated.

Chapter 4

A synthetic GD2 carbohydrate tetramer vaccine elicits tumor-killing antibodies and is therapeutic against GD2$^+$ tumors

Wenyong Tong[§,†], Michel Gilbert[‡], Anna-Maria Cunningham[‡], Yogesh Bramhecha [§, †], Gloria To[§], William D. Lubell [Ω], and H. Uri Saragovi [§,†,¶, *]

McGill University, [§]Lady Davis Institute-Jewish General Hospital,. [†]Pharmacology and Therapeutics, [¶]Oncology and the Cancer Center, Montréal, Quebec, Canada, H3T 1E2

[‡] Institute for Biological Sciences, National Research Council Canada, Ottawa, K1A 0R6.

[Ω] University of Montreal, Chemistry, Montréal, Quebec, Canada, H3T 1N8.

* Corresponding author

Lady Davis Institute-Jewish General Hospital

3755 Cote St. Catherine, E-535

Montreal, Quebec, CANADA H3T 1E2

Phone: (514) 340-8222 x 5055

FAX: (514) 340-7502

Email: uri.saragovi@mcgill.ca

Abstract

Gangliosides are neuraminic acid-containing glycosphingolipids that accumulate in plasma membrane rafts. Complex gangliosides such as GD2 and GD3 are validated tumor markers, and are targets for passive immunization using monoclonal antibodies (mAbs). We sought to develop a vaccine, but carbohydrates are notoriously poor immunogens. An approach is reported for eliciting selective immunity to GD2, by presenting this carbohydrate antigen in a dendrimeric form. Efficient biosynthesis and chemical conjugation of GD2 provided a dendrimer which retains the structural features of the natural ganglioside, and also forms of a raft-like carbohydrate aggregate. Immunization of mice with the dendrimer elicited a potent anti-GD2 humoral response. Antibodies were highly selective for GD2 as well as the structurally related GD3, but they do not bind other gangliosides. The antisera kill GD2-expressing cells in culture, in the absence of complement. In a prophylactic paradigm *in vivo*, vaccination before tumor challenge delayed the growth of syngeneic tumors. In a therapeutic paradigm *in vivo*, vaccination after tumor challenge was effective at delaying the growth of established syngeneic tumors, and prevented metastasis. This carbohydrate-dendrimer approach has provided an effective anti-tumor ganglioside vaccine, and may be elaborated to target other tumor-associated glycolipids.

Introduction

Gangliosides are neuraminic acid-containing glycosphingolipds, present in cell plasma membranes. Some gangliosides such as GD2 and GD3, derived from the b-pathway of biosynthesis in the Golgi apparatus, are prevalent tumor makers in neuroblastoma, melanoma, small cell lung cancer and glioma. Indeed, GD2 and GD3 are validated clinical targets. Partial therapy can be achieved with passive immunity by administering purified anti-GD2 (*106, 109, 112*) (*97*) or anti-GD3 monoclonal antibodies (mAbs) (*125-129*). However, the cost of passive immunity is high, the side effects are significant, and the efficacy is limited (*104*). As an alternative, many groups have pursued active immunotherapy (*8*).

In one example, GD2 lactone when chemically conjugated to keyhole limpet hemocyanin (KLH) is immunogenic, and can induce antibodies that delay tumor growth in mice (*150, 151, 160*). The antibodies induced by this vaccine act through a complement-dependent cytotoxicity (CDC) mechanism (*150, 151*). However, a bottleneck for developing a safe cancer vaccine is access to the GD2 antigen itself, because natural sources of gangliosides are limited, and chemical synthesis of complex glycolipids is difficult. Moreover, the KLH-ganglioside conjugation yields chemically heterogeneous products (*8, 137*), which is a serious drawback for clinical development. Ganglioside conjugates have shown poor immunogenicity and generally elicit a low and transient anti-ganglioside

antibody response (*161*). Even the most immunogenic ganglioside, a GM2-KLH vaccine did not provide clinical benefits (*152*).

In other examples, there are GD2-peptide mimotopes (*183-186*), GD2-mimicking peptides (*155, 156*), and GD2 mimotope DNA vaccines (*157*) that can induce cross-reactive immunity to GD2. However, immune responses are not very effective at protecting the host when challenged with ganglioside-expressing tumors in therapeutic paradigms (*184*).

Previously, we developed the chemoenzymatic synthesis of ganglio-oligosaccharides as a feasible alternative for their large scale production (*24-27*). In addition, we identified structural features of GD2 and of GD2-antibody interactions (*36*) that provided valuable insight into the appropriate presentation of GD2 as an antigen. With the synthetic method and structural information in hand, we sought to design homogenous GD2 glyconjugates that are immunogenic, for examination as vaccines in tumor-therapy paradigms.

Here, we report the design and characterization of a novel GD2 dendrimer which is effective as a cancer vaccine. A water-soluble amino phenyl ether-analog of GD2 carbohydrate, lacking the lipophilic ceramide and lipids, was synthesized and conjugated to a tetrameric dendrimer (hereafter “tetra-GD2”). Tetra-GD2 conserves native structural features such as the β-linkages of GD2. A tetra-GD2 vaccine elicited antibodies that bind to both GD2 and the highly related carbohydrate GD3, but not any other ganglioside. The antibodies were cytotoxic, in the absence of

complement. The tetra-GD2 vaccine delayed the growth and metastasis of $GD2^+$ tumors in syngeneic C57BL/6 mice, in prophylactic and in therapeutic paradigms. This work demonstrates an effective anti-ganglioside tumor vaccine, and the approach can be expanded to target other tumor-associated glycolipids.

Results and Discussion

Design and synthesis of GD2 dendrimers.

An amino phenyl ether-GD2 (AP-GD2) was produced, in which the ceramide and lipid moieties of gangliosides (**Figure 4.1A**) are replaced with an amino phenyl group (**Figure 4.1B**). The chemoenzymatic synthesis of AP-GD2 had a yield of ~90% pure material.

In gangliosides, the bond of ceramide to the first sugar is naturally in the β-configuration, and we have shown that this bond is critical for displaying a proper antigenic structure to the immune system (*36*). Thus, in the AP-GD2 analog the bond to the phenyl group was installed in the β-configuration, and it was verified as previously described by NMR spectroscopy (*36*).

For conjugation to a tetrameric PAMAM G0 linker, AP-GD2 was converted to its corresponding isothiocyanatophenyl GD2 (**Figure 4.2**). The isothiocyanatophenyl GD2 was then coupled to an amine-terminated tetravalent PAMAM dendritic core. The tetrameric product (**Figure 4.2**) was verified by 1D-^{1}H-NMR. The spectra indicated a 40:36:8 ratio of the amide NHs, NHC(S) NHPh, H-ortho, H-meta, NHAc/CH3/H_{ax} or H_{eq}, demonstrating that the GD2 dendrimer is indeed tetravalent (tetra-GD2) (**see Appendix III Figure S1**). The formation of the thiourea-bridge in AP-GD2 was verified by a carbon chemical shift at 180ppm that appears in the spectrum of HMBC (NHC(S) NHPh), as reported elsewhere (*224*).

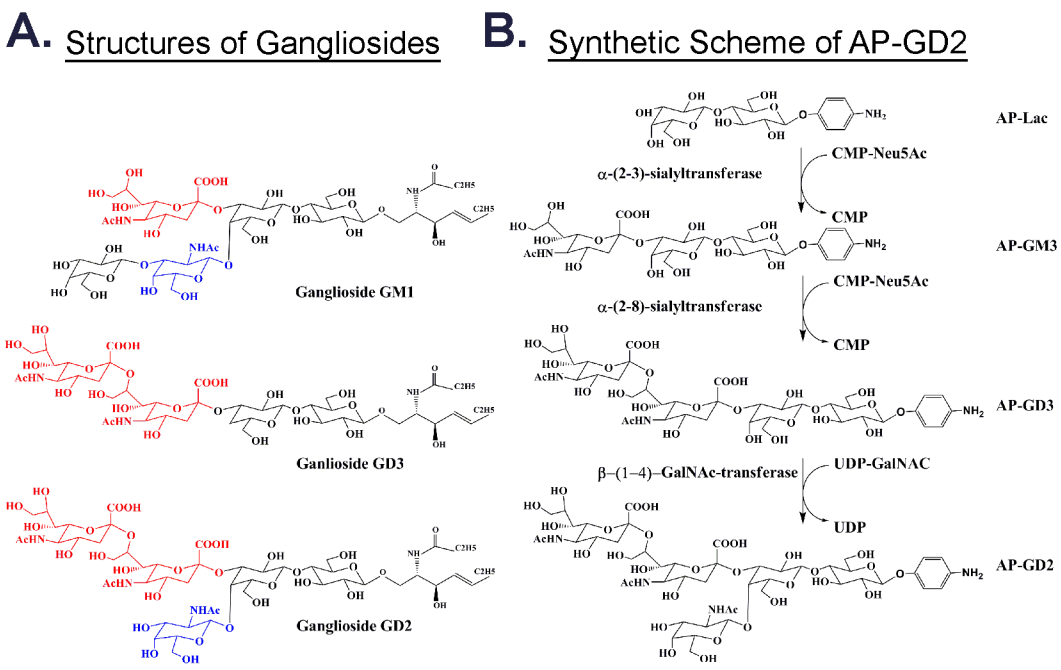

Figure 4.1. Synthesis of amino phenyl ether-GD2 (AP-GD2) and comparison to gangliosides

(A) Structures of ganglioside GM1, GD3 and GD2. The differences in the carbohydrates of these gangliosides are indicated by color. Ceramide, Glucose or Galactose (black); Neuraminic acid (red); and N-aceyl-galactosamine (blue). The first bond to the sugar is in the β-configuration.

(B) Synthetic scheme for GD2 carbohydrate analogs. The bond of amino-phenyl to the first sugar is in the native β-configuration.

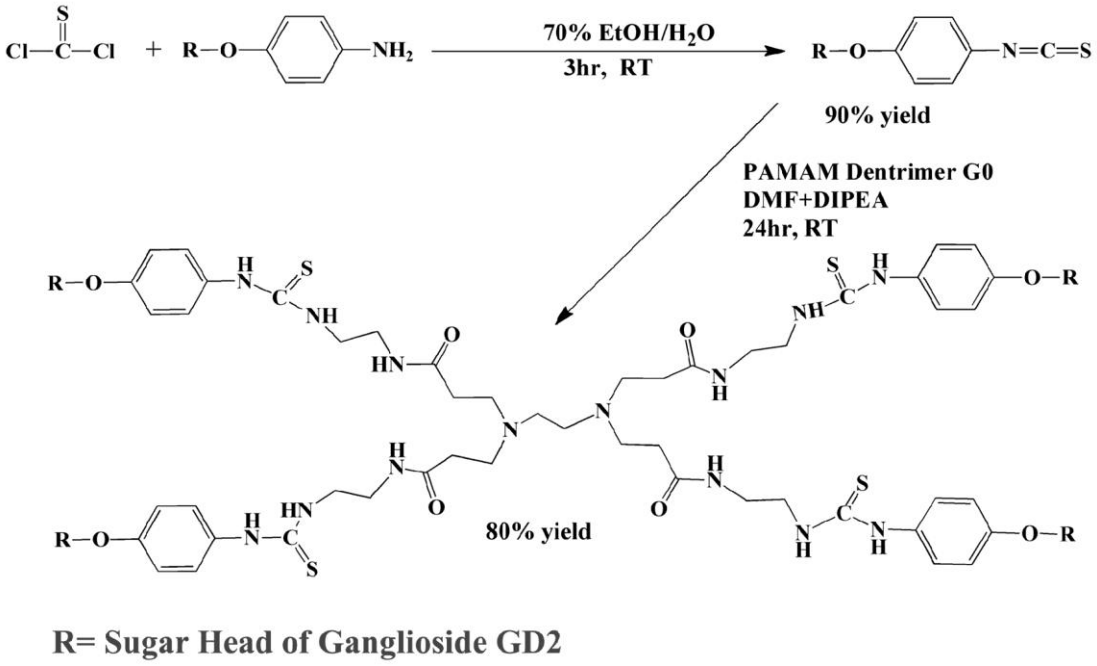

Figure 4.2. Synthesis of GD2 tetramers.

Conjugation of AP-GD2 analog to PAMAM G0. The 4:1 stoichiometry of the agent was verified by NMR.

Natural gangliosides are well-known to be poorly immunogenic, and this makes them not suitable for vaccines. Furthermore, they are difficult to employ as antigens, because of their poor water solubility and tendency to form micelles in solution. In addition, many gangliosides share homologous carbohydrate head structures, such as the ubiquitously expressed GM1, which differs from tumor-expressed GD2 by only two sugars (**Figure 4.1A**). Thus, the generation of a selective anti-tumor ganglioside response is difficult.

In tumor cells, the ganglioside carbohydrate head is exposed on the outer leaflet of the cell membrane, and is the antigenic portion. After presentation, the immune system may recognize a ganglioside as "self" and not elicit immunity or it may generate non-specific and widely cross-reactive pathological antibodies (e.g., Guillain-Barré syndrome is due to an anti-GM1 antibody).

To address the problems described above, our rationale for the design of a GD2 vaccine was based on the following concepts. First, presentation of the GD2-tetramer may more closely mimic the appearance of GD2 within tumor membranes, which is in the form of rafts that likely cluster GD2. The tetrameric display may increase immunogenity by mimicry of the rafted GD2, without creating steric hindrance or difficulties in antigen processing for the immune system. Second, the GD2 sugar head analogues (e.g. AP-GD2) can be easily conjugated to PAMAM linker at room temperature under mild conditions, in a scalable manner that is

amenable for biotechnology**.** PAMAM dendrimers can be used for the precise control of size, shape and placement of functional groups, thereby allowing predictable tuning of their biocompatibility (*225*) (*226*). Third, chemo-enzymatic synthesis guarantees the appropriate glycosidic linkage between each monosaccharide. For example, the β-configuration for the glycosidic bond between glucose and ceramide mimic (**Figure 4.1**) is critical to keep the overall conformation of the whole carbohydrate. Structural studies demonstrated that if this β-linkage is lost, other glycosidic bonds will show both α and β-configurations (*36*), resulting in loss of the native GD2 structures and increased heterogeneity in the antigen, which is undesirable for vaccine development.

GD2-dendrimers elicit antibodies against GD2.

Mice were immunized intraperitoneally and subcutaneously with the tetra-GD2 (see Methods). Sera were collected four days after immunization. Mice developed antibodies against GD2 and GD3 that reacted with these gangliosides on the cell surface (in FACScan assays) and with gangliosides immobilized on plates (in ELISA assays).

Representative FACScan data are shown in **Figure 3A**. EL4-GD2$^+$ cells express GD2 but not GD3. EL4-GD3$^+$ cells express GD3 but not GD2. Control Jurkat cells do not express either GD2 or GD3, but do express many other gangliosides such as GM1. Binding by anti-GD2 monoclonal antibodies and anti-GD3 monoclonal antibodies are shown as positive controls. Sera M1 and M3 had antibodies of the IgG and IgM isotypes

A.

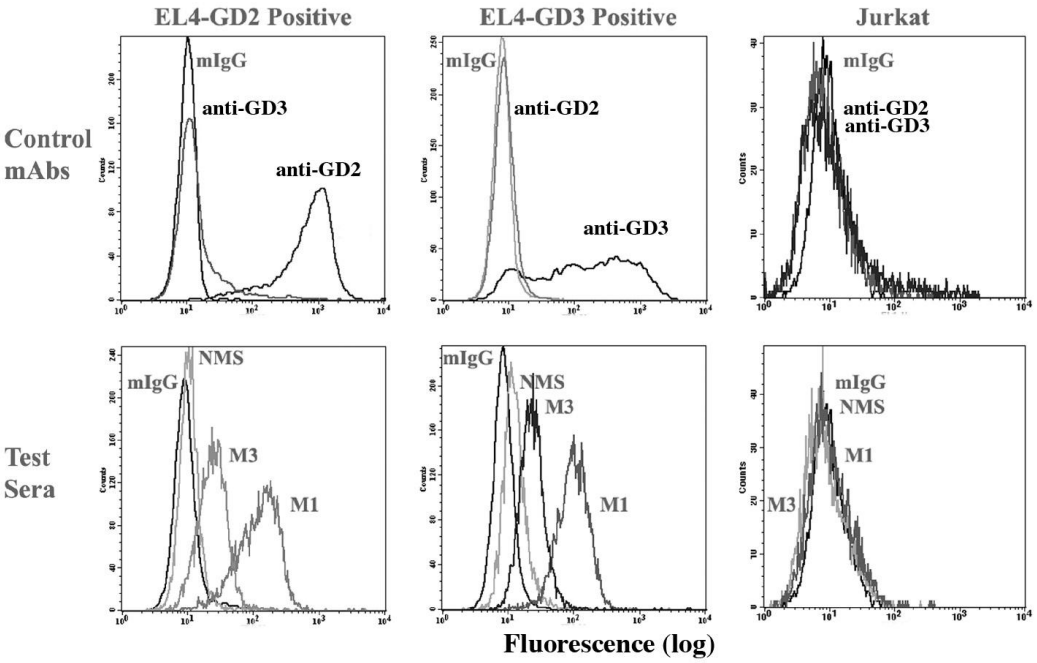
EL4-GD2 Positive
EL4-GD3 Positive
Jurkat
Control mAbs
Test Sera
mIgG
anti-GD3
anti-GD2
anti-GD2
anti-GD3
NMS
M3
M1
Fluorescence (log)

B.

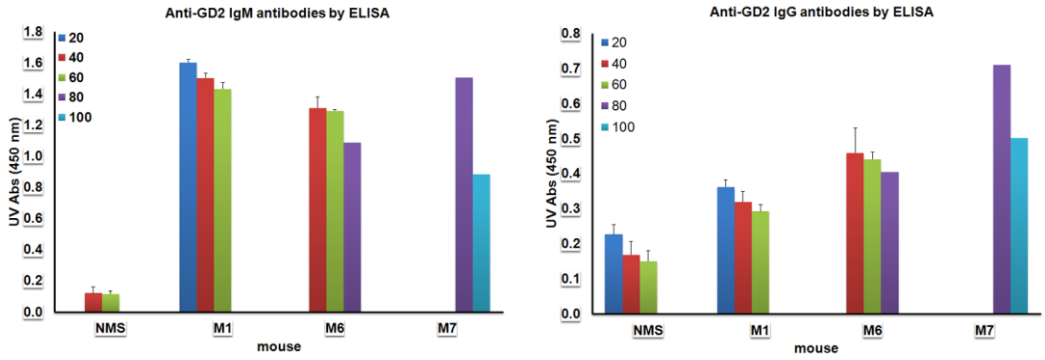
Anti-GD2 IgM antibodies by ELISA
Anti-GD2 IgG antibodies by ELISA
UV Abs (450 nm)
20
40
60
80
100
NMS
M1
M6
M7
mouse

Figure 4.3. Binding assays of mouse sera after vaccination.

(A) Representative FACScan data for sera from mouse 1 (M1) and mouse 3 (M3) showing the presence of anti-GD2–reactive antibodies of the IgG class. Similar analyses using anti-IgM secondary reagents demonstrated the presence of anti-GD2-reactive IgM sera as well (data not shown). Negative control Jurkat cells and positive control EL4-GD3^{+} cells show that antisera had no reactivity to other gangliosides other than to the closely related GD3.

(B) The presence of anti-GD2 antibodies of the IgM and IgG isotype was confirmed by testing in ELISA serial dilutions of sera against immobilized GD2, and specific anti-mouse IgM or anti-mouse IgG secondary reagents.

binding to EL4-GD2$^+$ and/or EL4-GD3$^+$ cells, but not to Jurkat cells. Negative control normal mouse serum pre-bleed (NMS) had no reactivity.

The presence of antibodies binding GD2 and/or GD3 were further confirmed by ELISA, and representative data are shown in **Figure 3B**. GD2, GD3, or controls were immobilized on ELISA plates and the indicated dilutions of test and control pre-bleed sera were assayed for direct binding. Sera from immunized mice exhibited reactivity to GD2 and/or GD3.

Results from the FACScan and ELISA tests are summarized in **Table 4.1**. Overall, immunization with tetra-GD2 generated antibodies against GD2 and GD3 in 14 out of 17 mice (83%), as quantified by flowcytometry and ELISA. Both IgG and IgM isotypes were generated. These data validate the use of the tetra-GD2 as an immunogen.

GD2 dendrimers elicit potent antitumor effects in vivo.

Given that tetra-GD2 elicits a potent humoral response, we studied its potential as a GD2-cancer vaccine *in vivo*.

In a tumor-preventive paradigm, immunocompetent C57/Bl6 mice were immunized four times intraperitoneally at one-week intervals, followed by subcutaneous implantation of syngeneic EL4-GD2$^+$ cells. In a tumor-therapeutic paradigm, mice were first implanted with EL4-GD2$^+$ cells, and when tumors were visible/palpable, the mice were immunized two times with tetra-GD2 or control vehicle. Tumor volume was measured at the indicated days post-tumor implantation.

Table 4.1. Anti-ganglioside reactivities of sera from mice immunized with tetra-GD2 dendrimer.

In FACScan assays, no reactivity above control pre-bleeds was seen for Jurkat cells lacking GD2 and GD3 gangliosides (at serum dilution 1: 25). In ELISA, no reactivity above background was seen for pre-bleed controls (at serum dilution 1: 30). The presence of anti-GD2 IgM isotype was also detected (data not shown).

Mouse	FACScan on cells (IgG)		ELISA (IgG)	
	EL4 GD2	EL4 GD3	Plated GD2	Plated GD3
M1	++++++++++	++++++++	++++	++++
M2	++	++	+++++	+++++
M3	++	++	+++++	+++++
M4	+	++	+++++	+++++
M5	+	++	+++++	+++++
M6	+++	++	+++++	+++++
M7	+++	+++	+++++++	++++++

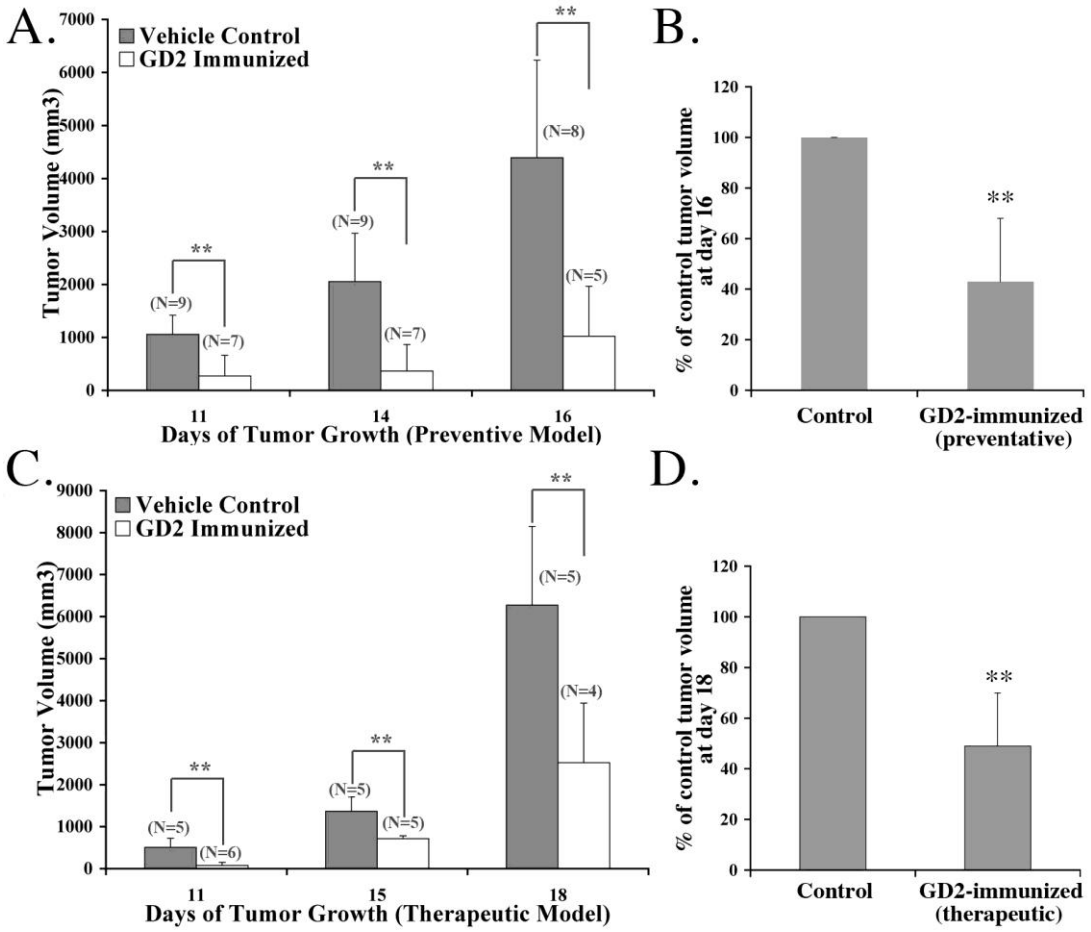
A.
Vehicle Control
GD2 Immunized
Tumor Volume (mm3)
Days of Tumor Growth (Preventive Model)
(N=9)
(N=7)
(N=9)
(N=7)
(N=8)
(N=5)
**
B.
% of control tumor volume at day 16
Control
GD2-immunized (preventative)
C.
Vehicle Control
GD2 Immunized
Tumor Volume (mm3)
Days of Tumor Growth (Therapeutic Model)
(N=5)
(N=6)
(N=5)
(N=5)
(N=5)
(N=4)
D.
% of control tumor volume at day 18
Control
GD2-immunized (therapeutic)

Figure 4.4. GD2 dendrimer vaccination provides protection from tumors.

Mice were vaccinated with GD2-dendrimers intraperitoneally (A) before subcutaneous tumor challenge, or (C) 3 days after subcutaneous tumor implantation (see details in Methods). Data are mean primary tumor volume ± sd, representative experiment of three similar independent experiments, and are analyzed by two-tailed t-tests, ** $p<0.01$. (B and D) Averages ± sd for all independent experiments. The data for the preventative paradigm (B, n=11) averages tumor volumes at day 16 post-tumor implantation. The data for the therapeutic paradigm (D, n=13) averages tumor volumes at day 18 post-tumor implantation. Tumor volume in control mice are standardized to 100%.

In the preventative paradigm, the mice immunized with the tetra-GD2 vaccine (n=7) had primary tumors of significantly smaller size than in control mice at all days measured (11, 14, 16 post tumor implantation) (**Figure 4.4A**). Notably, the immunized mice had no evidence of metastasis to the lymph nodes or thymus, organs which are the major sites of metastasis observed for EL4 tumors. The tumor-preventative vaccine experiments were reproduced in three independent experiments. In all three experiments we compared the tumor volume at day 16 post-tumor implantation, and control mice were standardized to 100%. Overall, the tumors in immunized mice were reduced to ~43% of the control (**Figure 4.4B**).

In the more clinically relevant therapeutic paradigm, mice immunized with tetra-GD2 vaccine after tumor implantation (n= 6) had significantly delayed primary tumor growth compared to control mice, at all days measured (**Figure 4.4C**). After 18 days of tumor growth, all the control mice developed primary tumors averaging ~6,000 mm^3, and extensive lymph node metastasis. In contrast, the immunized mice had primary tumors ~2,300 mm^3, and 5 out of 6 mice had no detectable metastasis to the lymph nodes or the thymus.

The tumor-therapeutic vaccine data were reproduced in four independent experiments. In all four experiments we compared the tumor volume at day 18 post-tumor implantation, and control mice were standardized to 100%. Overall, the tumors in immunized mice were reduced to ~49% of the control (**Figure 4.4D**).

Management of primary tumor growth and tumor metastasis in the realistic therapeutic paradigm, in which vaccine is given after the tumor is established, is a major milestone for cancer vaccines.

Vaccination with GD2 dendrimers elicits tumor-killing antibodies.

In the in vivo therapeutic paradigm there was no inverse correlation between tumor-volume and antibody titer (e.g. the smallest tumor volumes did not correlate with the highest antibody titers). Indeed, in mice bearing EL4 tumors there are very high titer of antibodies against the EL4 cell surface (some of which are anti-GD2 antibodies), even without vaccination. However, these antibodies are not protective to the host. Hence, we hypothesized that vaccination vaccination with tetra-GD2 alters the cytotoxic quality of the antibodies that the host generates against GD2, making them more able to kill tumor cells.

To test this hypothesis, we evaluated the titer and the *in vitro* activity of anti-ganglioside antibodies that were generated through (a) tumor challenge with vaccination, (b) tumor challenge without vaccination, (c) vaccination alone, and (d) naïve control. The presence of specific anti-ganglioside antibodies was evaluated by ELISA (not shown) and the presence of anti-EL4 cell antibodies was evaluated by FACS in sera from these groups of mice.

Vaccination elicited anti-EL4 cell antibodies whether or not animals had tumors (**Figure 4.5A**). In tumor-bearing mice anti-GD2 anti-EL4 cell

antibodies were also detected, even without vaccination. However, as reported above the antibodies elicited without vaccination did not inhibit tumor growth *in vivo*; while the antibodies elicited by vaccination provided protection to the host (e.g. see **Figure 4.4A** and **Figure 4.4C**).

Thus, we evaluated the tumor-cytotoxicity of the antibodies elicited in sera from these groups of mice. Antibodies from vaccinated mice inhibited the growth of EL4 cells in culture, even in the absence of complement or any effector cell, as determined in MTT assays (**Figure 4.5B**). We have previously shown that for EL4 lymphoid cells the MTT assay is equivalent to ^{3}H-thymidine incorporation (*227*). Moreover, EL4 cell killing by test sera was further verified by two other methods: counting cells stained with a viral dye (trypan blue) and by assessing their morphology (data not shown).

Cell killing by the vaccine-elicited antibodies was independent of whether or not mice had been injected with tumors: both the vaccinated mice and the tumor-bearing vaccinated mice produced cytotoxic antibodies. In contrast, in the absence of vaccination, tumor-elicited antibodies were ineffective at killing EL4 cells in culture (**Figure 4.5B**). These data are consistent with the results obtained *in vivo*, where only

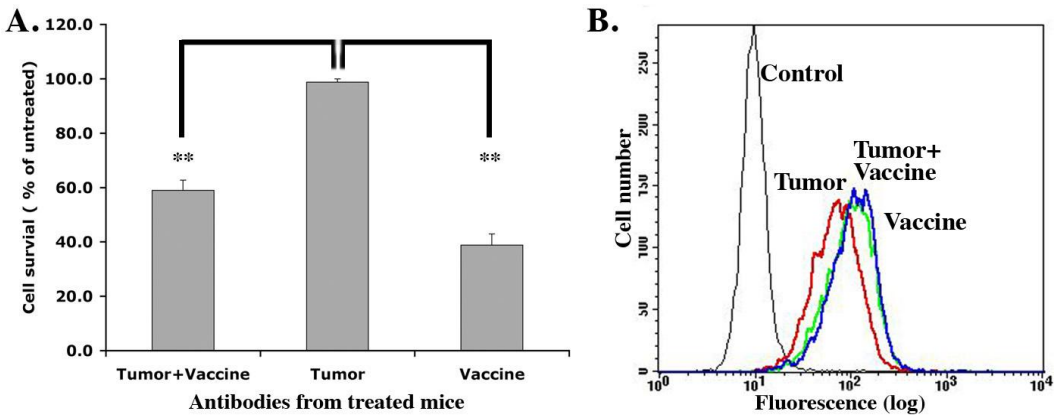

Figure 4.5. Vaccine-elicited antibodies inhibit the growth of EL4 GD2$^+$ cells. Sera were obtained from mice that were naïve (normal control), vaccinated, vaccinated while bearing a tumor, or bearing a tumor but without vaccination. (A) EL4-GD2$^+$ cells growing exponentially in complete media were cultured with the indicated antibodies (from tumor-bearing mice, from vaccinated-mice, from tumor-bearing mice that were vaccinated), and their survival/metabolism was quantified by MTT after 24 hours. Control anti-GD2 mAb 3F8 (cytotoxic), and control anti-GD2 mAb ME361 (non-cytotoxic) are shown as comparison. Data shown are mean ± sem (n=4) and are analyzed by one-way ANOVA with Tukey-Kramer multiple comparisons test. ** $P<0.01$. Representative from four independent MTT experiments, each in triplicate or quadruplicate. (B) FACS assays show binding of test antibodies to EL4-GD2$^+$ cells. Red=antibodies from tumor-bearing mice. Blue= antibodies from vaccinated-mice. Green= antibodies from tumor-bearing mice that were vaccinated. ELISAs with the same sera confirmed the FACS results (data not shown).

vaccination affords protection to the host bearing a tumor (e.g. see **Figure 4.4B** and **Figure 4.4D**).

Conclusion

A novel tetravalent GD2 carbohydrate dendrimer has been developed as a cancer vaccine. Biophysical characterization showed that the synthetic immunogen is a homogenous tetramer that maintains the desired β-configuration of the bonds. *In vivo* and *in vitro* biological studies showed that the tetra-GD2 vaccine can generate anti-GD2 humoral responses, and that the vaccine (but not the tumor itself) elicits cytotoxic antibodies that delay the growth and metastasis of established GD2-expressing tumors.

Advantages of this approach are that the GD2-tetramer may more closely mimic the rafted GD2 in tumor membranes, and the use of analogs that are carbohydrate-based (rather than mimotopes) and yet contain the appropriate glycosidic linkages. Presentation of carbohydrate structures to the immune system may stimulate more genuine and cytotoxic anti-tumor responses. This work represents a major step forward in vaccine development. Future work will explore the molecular mechanisms by which vaccination affords an improved cytotoxic antibody, and will expand the concept to GD3-expressing tumors.

Materials and Methods

Cells

Mouse lymphoma EL4-GD2$^+$ and Jurkat leukemia cells were obtained from ATCC. EL4-GD3$^+$ cells were developed in our laboratory by negative selection of EL4-GD2$^+$ with anti-GD2 mAbs, followed by sub-cloning. EL4-GD3$^+$ cells are stable and have the same in vitro growth properties and kinetics as EL4-GD2$^+$ cells. All cells were grown in RPMI 1640 medium (Wisent INC) supplemented with 5% fetal bovine serum, 2 mM glutamine, 10 mM Hepes and penicillin/streptomycin at 37°C in 5% CO_2 humidified atmosphere. Flow cytometry showed that all cell lines express equal levels of cell surface GM1. Flow cytometry, and thin layer chromatography of ganglioside extracts, confirmed that EL4-GD2$^+$ cells express GD2 but not GD3, that EL4-GD3$^+$ cells express GD3 but not GD2, while Jurkat cells do not express either GD2 or GD3.

Animals

C57/Bl6 (Harlan) mice were used for immunization. EL4 cells are syngeneic and grow and metastasize very rapidly in these mice. We have had 100% successful “take” over several years, in over 1,000 mice.

Synthesis of amino phenyl GD2 (AP-GD2)

The carbohydrates were synthesized as described (*24, 25, 27*), by modification of the process for phenylthio-GD2 (*36*) in which the thio-phenyl analog originally reported was substituted with an p-aminophenyl-

β-D-lactopyranoside (AP-Lac, from Toronto Research Chemicals), for subsequent conjugation to the dendrimer (see below). AP-GD2 was water soluble (>20 mg/ml), and purified by a size-exclusive column (Superdex 30 16 mm X 85 cm column, GE Health Care) to >99% purity. The measured molecular weight of AP-GD2 was 1218 g/mol and corresponded to expected values. Structures were verified by 1D and 2D NMR spectroscopy and mass spectrometry (EI-MS) (**see Appendix III Figures S1 and S2**).

Synthesis of tetra-GD2 dendrimer

Thiophosgene (2 μl) was added to a stirred solution of AP-GD2 (2mg) in 80% ethanol (300 μl), and the mixture was allowed to stand at room temperature for 3 h, when thin layer chromatography (ethyl acetate-methanol, 4:1) showed that all starting material had reacted and a single product had formed. Concentration almost to dryness gave a solid to which water was added. Filtration with washing of the product with water gave the isothiocyanatophenyl GD2 solution, which was freeze-dried to white powder (1.8 mg, 90% yield). The volatiles from a methanol solution of PAMAM G0 (Dendritech, Inc) were evaporated under reduced pressure, and the resulting residue was dissolved in dimethylformamide (DMF). A solution of isothiocyanatophenyl GD2 (1.8 mg) in DMF (110 μl) was added drop-wise to a stirred DMF solution (100 μl) of *N*,*N*-diisopropylethylamine (0.5 μl) and PAMAM G0 (2 μl of 0.854 μg/μl). The reaction was stirred at room temperature for 20 h, until no starting material was detected by TLC.

The reaction mixture was diluted with 3 ml of water and dialyzed against water (MW cutoff 2 kDa, Spectrum Laboratories Inc.). The resulting solution was freeze-dried to give tetravalent PAMAM based GD2 (**Figure 5.1**) as white powder in 80% yield (1.34 mg). The tetravalent PAMAM based GD2 was verified by 1D and 2D NMR spectroscopy (see **Appendix III Figure S1**).

Immunization for FACS and ELISA characterization of sera.

GD2-dendimer (50 μg) in PBS was administrated intraperitoneally to C57/Bl6 mice. After 10 days, the mice were re-immunized intraperitoneally (25 μg) + subcutaneously (25 μg) in PBS. Four days later, blood samples were collected for analyses.

FACScan: 2 x 10^5 cells of EL4-GD2$^+$, EL4-GD3$^+$, and Jurkat cells were washed with FACS buffer (PBS, 0.5% BSA, 0.05% NaN3), resuspended in 100 μl FACS buffer and incubated with 2 μl mouse antisera or positive control anti-GD2 mAb (13 nM) or anti-GD3 mAb (13 nM) for 20 minutes on ice. After 2x washing cells with ice-cold FACS buffer, FITC-conjugated anti-mouse IgG or anti-mouse IgM (Sigma) was added, and incubated for 20 minutes on ice. Cells were washed with FACS buffer and analyzed on flow-cytometer (Becton-Dickinson) using CellQuest software. Mouse IgG or IgM and normal mouse sera were used as negative control antibodies. Jurkat cells were used as negative control cells.

Direct binding ELISA: Gangliosides (Advanced ImmunoChemical Inc.) were immobilized onto polystyrene Corning Strip Well 96-well plates

(Fisher Scientific) by evaporation in a fume hood for 24 hours (10 ng/well). The wells were then “blocked” with phosphate buffered saline containing 0.5% bovine serum albumin (PBS-0.5% BSA) for one hour. Wells were incubated with primary antibodies for two hours, including test sera, control pre-bleed mouse sera, mouse IgG (Sigma), or specific anti-ganglioside monoclonal antibodies. The plates were washed three times with PBS-0.5% BSA, followed by secondary reagent horseradish peroxidase (HRP)-conjugated anti-mouse antibody (Sigma) specific for mouse IgG isotypes, or mouse IgM isotype. After three washes with PBS-0.5% BSA and two with PBS, the colorimetric substrate TMB One Solution (Promega) was added, and the reaction was stopped with 0.5 N H_2SO_4. Plates were read at 450 nm (Benchmark Plus, Bio-Rad).

Competitive ELISA: was as described above, except that ganglioside mimics were added to the wells as putative competitors together with anti-ganglioside antibodies or control anti-GM1 cholera toxin-B (CTB). Wells with no competitor were standardized as 100% binding. Wells with no anti-GD2 mAb added and wells with mouse IgG negative control were standardized as 0% binding (*36*).

Immunization for tumor-preventative studies

C57BL/6 mice were vaccinated intraperitoneally four-times, each one week apart (50 μg each time). Control mice received only vehicle injections. One week after the fourth vaccination, 5 x 10^5 EL4-GD2$^+$ were

injected subcutaneously. Ten days after tumor challenge, tumors were measured at the indicated times post-tumor implantation.

Immunization for tumor-therapeutic studies

5 x 10^5 EL4-GD2$^+$ cells were injected subcutaneously in C57BL/6 mice. After three days, when the tumor was visible/palpable, mice were randomized and were vaccinated twice intraperitoneally either with vehicle control, or with tetra-GD2-dendimer (50 µg in PBS). Tumors were measured at the indicated times post-tumor implantation.

Evaluation of tumor growth

The primary tumor was measured with a digital caliper, and data were analyzed by the following equation: V (mm^3)=0.5 $\times$ width $\times$ (length) ^{2}. After euthanasia, mice were dissected and examined microscopically for evidence of metastasis to lymph nodes and thymus (organs to which EL4 cells are known to home).

MTT assays

EL4-GD2$^+$ cells (5,000 /well, in 96-well plates, Corning) were cultured in RPMI 1640 medium (Wisent INC) supplemented with 5% fetal bovine serum, 2 mM glutamine, 10 mM Hepes and penicillin/streptomycin at 37°C in 5% CO_2 humidified atmosphere. Testing consisted of adding to the wells the following reagents or controls: anti-GD2 mAbs (positive control, 7 nM final concentration), normal mouse IgG control (negative control, 7 nM final concentration). For collection of mouse serum to be

tested in MTT, we followed timelines based on the therapeutic paradigm. Sera were collected from the following groups at day thirteen of the experiment: naïve mice (negative control), mice vaccinated twice intraperitoneally (at days 3 and 10), mice bearing tumors for thirteen days without vaccination, and mice bearing tumors for thirteen days that had been vaccinated twice intraperitoneally (at days 3 and 10). The cleared sera were semi-purified and ~50 µg of antibodies (of which only a fraction would be anti-ganglioside antibodies) were applied per well. The survival/metabolic profile of the cells was quantified after 24h using the tetrazolium salt reagent (MTT, Sigma) and UV absorption. Assays were done 5 times each in quadruplicate.

Statistics

For Figure 3, differences in tumor growth for the two groups were analyzed by two-tailed student t-tests; results were considered to be significant at $p<0.05$ (*) and $p< 0.01$ (**). For Figure 4, one-way ANOVA with Tukey-Kramer Multiple Comparisons Test compared the five different groups. A difference between results was considered significant when $p<0.05$ (*) and $p< 0.01$ (**).

Acknowledgments

WT was supported by a doctoral award from the FRSQ (Quebec). The work was supported by a grant from the Canadian Institutes of Health Research (to HUS).

Connecting text between Chapter 1, 2, 3 and Chapter 5

As described in chapter 1, adding exogenous gangliosides or blocking their biosynthesis through knockout or inhibition of glycosyltransferase cannot clarify the biology of individual ganglioside. Since GD2 peptide ligands and anti-GD2 mAbs are available (Chapter 2 and 3), we decided to use them to dissect the signaling pathway of bound GD2.

One example is in the next chapter. We demonstrated that the GD2-ligand induced-Src activation and this can enhance NMDA receptor activity via its NR2B units. This study defines some molecular mechanisms for GD2-mediated signal transduction.

Chapter 5

Ligand binding to the GD2 carbohydrate activate Src kinase, NMDA receptor, and regulates neuronal cell biology

Wenyong Tong [1,2], Martin Gagnon [1], and H. Uri Saragovi [1, 2,3,4,5,*]

McGill University.

[1]Lady Davis Institute-Jewish General Hospital;

[2]Pharmacology and Therapeutics;

[3]Oncology;

[4]Segal Center for Translational Research;

[5]Bloomfield Center for Neuroscience

Running title: Glycolipid-mediated activation of NMDA-R

* Corresponding author

Lady Davis Institute-Jewish General Hospital

3755 Cote St. Catherine, E-535

Montreal, Quebec, CANADA H3T 1E2

Phone: (514) 340-8222 x 5055

FAX: (514) 340-7502

Email: uri.saragovi@mcgill.ca

Abstract

Ganglioside GD2 is a plasma membrane glycosphinogolipid. It is expressed at low levels in a subset of peripheral neurons and the cerebellum, but it is over-expressed in neuroectoderm cancers. For cancer therapy, GD2 is targeted with anti-GD2 monoclonal antibodies. However, therapy causes severe pain not blocked by morphine, and which ceases on discontinuation of anti-GD2 treatment. Here, we studied mechanisms of GD2-induced pain. We provide evidence that ligand binding to cell surface GD2 carbohydrate moieties induce rapid and transient Src activation, Src-dependent phosphorylation of N-Methyl-D-aspartic acid receptor NR2B subunits at position Y1472 (NR2B-pY1472), activation of Ca^{++} flux, production of cAMP, and morphological changes in neuronal cell lines. These GD2-mediated signals differ in kinetics and in pharmacology from activation of the same signals through the TrkB growth factor receptor, suggesting biological specificity. These data link cell surface GD2 to regulation of Src activity that result in oncogenic transformation, and in pain through modulation of NR2B phosphorylation.

Keywords: Ganglioside GD2/Src kinase/NMDA receptor/anti-GD2 monoclonal antibody

Introduction

Ganglioside GD2 is a glycosphinogolipids expressed at high levels during embryonic development, but in the adult it is detectable only in a subset of normal cells of the peripheral nervous system and the cerebellum (*188, 189*). In some forms of cancer, especially those derived from neuroectoderm, GD2 is over-expressed. For example neuroblastomas, small-cell lung carcinomas, and melanomas (*4, 5, 190, 191*) over-express GD2 on the cell surface.

There is an association between GD2 re-expression and oncogenesis, as gangliosides have been shown to be important in cell-cell recognition, cell matrix attachment, cell growth or differentiation, and can cause the activation of Src-family tyrosine kinases (SFK) (*13, 193-195, 228*). In fact, GD2 has been validated for diagnosis and immunotherapy using anti-GD2 monoclonal antibodies (mAb) such as IgG3 mAb 3F8 (*97, 106, 192*). Recently, small peptides such as SS58 were developed that bind GD2 with high selectivity (*36*). Binding to cell surface GD2 carbohydrate moiety with mAb 3F8 or peptide SS58 cause activation of the SFK $p56^{Lck}$ in lymphoid cells (*36*).

Systemic administration of anti-GD2 mAbs in humans causes acute and severe visceral pain (*93, 97, 106, 109, 229, 230*). Pain is not neuropathic, and resolves rapidly after discontinuation of mAb infusion. Little is known about how anti-GD2 antibodies induce acute pain, but the pain is associated with ectopic activity in afferent C-fibers, and most

intriguingly it cannot be blocked by morphine (*231, 232*).

It is unclear how a glycosphingolipid can carry out the signals described above, because glycosphinogolipids have only a small extracellular component of carbohydrates, and a lipid component embedded in the outer leaflet of the plasma membrane. Since GD2 does not traverse the plasma membrane, a “client protein” may interact functionally with GD2 to carry out the biological signals that are associated with GD2 expression (*9*).

We asked what biological processes could be mediated by GD2 that can be associated with a transformed phenotype, with SFK activation, and with morphine-intractable pain. We focused on the nonreceptor tyrosine kinase Src and on NMDA (N-Methyl-D-aspartic acid) receptors (NMDA-R) for the following reasons: (i) Src is over-expressed/mutated as an oncogene (*206*); (ii) N-Methyl-D-aspartic acid receptors (NMDA-R), particularly the NR2B subunit, sensitize peripheral nociceptors in visceral pain (*233*); (iii) Src is a key regulator of NMDA-R activity (*234*). Thus, we postulated that membrane GD2 might regulate Src, which then regulates NMDA-R activity, and that this system could be affected by ligands of GD2 carbohydrate such as anti-GD2 mAbs or the peptide SS58 (*36*).

In this paper we provide evidence indicating that ligands of GD2 can selectively modulate NMDA-R function by activation of Src, in rather unique ways that differ from other means of activating these pathways. These data link GD2 expression/binding to Src pathways that lead to

oncogenesis and pain.

Results

GD2-ligands alter the phosphorylation of Src kinase

Flow cytometry confirmed that wild type SH-SY5Y, SH-SY5Y-TrkB and NMB-7 neuroblastoma express similar levels of cell surface GD2; and that the transfected SH-SY5Y-TrkB express cell surface TrkB receptors (data not shown).

SH-SY5Y-TrkB cells were treated with the indicated test GD2 ligands (3F8 mAb), negative controls (vehicle, or non-binding mouse IgG), or positive controls (BDNF). The time-dependent changes in phosphorylation of two Src tyrosine residues were quantified. Phosphorylation of Src-Tyr416 is required for full kinase activation, while phospho-Src-Tyr527 is a residue inhibitory of the catalytic activity and its de-phosphorylation is necessary for Src activation. These residues act as a “rheostat” to Src activity.

Ligand binding to GD2 caused phosphorylation of Src-Tyr416 within 7 min, but the signal was transient and decreased by 20 min (**Figure 5.1A**). Control BDNF induced strong phosphorylation of Src-Tyr416 within 7 min, and the signal was sustained after 20 min (**Figure 5.1B**). In pharmacological controls, the phosphorylation of Src-Tyr416 induced by mAb 3F8 can be inhibited by the Src kinase inhibitor PP2 (**Figure 5.1C**), indicating that it is a Src-dependent event. Interestingly, neither mAb 3F8 nor BDNF altered significantly the phosphorylation of another regulatory

tyrosine, Src-Tyr527 (**Figure 5.1A & 5.1B**). This suggests a differential regulation of the Src rheostat in a neuronal cell line.

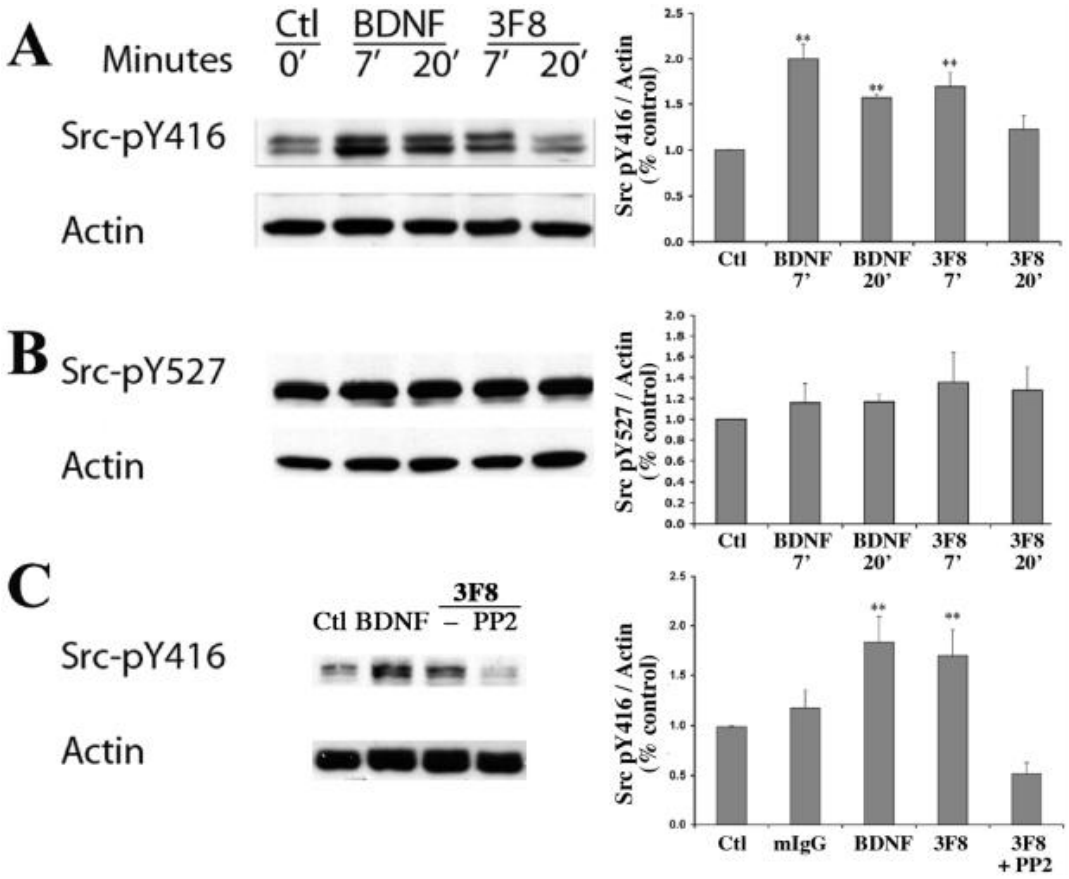

Figure 5.1. Anti-GD2 mAb 3F8 affects the phosphorylation of Src kinase. SH-SY5Y-TrkB cells were treated with mAb 3F8 (10 nM), control mIgG (10 nM) or positive control BDNF (4 nM) for the indicated times. Western blot analysis of whole cell lysates were done with specific anti-phospho-Src antibodies, and were quantified versus anti-β-actin or β-tubulin III. Untreated cells =1, n= 3-4 independent experiments each in triplicate ± SEM. ** $p<0.01$ versus control.(A) anti-GD2 antibody 3F8 induces the transient phosphorylation of Src-Tyr^{416}.(B) anti-GD2 antibody 3F8 has no effect the phosphorylation of Src-Tyr^{527}. (C) Pretreatment of SH-SY5Y-TrkB cells with the Src kinase inhibitor PP2 (20 μM) inhibited 3F8-induced phosphorylation of Src-Tyr^{416}.

Similar results for phospho-Src-Tyr416 were obtained after mAb 3F8 treatment of wild type SH-SY5Y (not expressing TrkB receptors) and the NMB-7 neuroblastoma cell line (data not shown). Moreover, we had shown previously in lymphoid EL4 cells the activation of an SFK family member $p56^{LCK}$ using ligands of GD2 mAb 3F98 and a small peptide termed SS58, which is a mimic of mAb 3F8 (*36*). In controls, GD2-ligands did not induce the phosphorylation of SFK in several cell lines devoid of GD2 (unpublished data). Together, these data indicate that the effect is GD2-ligand specific and it is not restricted to a cell line or a cell lineage.

GD2-ligands induce phosphorylation of NR2B via Src kinase

SH-SY5Y-TrkB cells were treated with ligands or controls as above, and time-dependent changes in phosphorylation of NR2B at Tyr1472 were quantified (**Figure 5.2**).

GD2 ligands caused phosphorylation of NR2B-Tyr1472 within 7 min, a signal that was transient and decreased by 20 min (**Figure 5.2A**). The positive control BDNF also induced phosphorylation of NR2B-Tyr1472, and sustained the signal after 20 min (**Figure 5.2A**), significantly longer than that induced by GD2-ligands (**Figure 5.2B**).

In pharmacological controls, treatment with PP2 or with ketamine did not block the ability of BDNF to induce NR2B phosphorylation (data not shown). In contrast, mAb 3F8-induced phosphorylation of NR2B-Tyr1472 can be inhibited by the Src kinase inhibitor PP2 or by the NMDA-R antagonist ketamine (**Figure 5.2C**). In the absence of GD2 ligands, the

pre-existing baseline NR2B phosphorylation was unaffected by treatment with PP2 or by ketamine. Quantification is shown in **Figure 5.2D**.

Thus, the signals activated by the TrkB ligand BDNF or the GD2 ligands 3F8 or SS58 have distinct kinetics and sensitivity to pharmacological inhibitors. These data indicate that the GD2 ligands and the TrkB ligand activate NR2B in different ways. It is noteworthy that neither mAb 3F8 nor BDNF change the phosphorylation of NR2A (*235*), so the effect appears to be selective for NR2B.

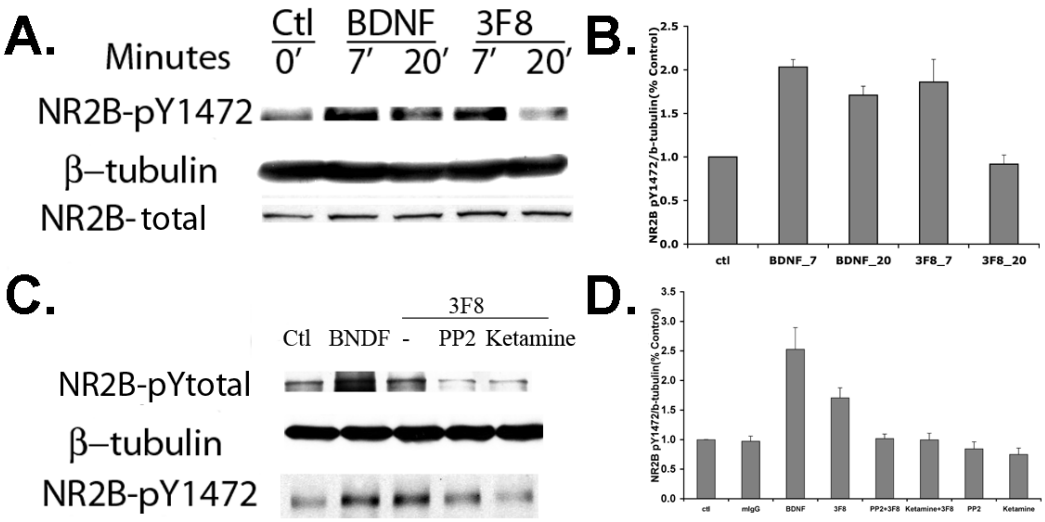

Figure 5.2. Anti-GD2 mAb 3F8 phosphorylates NR2B via Src kinase.

SH-SY5Y-TrkB cells were treated with mAb 3F8 (10 nM), control mIgG (10 nM) or positive control BDNF (4 nM) for the indicated times. Western blot analyses of whole cell lysates were done with specific anti-phospho-NR2B antibodies. Total NR2B levels did not change upon treatment (data not shown).

(A) anti-GD2 antibody 3F8 induces the phosphorylation of NR2B-Tyr^{1472}.

(B) Data from panel A were standardized to anti-β-actin or β-tubulin III levels, and were quantified versus untreated cells = 100%, n= 3-6 independent experiments each in triplicate ± SEM. ** $p<0.01$ versus control.

(C) Pretreatment of SH-SY5Y-TrkB cells with the Src kinase inhibitor PP2 (20 μM) or the NMDA receptor antagonist ketamine (20 μM) inhibited 3F8-induced phosphorylation of NR2B-Tyr^{1472}.

(D) Data from panel C were standardized to anti-β-actin or β-tubulin III levels, and were quantified versus untreated cells = 100%, n= 3-6 independent experiments each in triplicate ± SEM. ** $p<0.01$ versus control.

GD2-ligands increase intracellular calcium

To further confirm that mAb 3F8 can affect the NMDA-R activity through Src, Ca^{++} flux was studied in SH-SY5Y-TrkB cells. BDNF (**Figure 5.3A**), mAb 3F8 (**Figure 5.3B and 3C**), and SS58 (**Figure 5.3D**) can significantly increase the intracellular calcium concentration. The kinetics and the range of the Ca^{++} flux activation were the same for all ligands.

The Ca^{++} flux induced by 3F8 can be blocked by PP2 (**Figure 5.3B)** or by ketamine (**Figure 5.3C**); and the Ca^{++} flux induced by SS58 can be blocked by ketamine (**Figure 5.3D**) and by PP2 (data not shown). In contrast, Ca^{++} fluxes induced by BDNF are not blocked by PP2 or by ketamine (data not shown). These data are consistent with the previous data on Src phosphorylation and NMDA-R phosphorylation, suggest that Ca^{++} fluxes are dependent on Src and NMDA-R activity, and further substantiate the differences between the GD2-induced signaling pathways *versus* the TrkB-induced signaling pathways. We note that PP2 and ketamine block most of the calcium influx induced by mAb 3F8 but only partially block calcium influx induced by SS58. This may be due to the use of high concentrations of peptide SS58, required because it is a low affinity ligand.

Another difference between GD2 ligands and BDNF is that mAb 3F8 could not cause the phosphorylation of TrkB receptors or the phosphorylation of PLCγ-Tyr738 (**Figure 5.3E)**, while BDNF does.

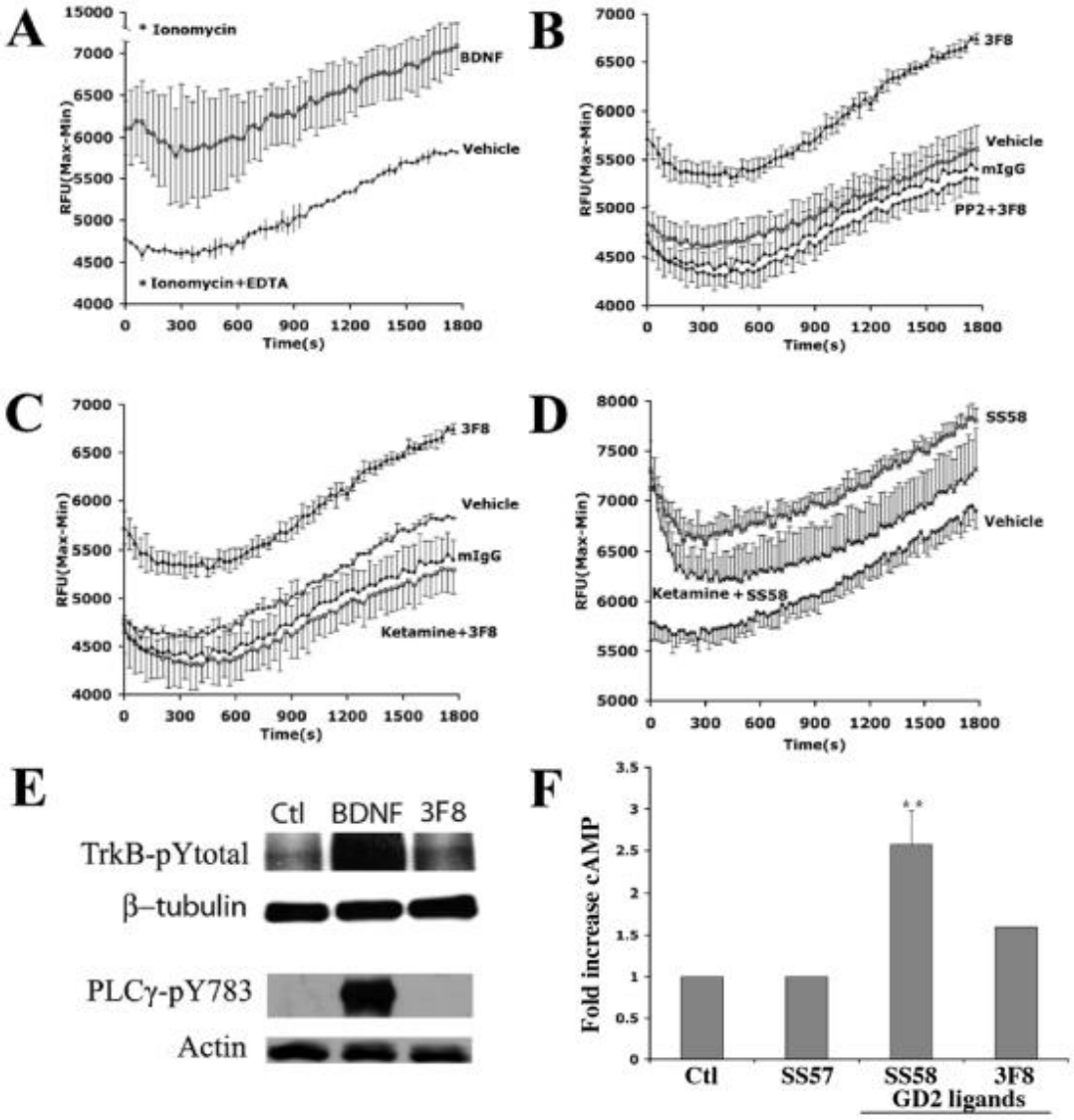
A
* Ionomycin
BDNF
Vehicle
* Ionomycin+EDTA
RFU(Max-Min)
Time(s)
B
3F8
Vehicle
mIgG
PP2+3F8
C
3F8
Vehicle
mIgG
Ketamine+3F8
D
SS58
Vehicle
Ketamine + SS58
E
Ctl
BDNF
3F8
TrkB-pYtotal
β–tubulin
PLCγ-pY783
Actin
F
Fold increase cAMP
Ctl
SS57
SS58
3F8
GD2 ligands

Figure 5.3. Anti-GD2 ligands regulate calcium fluxes through Src and NMDA-R.

SH-SY5Y-TrkB cells loaded with Fluo-8NW dye solution were treated with (**A**) positive control ionomycin (5 μM), or BDNF (4 nM), **(B, C)** mAb 3F8 (10 nM) and **(D)** SS58 (25 μM). Negative controls buffer or vehicle DMSO, ionomycin plus EDTA to quench Ca^{++}, and irrelevant mIgG (10 nM) were also tested. For pharmacological inhibition, the Src kinase inhibitor PP2 (20 μM) or the NMDA-R antagonist ketamine (20 μM) were added 30 minutes before treatment (data shown in **B and C,** respectively). For Ca^{++} assays, the data are a representative result of 4 independent experiments each done in quadruplicate ± SD. (**E**) Whole cell SH-SY5Y-TrkB lysates were studied by Western blot after treatment with mAb 3F8 (10 nM), negative control mIgG (10nM) or positive control BDNF (4 nM). Only BNDF induces phospho-TrkB and PLCγ-Tyr^{738}. (**F**) Anti-GD2 ligands regulate intracellular cAMP. Human NMB-7 neuroblastoma cells were treated with mAb 3F8 (10 nM) or control mIgG (10 nM), peptide SS58 (10 μM) or control peptide SS57 (10 μM). MAb 3F8 and peptide SS58 cause an increase of intracellular cAMP concentration significantly over controls.

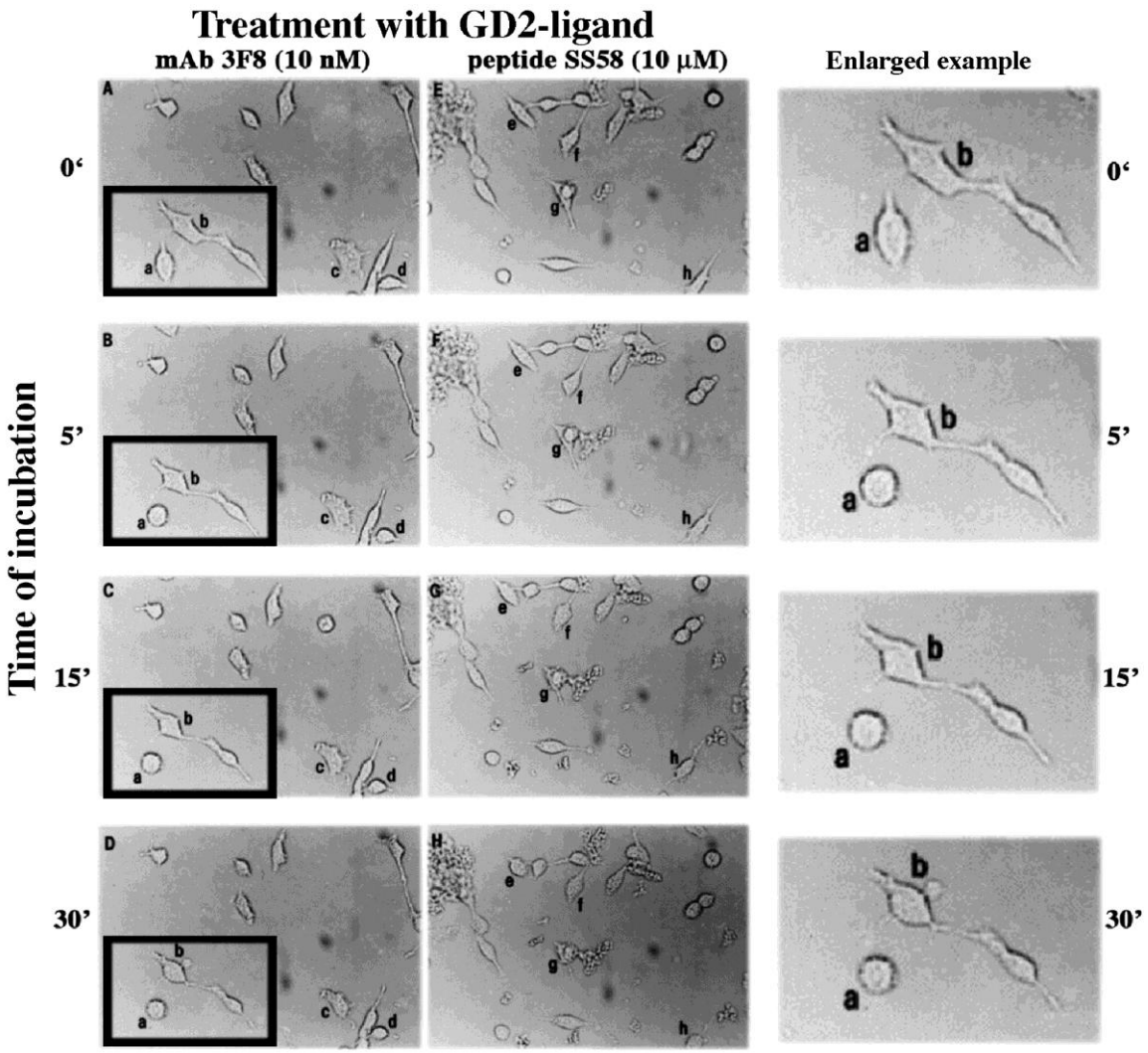

Figure 5.4. Morphological changes in neuroblastoma cells treated with GD2 ligands. NMB-7 cells grown in complete media were treated with 3F8 (50 nM, panels A-D) or SS58 (10 μM, panels E-H). Time-lapse photographs were taken at 100X magnification. Panels in large cap are times of incubation: (A, E) 0' (control starting time), (B, F) 5', (C, G) 15', (D, H) 30'. See the cells labeled with small letters (a-d and e-h), as their morphology changes over time. Enlarged figures (in squares in the panels) are shown as an example. No morphological changes were seen when cells were incubated with control peptide SS57 or with mouse IgG (data not shown).

Since mAb 3F8 did not activate PLCγ, the data suggest that Ca^{++} fluxes are likely not from internal stores, and this view is consistent with the fact that Ca^{++} fluxes are abolished when EDTA is used to quench extracellular Ca^{++} prior to treatment with mAb 3F8 (data not shown).

GD2-ligands increase intracellular cAMP

Consistent with the notion that GD2 ligands enhance Ca^{++} fluxes and NMDA-R activity, they also are able to increase the intracellular cAMP concentration. Both mAb 3F8 and peptide SS58 significantly increased cAMP levels, but their corresponding negative controls mIgG and non-binding peptide SS57 did not (**Figure 5.3F)**.

Morphological changes in neuroblastoma cells treated with GD2 ligands

Ligand-induced effects on cellular morphology were tested in NMB-7 human neuroblastoma cells. Addition of 3F8 or SS58 caused morphological changes characterized by swelling of cells and contraction of projections, an effect visible and almost maximal within 5 minutes (**Figure 5.4**). In controls, no changes were seen when non-binding peptide SS57 or mouse IgG were added to cultures (data not shown).

The simplest interpretation is that the activation of signaling pathways or calcium influx described above may be involved in triggering the morphological changes.

Discussion

We demonstrated that ligands of GD2 activate Src with transient kinetics, leading to increased Ca^{++} influx through activated NMDA-R (phosphorylated NR2B), and causing increased intracellular cAMP concentrations in neuronal cell lines. The mechanisms are Src-dependent (e.g. blocked by PP2) and NMDA-R-dependent (e.g. blocked by ketamine).

The activity of Src is regulated through a “rheostat” by phosphorylation at two distinct tyrosine residues. Phosphorylation of Src-Tyr416 is required for Src kinase activation. In contrast, the phosphorylation of Src-Tyr527 suppresses Src kinase activity (*236, 237*). The phosphorylation of Src-Tyr416 is mediated by the Src kinase itself (auto-phosphorylation). The phosphorylation of Src-Tyr527 is mediated by the Csk kinase. GD2 ligands, as well as BDNF, increased phosphorylation of Src-Tyr416; without detectable changes in the phospho-Src-Tyr527 levels compared to untreated control cells. This could be interpreted as a Csk kinase-insensitive mechanism of Src activation for GD2 ligands and for BNDF.

In our study, the BNDF-induced phospho-TrkB/phospho-Src/phospho-NR2B/Ca^{++} signals are positive controls because they have been documented before, but here we show that they are not blocked by PP2 or by ketamine. One possible explanation for this difference is that BDNF promotes NMDA-R phosphorylation via SFK-dependent and SFK-independent ways (*238, 239*). Another possible explanation for this difference is that BDNF induces a PLC-γ/IP3-dependent calcium store

depletion, which causes non-selective cation influx through other ion channels (*240*).

GD2–GD2-ligands activate Src with distinct kinetics and pharmacology compared to BDNF–TrkB cross-phosphorylation, suggesting biological specificity. Even though activated Src can cross-phosphorylate TrkB (*241*), GD2–GD2-ligands activated Src does not phosphorylate TrkB. Moreover, the GD2-mediated signals differ from BDNF-TrkB in their sensitivity to pharmacological inhibitors. Lastly, signals activated by GD2 ligands appear to target the cell surface pool of client receptors (e.g. phospho-NMDA-R can be blocked by ketamine). Hence, GD2 “activation” likely requires compartmentalization of all components at the cell surface. In contrast, GPCR-Src mediated TrkB phosphorylation occurs mainly at the intracellular TrkB receptors ((*242*) (*241*).

Together, our data suggest that GD2 ligands induced phospho-Src/phospho-NR2B/Ca^{++} signals. These signals promote an increase of intracellular cAMP, likely through activation of adenylyl cyclase (*243*), and significant morphological changes in the cells including retraction of pseudopodia or axons, and detachment from substrate. Pharmacological inhibition with PP2 and ketamine indicate Src and NMDA-R–dependent events.

Activation of NMDA-R and Ca^{++} fluxes by anti-GD2 mAbs may explain the cause of morphine-intractable visceral pain reported in animal studies

(*230-232*) and in human clinical trials using anti-GD2 mAbs (*93, 97, 106, 109, 229*).

Previously, experimental animal studies combined anti-GD2 mAbs with systemic gabapentin, to effectively reverse allodynia in a dose-dependent fashion (*244*). Gabapentin is an analgesic and anticonvulsant structurally related to the neurotransmitter GABA (gamma-aminobutyric acid). The mechanism of action of gabapentin is unknown, but it is unrelated to GABA or GABA receptors. Gabapentin is thought to bind to the α2δ subunits (*245, 246*) of the voltage-gated calcium channel in the central nervous system (*247*). Modulation of voltage-dependent calcium channels in the CNS might block afferent spinal glutamatergic systems acting through the NMDA-R. This is relevant because studies (*233*)report that NR2B-subunit containing NMDA-R may mediate peripheral sensitization and visceral pain. Also Gabapentin blocks the evoked C-fiber activity recorded in spinal cord cells of animals with severe peripheral inflammation (*248*) and this could be a mechanism for achieving allodynia during GD2-therapy.

Taken together, the literature and our study indicate that anti-GD2 antibody induced pain implicates NMDA-R activation and it is a target-mediated side-effect. The peripheral administration of ketamine could attenuate allodynia and visceral pain in patients. However, given the side effects of NMDA-R antagonists, pharmacological strategies to uncouple Src from NMDA-R (*249*) may be more promising to prevent pain. Also, a

recent *in vivo* study demonstrated that NR2B-containing NMDA receptor antagonist Ifenprodil attenuated NMDA-induced allodynia mediated by SFK (*250*)**.** Hence this drug might be used in conjunction with anti-GD2 cancer therapy.

In sum, we have shown an unexpected role for GD2 ganglioside in the modulation of phosphorylation and function of NR2B subunits, through the specific regulation of phosphorylation of Src-Tyr416 (but not Src-Tyr527), leading to increased intracellular Ca^{++} and cAMP, and changes in neuronal morphology. These findings may impact clinically on how anti-GD2 therapy is applied, and in cell biology on how we view the role of glycosphinogolipids. We postulate that other glycosphinogolipids, especially tumor-associated gangliosides may carry out analogous activities through other receptors.

Material and Methods

Cells

SH-SY5Y-TrkB cells are SH-SY5Y human neuroblastoma stably transfected with human TrkB receptor. NMB-7 are human neuroblastoma cells. Cells were grown in RPMI 1640 medium (Life Technologies) supplemented with 5% fetal bovine serum, 2 mM glutamine, 10 mM Hepes and penicillin/streptomycin at 37°C in 5% CO_2 humidified atmosphere. Flow cytometry indicated that these cell lines express similar levels of cell surface ganglioside GD2, and that the SH-SY5Y-TrkB stably expresses the transfected TrkB receptor (data not shown).

Cell treatments

Cells (1.5×10^6/well) were added to a 6-well plate and cultured for 20 hrs. Then the media was exchanged to serum free media (SFM, RPMI, 10 mM Hepes, 0.2% bovine serum albumin) and cells were cultured for 2 hrs to reduce baseline activity. The resting cells were then treated for the indicated times as follows: 10 nM anti-GD2 antibody 3F8 (*112*), control mouse IgG (mIgG, Sigma-Aldrich), 10 M GD2-binding peptide 58 which is a mimic of mAb 3F8, or 10 M of a non-binding control peptide 57 (*36*). For SH-SY5Y-TrkB cells, BDNF (4 nM) (Millipore) was used as a positive control. For pharmacological inhibition, the Src kinase inhibitor PP2 (20 μM) (Enzo Life Science) and the NMDA-R antagonist ketamine (Bioniche Animal Health) (20 μM) were added to the resting cells 30 minutes before the indicated treatments.

Biochemical assays

After treatment, cells were washed with ice-cold PBS (pH 7.4). Then cells were scraped from dishes in NP-40 lysis buffer (20 mM Tris-HCl pH 7.5, 137 mM NaCl, 2 mM EDTA, 1% NONIDET P-40 detergent, protease inhibitor (Roche) and 50 mM sodium orthovanadate) sonicated at 4°C with an ultrasonic processor (Sonics & Materials), cellular debris was removed by centrifugation and protein content in cellular lysates determined by the Bradford method (Bio-Rad). The samples were then electrophoretically separated on 6% and 8% SDS-PAGE under denaturing and reducing conditions. The resolved proteins were transferred to polyvinylidene

difluroride (PVDF) membranes (0.45 μm, Millipore), which were immunoblotted with antibodies directed to the following phosphotyrosine targets: phosphorylated NMDA receptor 2B subunit (NR2B) pY1472 (Enzo Life Science), phospho-Src pY416, phospho-Src pY527, phospho-PLC pY783 (Cell Signaling) and 4G10 anti-phosphotyrosine (Upstate Biotechnology). Blots were visualized using the enhanced chemiluminescence (ECL) system (NEN Life Science Products) and exposure to film (Source). Data were standardized to total protein loaded, by re-probing membranes with antibodies to total Src (Cell Signaling), total NMDA-R (Cell Signaling), anti-β-tubulin III (Sigma-Aldrich), anti-β-actin antibody (Sigma-Aldrich) and from coomassie blue staining of the gels. ImageJ (NIH) wa used for quantification of the films

Intracellular calcium studies

SH-SY5Y-TrkB cells (6×10^4/100 μl) were plated in 96-well black wall/clear bottom plates (BD Falcon) in regular growth medium and grown overnight. After removing the growth medium, 100 μl of Fluo-8NW dye solution, prepared according to Screen Quest ^{TM} Fluro-8 medium removal calcium assay kit (ABD Bioquest), was added to each well and plates were incubated at 37°C for 1 hr. Positive control ionomycin (5 μM) (Enzo Life Science) and negative control EDTA (5 μM) (Wisent INC) were used to determine the range of the signal. DMSO was the vehicle for PP2. PBS was the vehicle for everything else. The indicated concentrations of ligands were added to the wells, and the assay proceeded for the times

shown. Fluorescence detection was done with a filter set of Ex/Em=490/525 nm using FLUOstar OPTIMA (BMG LABTECH).

cAMP detection assay.

Intracellular cyclic AMP (cAMP) levels were quantified using the direct cAMP enzyme immunoassay kit (Assay Design Inc). Briefly, Human NMB-7 neuroblastoma cells were plated in 96-well culture plates in medium at a density of 9×10^5 cells/well. Cells were treated with 3F8 (10 nM), SS57 irrelevant control peptide or SS58 GD2 ligand (25 μM). Forskolin (50 μM) was the positive control. After 10 minutes, the treatment was terminated by the aspiration of the culture medium and addition of the lysis buffer included in the kit. cAMP was measured using the nonacetylation assay procedure provided by the manufacturer.

Morphological assays

NMB-7 cells were grown in 35 mm dishes (Falcon) and cultured in RPMI 1640 medium (Life Technologies) supplemented with 5% fetal bovine serum. 3F8 (50 nM) and SS58 (10 μM) were added and time-lapse photographs were taken at 100X magnification using a Nikon camera and a microscope adapted with a 37°C chamber.

Statistical analysis

One-way ANOVA with Tukey-Kramer Multiple Comparisons Test was used to compare the different results. Results are reported as significant *P<0.05 and **P<0.01.

Acknowledgments

Dr. Nai-Kong V. Cheung (Memorial Sloan-Kettering, NY) supplied the anti-GD2 3F8 mAb, Dr. Nina Schor supplied SH-SY5Y-TrkB cells, and Nelson Lezcano performed some cAMP assays. WT received a scholarship from the FRSQ. Supported by a Canadian Institutes of health Research grant to HUS.

Chapter 6 General discussion and conclusion

Effective therapies typically are expected to target diseased tissues without affecting healthy tissues. A tumor-related glycosphingolipid (GSL), such as ganglioside, is one of the molecular targets that distinguish diseased cells from healthy ones, which may vastly amplify therapeutic opportunities. In order to improve the therapy targeting of GD2-related cancer, the first GD2 direct-binding peptide ligands, as well as a novel type of GD2 vaccine, were designed as a result of structural studies and investigated *in vitro* and *in vivo*. So far, the well-defined GD2 vaccine may be a more promising therapy than GD2 peptide ligands, but these directing GD2 binding ligands are still valuable for exploring the signaling modulated by GD2 and open ample possibilities for improvement in selectivity, affinity and stability. In this section, the implication of our results and future directions will be discussed at the molecular, cellular and animal levels.

Structure-based design and interaction study by NMR (atomic and molecular levels).

The structure-based design by NMR and molecular modeling that we proposed (**see Chapter 2 and Appendix II**) can be expanded not only to other clinically relevant carbohydrates, but also to other types of small molecules that interact with receptors, enzymes or DNA/RNA. The design can be done with or without crystallography, but crystal structures are definitely helpful for progress in this matter.

Because most drug targets are proteins or DNA/RNA, the structure-based design is more about the optimization of small molecules. In our study, ligands were designed from an antibody that is a big “ligand” for a small glycolipid “receptor,” and that is why it is much harder to develop. Since the surface of the binding site of GD2/antibody is a relatively flat and shallow surface, peptides can only mimic some parts of the main interaction CDR loop, which will lead to diminished affinity. A dimer or multimer peptide may keep a better three-dimensional binding site. For example, the dimerization of a glycopeptide BCE against vancomycin-resistant bacteria may strongly enhance the binding to bacterial cell-wall precursor analogues (*251*). Bivalent peptidomimetic ligands, as biased agonists TrkC receptors, may selectively induce neuritogenesis or potentiate neurotrophin-3 trophic signals (*252*). In the future, our bound peptide conformational study may provide extremely valuable information for lead compound design.

One main characteristic of this structure-based design is guided by the dynamic interactions between the antibody and the carbohydrate in an aqueous buffer, which may not be amenable to crystallography. STD-NMR was employed to identify which functional groups or protons in a ligand are most important in establishing the intermolecular interaction with its target. It has been observed that the STD intensities can be influenced by the T1 relaxation rate of the ligand’s proton (*202*). The rate at which the STD signal builds up at short relaxation times may be a more accurate

indication of a binding epitope. In practice, it may not always be possible to obtain a good signal-to-noise ratio in spectra that are recorded with very short saturation times. In order to solve this problem and to obtain accurate epitope mapping, other methods for the study of interactions, such as trNOE or diffusion NMR (*199*), should be applied and may form a good complement.

Bound ligand conformations can be directly calculated from a trNOE spectrum, as we did in Chapter 2. However, the trNOE/ROEs were not detected for the complex of GD2 and its mAb 3F8. This may imply that GD2 3D-structures derived from NMR can adopt a transitional status conformation between an unbound and bound status. Possibly, an induce-fit mechanism can regulate the anti-GD2 antibody (protein) to bind to GD2 (carbohydrates).

There is little 3D-structural information about oligosaccharides (*8*). Few underivated oligosaccharides crystal structures are available due to their inherent flexible structures. Thus, NMR has become a common technique for the determination of conformations of oligosaccharides. There are still some limitations to the calculation of flexible carbohydrates structure by NMR, namely few long-term NOEs and the fact that the parameters measured are the average across all populated conformational states (*253*). These issues may not, however, apply to rigid carbohydrate molecules, such as Lewis and GD2. The overall

conformational behaviors of these oligosaccharides are generally found to be of a much more restrained nature.

Finally, this structure-based design by NMR is complemented by a computational modeling, such as docking, molecular mechanic and dynamic simulation. The quality of binding models can always be checked by comparison with NMR data or crystal structures.

Ganglioside-modulated signaling transduction (molecular and cellular levels).

The dramatic changes in gangliosides, composition and metabolism are associated with oncogenic transformation. The up- and down-regulation of ganglioside are caused by the over-expression and shutdown of related biosynthetic glycosyltransferase genes. Consequently, changes in particular ganglioside composition in lipid rafts result in the alteration of antigenicity, immunogenicity and malignancy. GD2 is such an example that is related to tumors. First, it is a tumor marker. Second, GD2 has a low immunogenicity and protects the tumor cells by suppressing the immune system. Third, GD2 is involved in tumor growth and metastasis through interactions with growth receptors and adhesion molecules within lipid rafts. However, it is unclear how the transcriptional activation of glycosyltransferase genes is regulated (*254*) and whether these tumor-related gangliosides can affect the gene expression of glycosyltransferase.

Although current observational studies indicate that gangliosides are involved in tumorigenesis, metastasis, and angiogenesis, it is still unclear what roles the different types of gangliosides play in cancer and which signaling proteins are involved in pathways that are modulated by gangliosides. Glycomics may be a better approach to use to investigate the structural and functional relationships (SAR) of gangliosides (*255*). One on-going project in our group is the investigation of ganglioside-binding proteins through a GD2-conjugated affinity column. The next step will be to investigate how GD2 modulates these protein functions and how these GD2/protein interactions can be pharmacologically interrupted. The most difficult challenge is to elucidate how clustered GD2s within lipid rafts govern the intra- or extra-cellular signaling transduction and cell-to-cell communications through multivalent interactions with proteins or carbohydrates.

In our study (**Chapters 2 and 5**), we reported that the exact mechanism of interaction between GD2 in the outer leaflet of cell membrane and cytoplasmic Src family kinases (SFKs) is still unknown. However, it is well established that SFKs can be only activated by GD2 when the anti-GD2 mAb or peptide ligands bind to GD2. In fact, other gangliosides bound by mAbs, such as GD3, can also recruit different SFKs, depending on the cell types.

We also demonstrated that a GD2-mediated enhancement of NMDA receptors (NMDAR) through SFKs in neuroblastoma cells may be

responsible for the pain sensations that are felt following an anti-GD2 antibody treatment in clinical trials (**Chapter 5**). The next step for this work is probably to conduct an electrophysiological study at the cellular or periphery nerve level and to further test whether NMDAR antagonists, especially NR2B-selective antagonists, can block anti-GD2 antibody-induced allodynia and visceral pain in animal pain models.

One interesting observation is that the NMDA receptor antagonist ketamine could abolish the sequential activation of SFK-NR2B that is caused by the anti-GD2 antibody 3F8 binding to GD2 (**Chapter 5**). The NR2B unit may be uncoupled by the channel blocker ketamine from the complex of NMDAR/SFK. The N2B-mediated NMDAR internalization (*256*) may be another mechanism that accounts for the ketamine effects on the phosphorylation of c-terminal of NR2B unit.

In summary, future work for ganglioside-modulated cellular signaling needs to address the roles of lipid rafts, to identify ganglioside-binding proteins and to investigate how the carbohydrate/protein and carbohydrate/carbohydrate interactions induce intra- and extra- cellular signaling transduction.

Ganglioside cancer vaccines (*in vitro* and *in vivo* levels)

Altered ganglioside patterns distinguish some malignant cells from their normal cell counterparts. This is the rationale for carbohydrate-based

cancer vaccines that are primarily used after completion of primary therapy (e.g., surgery, radiation and chemotherapy).

Gangliosides are poorly immunogenic. Moreover, they are antigens that are presented on the host tumor's cell surface, which are supposed to be recognized as "self" by the immune system. Therefore, the development of a vaccine to break the immunotolerance of ganglioside antigens is indeed an ambitious goal.

There are a number of mechanisms by which tumors may evade an immune response (e.g., blocking of the T-cell effector function by TGF-β, evasion of T-cell recognition and immunosuppression of shed gangliosides). However, it is still not clear how exogenous carbohydrate antigens (vaccines), instead of the same antigens expressing the tumor cells, can induce an effective immune response. Our study (**Chapter 4**) showed that the anti-GD2 antibodies elicited by the tumors did not provide protection against tumor growth *in vitro and in vivo*. On the other hand, the antibodies that were elicited by the GD2 vaccine delayed tumor growth. The quality of the vaccine-induced antibodies seems to be superior to those induced from tumors. The next step is to identify the immunized effector cells and to evaluate the T-cell response during the vaccination progress. Overall, the elucidation of the underlying molecular mechanisms for breaking the tumor immune escape may improve the effectiveness of carbohydrate-based cancer vaccines.

At the same time, future work may also focus on the optimization of the current GD2 vaccine, based on some parameters, such as the epitope clustering, the length and the structure of linker (*257*). For the clustered epitope, either the change of the GD2 assembly pattern or the increaseed number of GD2 may strengthen the antibody response. The length of linker will also affect the pattern of epitope clustering. Except for PAMAM G0, other generations of PAMAM are possibly used to make GD2 multimers to increase the immunogenicity. The incorporation of helper T-cell epitopes to linkers may achieve a strong, long-lasting and class-switched antibody response (*8*). As well, various kinds of low-toxicity adjuvants (e.g., Alum and QS-21) deserve further investigation to improve the immunogenicity of the tetra-GD2 vaccine. Finally, multi-antigenic vaccines composed of gangliosides or other tumor-associated antigens will be another alternative to developing ganglioside vaccines.

The next step following optimization is to test GD2 conjugates in the syngeneic murine neuroblastoma, melanoma and SCLC models (*156, 258*). If necessary, tumor models may be generated in nude mice.

With regard to toxicities, whether or not the GD2 vaccine, like anti-GD2 anti-bodies (**Chapter 5**), induces pain remains a question. So far, our observations showed that none of the immunized mice have experienced any pain syndrome. Pain was not reported in GD2 (*151*) and GM2-KLH (*152, 167*) clinical trials either. The titer and affinity of circulating anti-GD2

antibodies induced by vaccines are lower than infused ones, which may account for this paradoxical phenomenon (*151*).

Conclusion

Ganglioside GD2 can be druggable, not only because it is a cancer-maker, but also because it plays a critical role in tumor growth.

In the work presented herein, direct GD2-binding ligands and a novel type of immunogenic teta-GD2 dendrimer were designed on the basis of structural studies by NMR. The *in vitro* and *in vivo* studies demonstrated that the tetra-GD2 dendrimer can be a promising cancer vaccine. Although direct GD2-binding ligands have not shown therapeutic potential, they are still valuable for biochemical studies. With the use of peptide ligands and the anti-GD2 antibody 3F8, it was demonstrated that NMDAR might be involved in anti-GD2 antibody induced pain.

Ongoing glycomic study may accelerate research on GD2 functions and the development of better GD2-direct binding ligands. The optimizations of the current GD2 vaccines and understanding the immune-mediated tumor rejection are proposed as the objectives of future work.

Appendix I Supporting information for Chapter 2

Small Molecule Ligands of GD2 Ganglioside, Designed from NMR Studies, Exhibit Induced-Fit Binding and Bioactivity.

Wenyong Tong, Martin Gagnon, Tara Sprules, Michel Gilbert, Shafinaz Chowdhury, Karen Meerovitch, Karl Hansford, Enrico O. Purisima, John W. Blankenship, Nai-Kong V. Cheung, Kalle Gehring, William D. Lubell, H. Uri Saragovi *

Index

Figures

Tables

Table S4. Comparison of the experimental and calculated percentage fractional STD intensities for GD2/3F8 complex (T_{sat} = 3s) and the respective T1 relaxation time.

Table S5. Proton Chemical shift of peptide M1 at pH=6.8 and T=288k in 10%D2O/90%H2O. Proton Chemical shift of peptide SS58 at pH=6.0 and T=288k in 10%D2O/90%H2O.

Table S6. Proton Chemical shift of peptide M50B at pH=6.0 and T=288k in 10%D2O/90%H2O.

Table S7. Statistics for the NMR structure calculations of the peptides in water.

Methods

Cell Culture.

NMR spectroscopy of ganglioside GD2 and thiophenyl GD2.

STD NMR spectroscopy.

Structure calculations.

Docking Studies.

Structure prediction, model building and refinement.

Molecular docking of GD2 and CORCEMA-ST calculations.

References

A

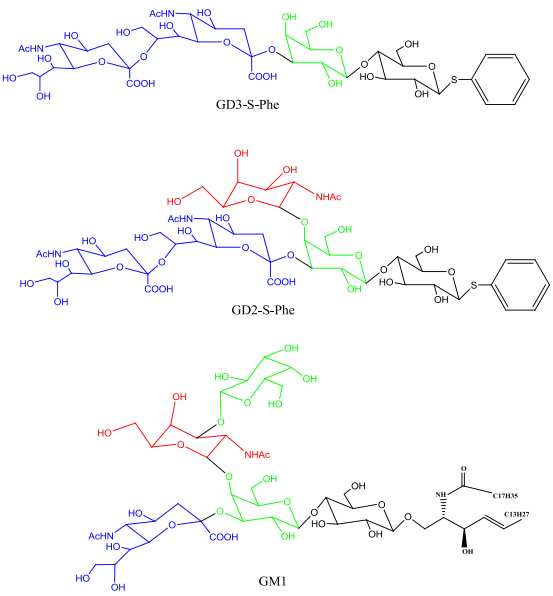

B

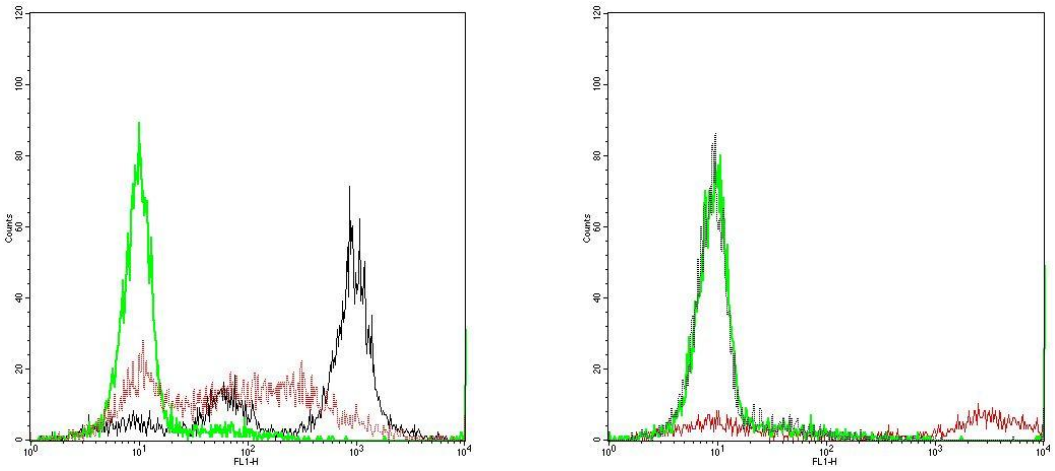

Figure S1. Structures and antibody binding of EL4 GD2 positive cells and EL4 GD2 negative cells. (A) Structure of Thiophenyl GD2, Thiophenyl GD3 and ganglioside GM1. Glucose (black), Galactose (green), N-acetyl galactose (red) and Neuramic acid (blue) are shown in different colors. (B) 3F8 (black) specifically binds to EL4-GD2 positive cells and does not bind to EL4-GD2 negative cells. Anti-GD3 ganglioside mAb R24 (red) is a control for expression of ganglioside GD3, and mIgG (green) is a negative control for background.

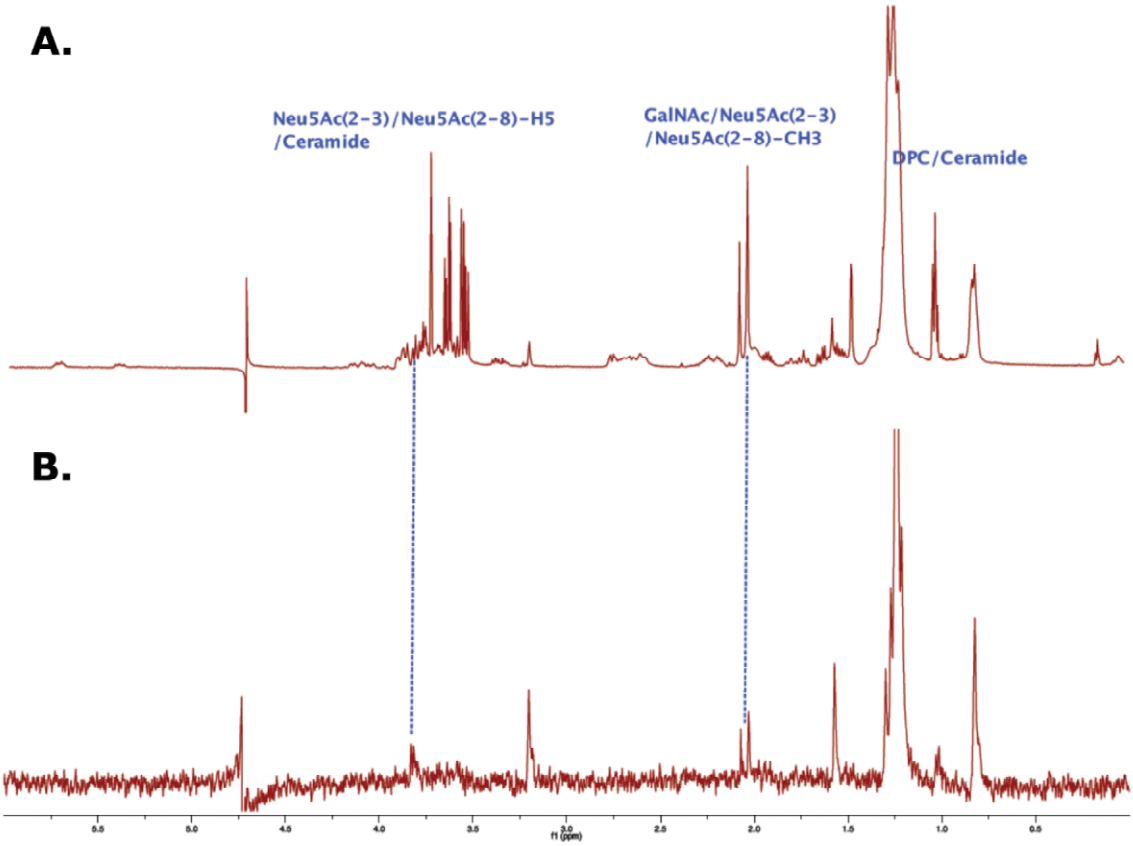

Figure S2. STD NMR spectra for a mixture of ganglioside GD2 in DPC micelles and 3F8. (A) Reference spectrum of a mixture of ganglioside GD2 (500 µM) in the DPC micelles (molar ratio 40:1) and 3F8 (20 µM binding sites) at a ratio of 25:1 (ligand excess). (B) STD NMR spectrum of the same sample (T_{sat}= 5 s).

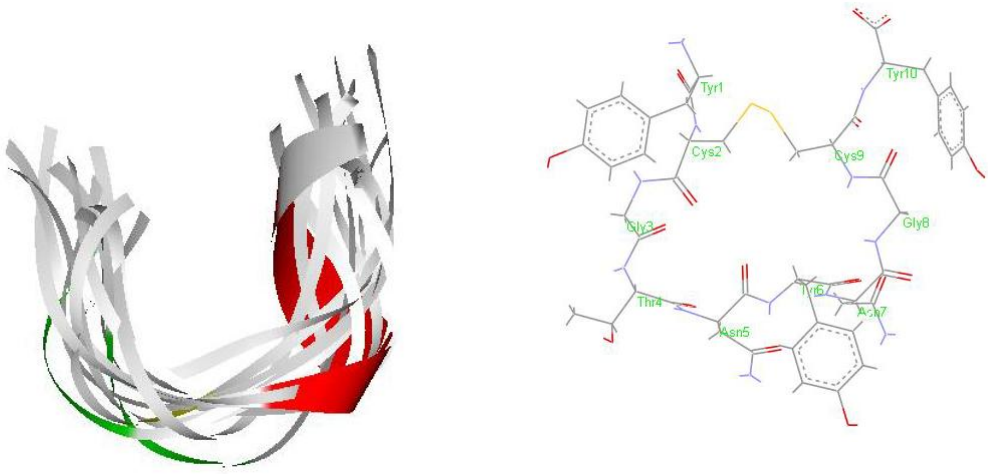

Figure S3. Ensemble of 12 lowest-energy structures calculated for the GD2-binding peptide M1. The ensemble of structures is in flat ribbon representation, and the average structure is in line representation (water molecules are removed). The α helix is in red, the β turn is in green and the random coil is in gray.

A

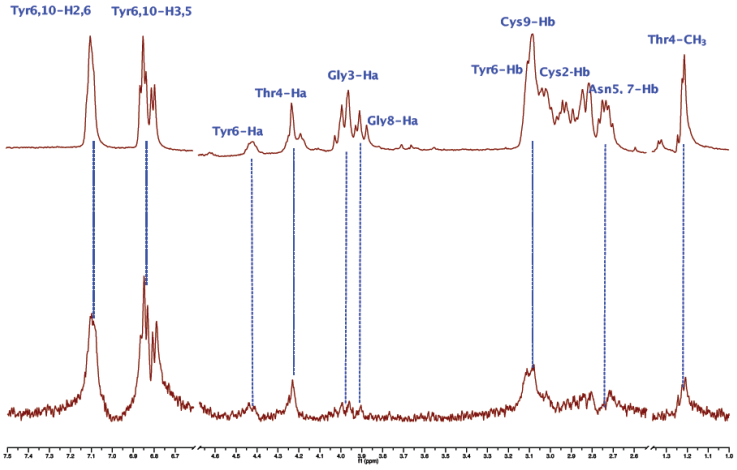

B

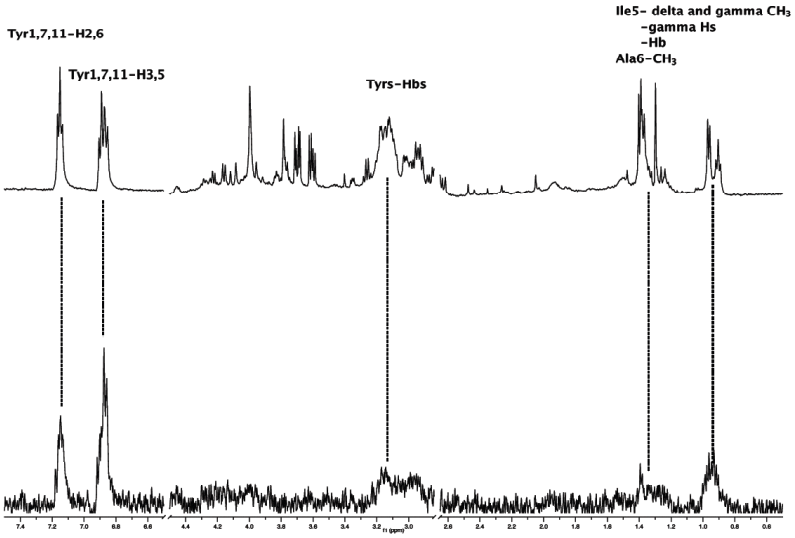

Figure S4. STD NMR spectra for a mixture of ganglioside GD2 micelles and M1/SS58. (A) Reference spectrum of a mixture of ganglioside GD2 micelles (200 μM) and peptide ligand M1 (1 mM) in a ratio of 1:5 (top panel). STD NMR spectrum of the same sample at 298 K (*T*sat= 5 s, bottom panel). (B) Reference spectrum of a mixture of ganglioside GD2 micelles (100 μM) and peptide ligand SS58 (500 M) in a ratio of 1:5(top panel); STD NMR spectrum of the same sample at 298 K (Tsat=5s, bottom panel).

```
L1                L2
3F8VL  SIVMTQTPEFLFVSAGDRVTITC**KASQSVSNDVT**WYQQKAGQSPKLVIY**SASNRYS**GVPD
2PSKVL QIVLTQSPAIMSASPGEKVTITC **SASSSVSN**-**IH**WFQQKPGTFPKLWIY**STSTLASG**VPG
                     L3
3F8VL  RFTGSGYGTAFTFTISTVQAEDLAVYFC**QQDYS---S**FGGGTKLEILRADAA
1PSKVL RFSGSGSGTSYSLTISRMGAEDAATYYC**QQRSGYPFT**FGSGTKLEIKRADAA
                     H1              H2
3F8VH  QVQLKESGPGLVAPSQSLSITCTVSGFSV**TNYGVH**WVRQPPGKGLEWLG**VIWAG-GITNY**
1PSKVH EVQLQQSGPELVKPGASVKISCKTSGYTF**TKYTMH**WVKQSHGKSLEWIG**DINPNNGGTNY**

                                                  H3
3F8VH  **NSAFMS**RLSISKDNSKSQVFLKMNSLQIDDTAMYYCAS**RGGHYGYALDY**WGQGTSVTVSS
1PSKVH **NQKFKG**TATLTVHKSSTTAYMELRSLTSEDSAVYYCTS**K**------**SFDY**WGQGTTLTVSS
```

Figure S5. Sequences from anti-GD2 antibody Fab fragment of ME36.1 (pdb code 2psk) and 3F8 were aligned using the program ClustalW V8.13. There is 59% and 46% identity observed between the two sequences. The CDR's of light (VL) and heavy (VH) were designated by L1 (red), L2 (blue), L3 (orange) and H1 (red), H2 (blue), H3 (orange) respectively.

```
                     L1              L2
3F8VL   SIVMTQTPEFLFVSAGDRVTITC**KASQSVSNDVT**WYQQKAGQSPKLVIY**SASNRYS**GVPD
2Q8AVL  SIVMTQTPKFLPVSAGDRVTIIC**KASQSVSNDVV**WYQQKPGQSPKLLIY**YASIRYTG**VPD
                     L3
3F8VL   RFTGSGYGTAFTFTISTVQAEDLAVYFC**QQDYSS**---FGGGTKLEILRADAA
2Q8AVL  RFTGSGYGTDFTFTISTVQVEDLAVYFC**QQGFSS**PRTFGGGTKLEINRADAA
                        H1        H2
3F8VH   QVQLKESGPGLVAPSQSLSITCTVSGFSVT**NYGVH**WVRQPPGKGLEWLG**VIWAGGITNYN**
2GJZVH  QVQLKESGPGLVAPSQSLSITCTVSGFSLT**NYGVD**WVRQPPGKGLEWVG**VIWSGGSTNYN**
                        H3
3F8VH   **SAFMS**RLSISKDNSKSQVFLKMNSLQIDDTAMYYCAS-**RGGHY-GYALDY**WGQGTSVTVSS
2GJZVH  **SALMS**RLSISKDNSKSQVFLKMNSLQTDDTAVYYCAKH**WGGYYIPYGMDH**WGQGTTVTVSS
```

Figure S6. Structure based sequence alignment. Sequence alignment of the Fab fragment of VL of 3F8 and Fab of VL of malaria antigen AMA1 (pdb code 2q8a) showed 84% identity. Also Fab VH of 3F8 showed 84% identity with the sequence of 13G5 antibody (pdb code 2gjh). The alignment was obtained by ClustalW V1.83. The CDR's of light (VL) and heavy (VH) chains were designated by L1 (red), L2 (blue), L3 (orange) and H1 (red), H2 (blue), H3 (orange) respectively.

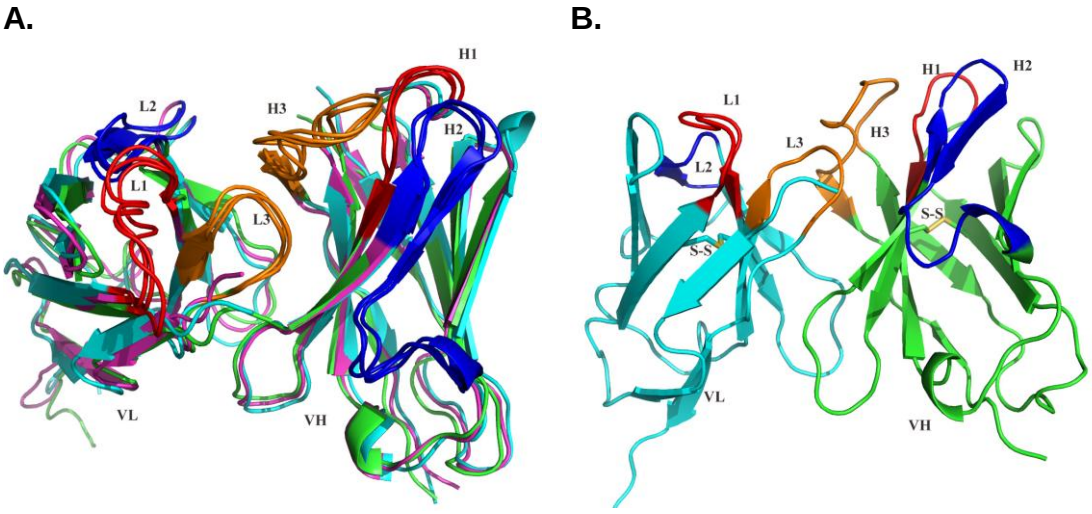

Figure S7. Molecular model of 3F8 Fab fragment obtained from the average structure. (A) The superimposed molecular dynamics (MD) average structure of the of simulation trajectory of 3F8 Fab. The CDR's of light (VL) and heavy (VH) chains were designated by L1 (red), L2 (blue), L3 (orange) and H1 (red), H2 (blue), H3 (orange) respectively. (B) The final MD average structure of Fab of 3F8 anti GD2 antibody used for the docking study.

Table S1. Proton NMR chemical shifts of ganglioside GD2 in DPC micelles and thiophenyl GD2 at pH=6.0 and T=288 K in D_2O (note: reference number is shown in table)

Residue	H	Chemical shifts (ppm)				
		GD3-S-Phe(***35***)	GD2-S-Phe	GM1-Neu5G(*259*)	GM1(*33*)	GD2
βGlc	1	4.83	4.83	4.48	4.45	4.43 ($J_{1,2}$=7.34Hz)
	2	3.41	3.40	3.37	3.34	3.33 ($J_{2,3}$=8.34Hz)
	3	3.67	3.68	3.66	3.64	3.62
	4	3.71	3.65	3.63	3.61	3.60
	5	3.64	3.63	3.62	3.66	3.57
	6	3.84	3.84	3.82	3.80	3.79
	6′	3.98	3.98	4.01	3.99	3.97
βGal (1-4)	1	4.52	4.50	4.56	4.54	4.49 ($J_{1,2}$=7.10Hz)
	2	3.56	3.39	3.39	3.39	3.38 ($J_{2,3}$=8.88Hz)
	3	4.09	4.15	4.19	4.17	4.15 ($J_{3,4}$=4.18Hz)
	4	3.96	4.04	4.17	4.13	4.04
	5	3.72	3.71	3.78	3.78	3.71
	6	3.74	3.77	3.79	3.66	3.75
	6′	3.74	3.77	3.79	3.87	3.75
αNeuAc (2-3)	3ax	1.74	1.78	1.97	1.95	1.79($J_{3a,4}$=11.95Hz)
(α-Neu5Gc)	3eq	2.68	2.68	2.71	2.69	2.65($J_{3e,4}$=12.01Hz, $J_{3a,3e}$=3.59Hz)
	4	3.60	3.66	3.92	3.84	3.69
	5	3.82	3.82	3.93	3.84	3.80
	6	3.69	3.57	3.65	3.57	3.54
	7	3.86	3.86	3.63	3.61	3.86
	8	4.14	4.10	3.80	3.60	4.10
	9	3.74	3.71	3.66	3.76	3.69
	9′	4.17	4.17	3.90	3.90	4.14
	NAc	2.07	2.07			2.07
	NH		8.00			
βGal NAc (1-4)	1		4.70	4.83	4.78	4.71($J_{1,2}$=8.78Hz)
	2		3.88	4.08	4.04	3.89
	3		3.91	3.83	3.84	3.91
	4		3.77	4.19	4.18	3.74
	5		3.68	3.76	3.73	3.69
	6		3.76	3.85	3.76	3.75
	6′		3.76	3.85	3.764	3.75
	NAc		2.03		2.02	2.02
	NH		7.84			
αNeuAc (2-8)	3ax	1.74	1.74			1.72($J_{3a,4}$=12.01Hz)
	3eq	2.78	2.76			2.75($J_{3e,4}$=12.09Hz, $J_{3a,3e}$=4.24Hz)
	4	3.67	3.67			3.66
	5	3.83	3.83			3.80
	6	3.61	3.61			3.59
	7	3.59	3.59			3.58
	8	3.90	3.90			3.88
	9	3.64	3.64			3.63
	9′	3.88	3.88			3.86
	NAc	2.03	2.02			2.04
	NH		8.04			
Ceramide	1			4.20	4.20	4.19
	1′			3.75	3.74	3.70
	2			3.94	3.92	3.89
	3			4.10	4.08	4.06
	4			5.35	5.42	5.40($J_{4,5}$=14.80Hz, $J_{3,4}$=7.77Hz)
	5			5.77	5.74	5.73($J_{4,5}$=14.27Hz, $J_{5,6}$=7.77Hz)
	6			2.02	2.00	1.97
	7				1.34	1.34

Table S2. Carbon NMR chemical shifts of ganglioside GD2 in DPC micelles and thiophenyl GD2 at pH=6.0 and T=288 K in D_2O

Residue		Chemical shifts (ppm)				
	C	GD3-S-Phe	GD2-S-Phe	GM1-Neu5Gc	GM1	GD2
βGlc	1	88.0	88.02	103.0	103.26	103.83
	2	72.4	72.32	72.70	72.77	73.45
	3	76.5	76.54	72.71	72.44	70.44
	4	78.5	78.74	79.17	78.98	79.46
	5	79.7	79.64	74.76	74.01	72.66
	6	60.9	60.90	59.20	60.21	60.82
βGal (1-4)	1	103.4	103.60	102.70	102.83	103.60
	2	70.1	70.61	70.01	70.13	70.49
	3	76.3	75.43	74.42	74.64	75.12
	4	68.4	76.83	77.40	77.10	77.30
	5	76.1	75.16	72.28	72.17	75.12
	6	62.0	61.68	60.66	63.10	61.45
αNeuAc (2-3) (α-Neu5Gc)	3	40.5	39.99	36.91	36.93	39.61
	4	68.9	69.04	N/A	68.50	69.10
	5	53.1	53.24	51.40	51.51	53.26
	6	74.9	74.62	74.56	73.14	74.54
	7	70.2	70.15	67.90	68.15	70.19
	8	79.0	79.18	74.21	74.75	78.94
	9	62.4	62.36	62.60	60.86	62.26
	NAc	23.1	23.22		22.27	23.14
	C=O				175.3	175.6
	COOH					174.1
βGalNAc (1-4)	1		103.61	102.70	102.65	103.54
	2		53.23	50.80	52.28	53.24
	3		68.58	81.59	80.47	68.56
	4		71.71	67.71	68.07	71.82
	5		75.33	74.81	74.76	75.12
	6		61.85	60.32	62.13	61.71
	NAc		23.41		22.66	22.88
	C=O				174.90	175.6
αNeuAc (2-8) (α-Neu5Gc)	3	41.2	41.35			41.20
	4	69.4	69.37			69.10
	5	52.6	52.64			52.68
	6	73.5	73.56			73.48
	7	68.9	69.02			68.85
	8	72.6	72.62			72.49
	9	63.4	63.44			63.38
	NAc	23	22.92			23.16
	C=O					175.6
	COOH					174.1
Ceramide	1			69.86	69.74	70.48
	2			53.20	53.40	54.01
	3			70.63	70.84	71.58
	4			130.37	130.18	130.90
	5			133.75	133.23	134.19
	6			32.65	32.95	33.55
	7				30.58	30.46
	C=O					175.4

Table S3. Values of dihedral angels in the conformers obtained by annealing simulation with refinement of NMR data

Simulation	Conformation (°)			
	(ϕ2,φ2)	(ϕ3,φ3)	(ϕ4,φ4, ω4,χ4)	(ϕ5,φ5)
Thiophenyl GD2 (N=14)	-81.3±2.1 132.4±2.0	-143.6±1.6 -146.2±1.6	-173.3±1.4 118.0±2.5 -69.8±1.8 152.0±3.0	-87.0±2.6 -88.6±1.1
GD2 (N=16)	-119.8±0.8 161.0±0.8	-170.4±0.7 -137.1±0.9	170.1±1.5 89.5±3.5 48.2±1.5 152.4±1.2	-100.3±0.6 -71.9±2.6

The glycocidic angles are defined as follows: φ=O5-C1-O-CX' (C1-C2-O-C3' in Neu5Ac-α2-3-Gal) and ψ=C1-O-CX'-C(X-1)'. For the Neu5Ac-α2-8-Neu5Ac, φ=C1-C2-O-C8', ψ=C2-O-C8'-C7', ω=C6-C7-C8-C9 and X=C5-C6-C7-C8.

Table S4. Comparison of the experimental and calculated percentage fractional STD intensities for GD2/3F8 complex (T_{sat} = 3s) and the respective T1 relaxation time.

Proton	Experimental STDs (%)	STDs from CORCEMA-ST calculation (%)	T1(s)
NeuAc (2-3): H3E	9.3	7.6	0.67
NeuAc (2-3): CH3	5.5	2.0	1.64
NeuAc (2-8): CH3	4.4	2.9	1.68
GalNAc: CH3	4.6	1.8	1.12
Glc/Gla: H2	2.7 [a]	3.8 [b]	2.16 [a]

[a] These resonances overlap

[b] The calculation is for Gal:H2

Table S5-1. Proton Chemical shift of peptide M1 at pH=6.8 and T=288 K in 10%D_2O/90%H_2O

Residue	Chemical shift (ppm)				$^3J_{HN-H\alpha}$ (Hz)
	HN	Hα	Hβ	Others	
Tyr1	-	4.16	2.99,3.08	-	
Cys2	-	4.64	2.92, 3.03		
Gly3	8.01	3.96			5.00
Thr4	8.19	4.22	-	CH_3 1.20	6.00
Asn5	8.43	4.59	2.74, 2.79	NH_2 7.38, 6.90	5.52
Tyr6	8.05	4.41	3.00, 3.08	$H^{2,6}$ 7.08; $H^{3,5}$ 6.83	6.50
Asn7	8.29	4.65	2.71, 2.81	NH_2 7.43, 6.95	5.65
Gly8	8.20	3.88, 3.97			5.50
Cys9	8.06	4.60	2.89, 3.06		7.07
Tyr10	7.87	4.39	2.86, 3.07		8.00

Table S5-2. Proton Chemical shift of peptide SS58 at pH=6.0 and T=288 K in 10%D_2O/90%H_2O

Residue	Chemical shift (ppm)				$^3J_{HN\alpha}$ (Hz)
	HN	Hα	Hβ	Others	
Tyr1	-	4.25	3.05, 3.12	-	
Cys2	8.72	4.69	2.89, 3.06		7.44
Gly3	8.24	3.94			5.54
Gly4	8.18	3.92, 4.03			5.58
Ile5	8.07	4.08	1.86	Hγ 1.44,1.17; CH3γ 0.90; CH3δ 0.86	6.50
Ala6	8.41	4.15	1.31		5.63
Asn7	8.09	4.55	2.72, 2.79	NH2 7.57, 6.88	6.00
Tyr8	7.88	4.50	2.96, 3.02	$H^{2,6}$ 7.09; $H^{3,5}$ 6.80	6.11
Asn9	8.36	4.62	2.58, 2.71	NH2 7.54, 6.90	7.75
Cys10	8.08	4.62	2.92, 3.05		6.50
Try11	7.95	4.45	2.90, 3.09	$H^{2,6}$ 7.08; $H^{3,5}$ 6.82	7.50

Table S6. Proton chemical shift of peptide M50B at pH=6.0 and T=288 K in 10%D_2O/90%H_2O

Residue	Chemical shift (ppm)				$^3J_{HN-H\alpha}$ (Hz)
	HN	Hα	Hβ	Others	
Tyr1	-	4.16	3.00, 3.05	$H^{2,6}$ 7.08; $H^{3,5}$ 6.81	-
Cys2	-	4.67	2.90, 3.06		-
Gly3	8.08	3.92			5.62
Ile 4	7.90	4.08	1.82	Hγ 1.42,1.13; $CH_3\gamma$ 0.89; $CH_3\delta$ 0.81	6.76
Ala5	8.37	4.17		$CH_3\beta$ 1.32	5.61
Asn6	8.12	4.53	2.75	NH_2 7.52, 6.88	7.21
Tyr7	7.98	4.52	2.96,3.04	$H^{2,6}$ 7.10; $H^{3,5}$ 6.77	6.55
Asn8	8.41	4.56	2.68, 2.80	NH_2 7.59, 6.92	6.53
Gly9	8.09	3.86, 3.94			6.31
Cys10	8.01	4.55	2.87, 3.05		7.72
Tyr11	7.82	4.37	2.84, 3.06	$H^{2,6}$ 7.05; $H^{3,5}$ 6.77	8.13

Table S7. Statistics for the NMR structure calculations of the peptides in water

Parameter	M1	M50 (free state)	M50 (bound state)
Number of residues	10	11	11
Distance restrains	**63**	**75**	**134**
Intra-residue	47	58	64
Sequential	14	17	34
Short	2	0	25
Medium	0	0	2
Long	0	0	9
ϕ Angel restrains	8	10	0
Number of S-S bond restrains	1	1	1
NMR constraints violations			
NOE rms	0.021±0.008	0.049±0.005	0.058±0.004
NOE violation >0.5Å	0	0	0
J coupling restraints	0.56±0.11	0.59±0.12	N/A
Bond (Å)	0.0036±0.0003	0.0039±0.0002	0.0057±0.0003
Angle (º)	0.49±0.063	0.53±0.069	0.82±0.0074
Improper torsion (º)	1.3±0.25	1.2±0.26	2.29±0.36
Only hydrogen bond	0	0	0
Empirical total energy (kacl.mol^{-1})	-272.1±11.4	-299.6±38.1	-208.7±34.7
R.m.s deviation from the mean structure (Å)			
All residue over backbone, 2nd structure	1.43±0.24	1.78±0.32	0.55±0.51
All heavy atoms, 2nd structure	2.53±0.57	2.99±0.39	0.84±0.83
Ramachandran statistics			
Residues in allowed region	95.0%	90%	100%
Residues in disallowed region	5.0%	10%	0%

METHODS

Cells. EL4 GD2-positive murine lymphoma were grown in RPMI 1640 medium (Life Technologies, Carlsbad, CA) supplemented with 5% fetal bovine serum (FBS), 2 mM glutamine, 10 mM HEPES and penicillin/streptomycin at 37°C in 5% CO_2 humidified atmosphere.

NMR spectroscopy of ganglioside GD2 and thiophenyl GD2. Mixed micelles were prepared by dissolving ganglioside GD2 (1 mM) and the detergent dodecylphosphocholine-d38 (DPC, molar ratio 1:40) in deuterated 50 mM phospate buffer (pD 6.6); the mixture was exchanged three times with D_2O, with intermediate lyophilization, dried under high vacuum at –56° C, and finally dissolved in 300 μL of buffer (*33*). Thiophenyl GD2 was dissolved in deuterated 50 mM phosphate buffer (pD 6.6). Spectra were obtained at 308 K or 298 K, respectively. ^{1}H-^{1}H homonuclear experiments included gradient-selected COSY spectra, DQF-COSY, TOCSY with 75 ms 7.5 KHz DIPSI spinlock, ROESY with 200 ms 2 KHz spinlock and NOESY spectra with mixing times of 50-200 ms. In general, data sets were recorded with sweep widths of 10 ppm in both dimensions, with 512 increments in the indirect dimension and 2000 data points recorded in the acquisition dimension. Relaxation delays of 1.2-1.5 s were used. Solvent suppression was achieved with presaturation during d1 when necessary. To aid in assignment of ganglioside GD2, ^{13}C HMBC and HSQC spectra were also recorded. The gradient selected HMBC was recorded with sweep widths of 240 ppm in the carbon

dimension and 10 ppm in proton, with a 400 x 1706 point data matrix. The gradient-selected HSQC was recorded with a sweep width of 80 ppm in carbon and 10 ppm in proton and a 512x640 point data matrix. ^{1}H chemical shifts were referred to an internal sodium 2,2-dimethyl-2-silapentane-5-sulfonate standard (DSS) at 0.00 ppm. ^{13}C chemical shifts were indirectly referenced to the proton frequency.

STD NMR spectroscopy. A 1D saturation transfer difference pulse sequence with internal subtraction via phase cycling was employed to record difference spectra (*210*). Residual H_2O signal was removed using a 3-9-19 WATERGATE pulse sequence, with a 150 ms interpulse delay. On-resonance irradiation was performed at 0 ppm, for mAb 3F8, or -1 ppm for ganglioside GD2 micelles, with off-resonance irradiation at 34.8 ppm. Reference spectra were recorded using the same pulse sequence with saturation pulses applied at 34.8 ppm, and no internal subtraction. The irradiation power was ($\gamma/2\pi$) B1= 65 Hz applied through a train of 50 ms eburp1 pulses with a 1 ms delay between the pulses. Experiments were recorded with saturation times of 5 s, 3 s, 2 s and 1 s. The relaxation delay was set to 0.1 s in all cases. A 30 ms spin-lock pulse with a strength of (g/2p) B1= 1300 Hz was used to eliminate background antibody/ganglioside signals. Spectra were recorded with 32000 points, a sweep width of 16 ppm, and 1024 to 2048 transients. 1D STD spectra were processed by MestReNova-Lite v5.2.1-3586 (Mestrelab Research SL, Santiago de Compostela, SPAIN).

Structure calculations. Different mixing times of NOESY spectra were used to evaluate the linear build-up of NOEs. Molecular dynamics simulations with NMR refinement in AMBER 9 GB Model (*211*) were employed to determine the energetically favorable conformations of the two types of unbound ganglioside. The distance restraints derived from NOE or ROE data were produced by the software Felix 2004 (Accelrys, Inc). The S-M-W bins method, which categorizes connectivities based on distance as strong (2.5 Å), medium (3.5 Å), and weak (6.0 Å) was used to convert the calculated distances to restraints and generate qualitative upper-bound restraints. The intra-residue distance of 1.78 Å between the H3ax and H3eq of N-acetyl neuraminic acid was used as a reference for distance calibration (*34*). In the simulation, the lipid portion of molecular was replaced by a truncated ceramide (Figure 1, panel A). The topology file of truncated ceramide was produced by ANTECHAMBER (*214*). The energy minimization and simulation with distance restrains used the SANDER module of the AMBER 9 program with the AMBER force field (Glycam_04.dat (*212*) and GAFF (*213*)) with a dielectric constant of 80. After minimization, the system was heated up to 350 K from 5 K, and then was cooled down to 5 K. Total simulation time was 1 ns. The simulated annealing was repeated five times until there was no improvement on potential energy. This final NMR structure was used as a starting input into 1ns restrained molecular dynamics simulations (rMD) to produce 8 families of conformers according to the combinations of dihedral angles.

And one conformer from each family was then as a starting structure for an additional simulated annealing step with NMR refinement again. The AMBER 9 suite of programs together with the AMBER force field (Glycam_04.dat and GAFF) was used to perform 10ns MD simulations of the two types of GD2. Each GD2 conformation was solvated in a truncated octahedron TIP3P water box. Sodium counterions were added to maintain electroneutrality of the system. The system was minimized first, followed by heating from 100 K to 303 K over 10 ps in the canonical ensemble (NVT), and by equilibrating to adjust the solvent density under 1 atm pressure over 10 ps in the isothermal isobaric ensemble (NPT) simulation. After an additional 100 ps simulation, a 1 ns production NPT run was obtained with snapshots collected every 1 ps. Langevin dynamics was used for temperature control. Bond lengths involving bonds to hydrogen atoms were constrained by SHAKE. The conformations of the peptides are constrained by an intra-chain disulfide between two cysteines. Cross-peaks from a NOESY spectrum with a mixing time of 100 and 200 ms, which lies within the initial build-up of the NOE curve, were measured with SPARKY. Coupling constants (^3JH_N-H_α) measured from 1D proton and 2D COSY spectra were used to constrain the backbone ϕ angles. 3D structures of peptide ligands were calculated by the software ARIA 2.2/CNS 1.2 with the network anchoring approach (*215*). From the 200 structures calculated for each peptide, the 20 lowest energy ones were chosen and clustered by MMTSB (*216*). Structures were visualized using

Discovery Studio 1.7 (Accelrys, Inc), PyMOL and VMD-Xplor on Mac OS X.

Docking Studies.

Structure prediction, model building and refinement. The 3-D structure of another GD2 antibody ME36.1 Fab fragment of lower affinity is available (*260*). The sequence identity observed between the Fab (fragment for antigen binding) of the light chain (VL) and the heavy chain (VH) of the 3F8 and the Fab of the VL and VH of ME36.11 antibody are 59% and 46% respectively. The ME36.1 was not selected as a template as sequence identity was not significant at the CDR regions and a number of insertions and deletions are needed to build the 3-D model (Figure S5). Instead crystal structure of malaria antigen AMA1 antibody Fab (pdb code 2q8a) (*217*) and 13G5 antibody Fab (pdb code 2gjz) (*218*) were selected as templates for light chain (84%) and heavy chain (84%) of 3F8 respectively. With these templates, the CDR's of both chains were readily aligned (Figure S6).

As 3F8 corresponds to IgG class, each Fab fragment of light and heavy chain has one conserved intrachain disulfide bridge which is important for creating and maintaining CDR's loops (L1, L2 and L3 for light chain and H1, H2 and H3 for heavy chain). For these intrachain inter-beta-strand disulfide bonds, the sequence alignment and template structure place the cys residues within the disulfide bonding distance. The homology modelling was carried out using the program COMPOSER in

SYBYL 7.3 (Tripos Inc, St Louis, MO). Two and three structurally conserved regions (SCRs) were used to build an initial model of Fab of the 3F8 light chain and heavy chain respectively. Only one insertion for light chain and two insertions for heavy chain were required relative to the template. Structural refinement of the complex was done by stepwise energy minimization in Sybyl using the AMBER all atom force field (*261*) to a gradient of 0.05 kcal/mol/Å. First, only the side chains of the SCRs were energy-minimized followed by energy minimization of the entire structure.

The energy-minimized model was then used as starting point for molecular dynamics (MD) simulation, using the AMBER ff03 force field in the AMBER 9 suite of programs (*211*). The protein was solvated in a truncated octahedron TIP3P water box (*262*). The distance between the wall of the box and the closest atom of the solute was 12.0 Å and the closest distance between the solute and solvent atoms was 0.8 Å. Counterions (Na^+) were added to maintain electroneutrality of the system. The solvated system was energy-minimized with harmonic restraints of 10 kcal mol^{-1} $Å^{-2}$ on all solute atoms, followed by heating from 100 K to 300 K over 25 ps in the canonical ensemble (NVT). Then, the solvent density was adjusted by running a 25-ps isothermal isobaric ensemble (NPT) simulation under 1 atm pressure. The harmonic restraints were then gradually reduced to zero with four rounds of 25-ps NPT simulations. After an additional 25-ps simulation, a 5 ns production NPT run was carried out with snapshots collected every 1 ps. For all simulations, a 2 fs

time-step and 9 Å non-bonded cut-off were used. The Particle Mesh Ewald (PME) method was used to treat long-range electrostatic interactions (*263*), and bond lengths involving bonds to hydrogen atoms were constrained by SHAKE (*264*). The MD average structure was obtained from the most stable part of the trajectory for docking study (Figure 4).

The modeled structure preserves all immunoglobulin folds common to all Fab structures. The 3-D model of Fab fragment of light and heavy chain consist of antiparallel β-sheets linked by an intra domain disulfide bonds which are completely buried in the core of each domain, also preserved in this 3-D model of 3F8 Fab fragment of antibody. The hypervariable complementarity determining regions (CDRs) are located in the loops connecting β starnds of the Fab fragments of the heavy and light chain. Visual inspection of the trajectory showed the global fold remain essentially intact. The PROCHECK program (*265*) does not flag any conformational problems with the structure. Figure S7 shows superimposition of three average structures during three different time frames in the trajectory. The antigen-binding site is predicted to be a wide shallow grove formed mainly by the CDRs loops (L1, L2 and L3 and H1, H2 and H3) of both chains. Superimposition of the model of 3F8 and solved crystal structure of another anti GD2 antibody (ME36.1) (data not shown) showed more elongated H3 loop of heavy chain, which created

broader area for antigen binding and may explain stronger affinity of GD2 for 3F8 and then ME36.1.

Molecular docking of GD2 and CORCEMA-ST calculations. Theoretical STD values were predicted by the CORCEMA-ST protocol (*221*) based on the binding mode generated from MD simulations for interactions of thiophenyl-GD2 and a 3F8 Fab fragment. Spectral densities were calculated only for proton pairs having a distance of 6 Å or less. In the calculations, thiophenyl-GD2 and the 13 amino acid residues within the binding pocket were included. The calculations were performed using the following parameters: order parameters S^2 = 0.25 for intra-methyl relaxation, S^2 = 0.85 for methyl–X relaxation; the concentration of ligand was 500 μM and the ratio of ligand: protein was 50:1; k_{on} was set to $5x10^7$ s^{-1} M^{-1} for the best fitting results. The value of the dissociation constant (K_D) for thiophenyl-GD2 that was used in the calculation was 10^{-6} M, calculated from a long-term MD simulation. The final optimized values of the correlation times (τ) were 1.2 ns and 80 ns for the ligand in the free and bound states respectively. STD values were calculated as [(*I*(*t*)(*k*)-(*I*0(*k*))/I0(*k*))x100], with *I*0(*k*) being the intensity of the signal of proton *k* without saturation transfer at time *t*=0, and *I*(*t*)*k* being the intensity of proton *k* after saturation transfer during the saturation time *t*. For the comparison to the experimental STD values, an NOE *R*-factor is defined as:

$$\text{R-factor} = \sqrt{\frac{\sum (S_{expt,\,k} - S_{calk,\,k})^2}{\sum (S_{expt,\,k})^2}}$$

In these equations, $S_{expt,k}$ and $S_{calc,k}$ refer to experimental and calculated STD values for proton *k*.

The values for k_{on} and τ were optimized in the CORCEMA-ST calculations. k_{on} is in the range of diffusion controlled association with no major conformational rearrangement of ligand or receptor upon binding, which is consistent with MD results. The correlation times (τ) are reasonable given the sizes of the ligand (~1,200 MW) and receptor (~155,000 MW). K_D was taken from MD simulations, and falls within the range of dissociation constants (10^{-3}-10^{-8}) that result in efficient build up of saturation. Also we note that the K_D estimated for the ligand from the competitive ELISA corresponds well to the values used for CORCEMA-ST calculations. The S^2 values are as usually defined within the software.

Appendix II

A book chapter in Methods in Molecular Biology

-Rational design of peptide ligands against a glycolipid by NMR studies

Wenyong Tong[1, 2 *], Tara Sprules[5 *], Kalle Gehring[3, 5], H. Uri Saragovi [1, 2, 4, *]

[1]Lady Davis Institute-Jewish General Hospital, Montréal, Quebec, Canada, H3T 1E2.

Departments of [2]Pharmacology and Therapeutics, [3]Biochemistry, [4]Oncology and the Cancer Center, McGill University, Montréal, Quebec, Canada H3G 1Y6.

[5]Quebec/Eastern Canada High Field NMR Facility, McGill University, Montréal, Quebec, Canada, H3A 2A7.

* co-first authors

* * Correspondence should be addressed to HUS.

Lady Davis Institute-Jewish General Hospital

3755 Cote St. Catherine, E-535

Montreal, Quebec, CANADA H3T 1E2

Summary

Ganglioside GD2 is a cell surface glycosphingolipid that is targeted clinically for cancer diagnosis, prognosis and therapy. The conformations of free GD2 and of GD2 bound to anti-GD2 mAb 3F8 were resolved by saturation transfer difference NMR and molecular modeling. Then small molecule cyclic peptide ligands that bind to GD2 selectively were designed, and shown to affect GD2-mediated signal transduction. The solution structure of the GD2-bound conformation of the peptide ligands showed an induced-fit binding mechanism. This work furthers the concept of rationally designing ligands for carbohydrate targets; and may be expanded to other clinically relevant gangliosides.

Key words: Saturation transfer difference NMR, Transferred NOE, Antibody-carbohydrate interactions, Peptide-carbohydrate interaction, NMR structure calculations, Molecular modeling, ganglioside GD2, Peptide mimetics, Cancer

Introduction

Nuclear magnetic resonance (NMR) spectroscopy has become a very important tool for drug discovery, not only because of its ability to elucidate molecular structure, but also for its great potential to monitor intermolecular interactions at the atomic level. NMR can be used for assessing target druggability, for pharmacophore identification, for hit validation, and for structure-based design **(*266*)**. NMR can detect interactions in systems that may not be amenable to crystallography.

In particular, techniques such as saturation transfer difference (STD) NMR and transferred nuclear Overhuaser effects (trNOEs) are very useful when working with ligands with dissociation constants K_D in the range of 10^{-3}-10^{-8} M. This is because the approach takes advantage of the different NMR relaxation properties of large and small molecules to transfer information from the bound, NMR “invisible” state of the ligand, to the free, “visible” state. The STD experiment can identify which functional groups or modules in a ligand are most important for establishing the intermolecular interaction with its target. In the case of monoclonal antibodies (mAbs), it is possible to identify the binding epitope **(*199*)**.

Transferred NOEs can be used to calculate a three-dimensional (3D) structure of the bound ligand. The NOE experiments provide important information by measuring the average inter-atomic distances to ~6 Å. Distance information is supplemented by the measurement of torsion angles from through-bond scalar J-couplings. These restraints are input

into a molecular modeling algorithm to generate a family of representative structures. Finally, NMR data is complemented by the use of molecular dynamics simulation (MD). The results can then be applied to rationally design a more potent compound **(*267*).** These approaches have been used successfully for protein targets.

Here, a novel example of NMR based structure design is presented targeting the carbohydrate portion of a cell membrane glycolipid by using saturation transfer difference NMR and transferred nuclear Overhauser effects (**Fig. 1**) **(*36*)**. Some glycolipids such as ganglioside GD2 (**Fig. 2**) are highly expressed in cancer tissues, for example neuroblastomas, small-cell lung carcinomas, and melanomas, but have a very low level of expression in normal tissues. GD2 is thus targeted clinically for diagnosis and immunotherapy using anti-GD2 monoclonal antibodies (mAb), such as IgG3 mAb 3F8 **(*192*)**. The importance of gangliosides in tumorigenesis, tumor progression and tumor metastasis may be due to their biological functions that include cell recognition, cell matrix attachment, cell growth and differentiation **(*13, 193*)**. Since those cell surface glycolipids can induce the signal transduction cascade, we studied whether NMR-based approaches can generate GD2-selective ligands with biological activity.

STD NMR spectroscopy was used to study the binding characteristics of anti-GD2 mAb 3F8 to two forms of GD2; (i) intact ganglioside GD2 incorporated in dodecylphosphocholine micelles (DPC, that forms micelles as a plasma membrane mimic), and (ii) a water soluble phenylthioether-

analog of GD2 that lacks ceramide and lipids, the “GD2 carbohydrate head”. With the aid of molecular modeling, docking and theoretical STDs calculated by the CORCEMA-ST program **(*221*)**, a model of GD2/3F8 was proposed that matched the experimentally determined binding epitope. Then three GD2-selective peptidic ligands, which mimic mAb 3F8, were synthesized by using mAb mimicry designs to keep the β-turn conformation **(*200*)**. The detergent-like properties of gangliosides **(*204*)** were utilized to form lipid raft-mimicking GD2 micelles to study the peptide/carbohydrate interaction by NMR. However, the intensities of observed STDs are primarily dependent upon the longitudinal relaxation rate of the free ligand protons at long saturation times (T1 effects). At the relaxation times used for peptide/GD2 micelle experiments (>2 s) the STD intensities were dominated by T1 effects**(*202*).** The conformation of the peptidic GD2 ligands bound to the head group of GD2 was therefore further characterized by trNOE experiments in order to accurately map the binding epitope.

2. Materials

2.1 Chemicals and regents

1. Dodecylphosphocholine-d_{38} (DPC).
2. Amicon centrifugal filters, 10 kDa cutoff, Millipore.
3. Deuterated water.
4. 50 mM of deuterated phosphate buffer (pD 6.2) made with 70 mg potassium dideuteriumphosphate and 17 mg dipotassium

deuterium phosphate in 12.5 ml of 100% D_2O (Ionic strength 0.065).

2.2 Instrumentation

1. Waters 600 HPLC and C-18 semipreparative column.
2. 500 MHz Varian INOVA NMR spectrometer with an H {CN} triple resonance cold probe with Z-gradients and variable temperature control (5-50C), and BioPack pulse sequence library.
3. Agilent capLC-MSD Quad.
4. pH meter, with microelectrode that will fit in microfuge tubes or NMR tubes.
5. Heto powerDry 3300 lyophilizer.
6. Nano-drop 1000, UV meter, Wilmington.

2.3 Software for the analysis of NMR data

1. Molecular modeling software: ANTECHAMBER**(*214*)** and AMBER 9**(*211*)**with the AMBER force field (Glycam_04.dat and GAFF), ARIA 2.2/CNS 1.2**(*215*)** and MMTSB for clustering**(*216*)**.
2. NMR software: Felix 2004 (Accelrys, Inc), SPARKY (T. D. Goddard and D. G. Kneller, University of California, San Francisco), NMRPipe **(*209*)**, MestReNova-Lite v5.2.1-3586 (Mestrelab Research SL), CORCEMA-ST program provided by Dr. N. R. Krishna, University of Alabama at Birmingham.

3. Structure presenting software: DiscoveryStudio 1.7 (Accelrys, Inc), PyMOL and VMD-Xplor.

3. Methods

3.1 Sample preparation for STD NMR experiments to study the interaction between antibody and carbohydrate

1. Thiophenyl GD2 (**Note 1**) (**Fig. 2**) was synthesized from thiophenyl GD3**(*35*)** using a recombinant β-1,4-*N*-acetylgalactosaminyltransferase (CgtA, construct CJL-30) and an UDP-GlcNAc 4-epimerase (Gne, construct CPG-13) originally cloned from *Campylobacter jejuni* **(*26, 207*).** The sample was purified (>98%) by HPLC using a C-18 semipreparative column, and was verified by mass spectrometry (ESI-MS) and NMR. The measured molecular weight of thiophenyl GD2 corresponded to expected values. Thiophenyl GD2 was dissolved in 50 mM deuterated phosphate buffer (pD 6.2).
2. Mixed micelles were prepared by dissolving ganglioside GD2 (1 mM) and the detergent dodecylphosphocholine-d_{38} (DPC) in a molar ratio of 1:40 in 50 mM deuterated phosphate buffer (pD 6.2); the mixture was exchanged three times with D_2O, with intermediate lyophilization, dried under high vacuum at –56° C, and finally dissolved in 300 μL of buffer (*see* **Note 2**).

3. 3F8 was concentrated using Amicon centrifugal filters and exchanged several times with a 50 mM deuterated phosphate buffer (pD 6.2). The mAb preparations were combined with freeze-dried thiophenyl GD2 or ganglioside GD2 in DPC micelles at molar ratios ranging from 1:25 to 1:200; the final oligosaccharide concentrations were between 0.125 and 1 mM.

3.2 STD NMR experiments to study the interaction between antibody and carbohydrate

1. NMR assignments. 1D proton spectra, as well as 2D TOCSY, COSY, NOESY, ROESY, ^{13}C HSQC and ^{13}C HMBC experiments were recorded using the spectrometer's standard pulse sequences for both thiophenyl GD2 (25°C) and GD2-DPC micelles (35°C) in the absence of mAb3F8. These experiments give complete ^{1}H and ^{13}C assignments for the two compounds. T1 relaxation rates were measured for thiophenyl GD2 using a standard inversion-recovery pulse sequence (*see* **Note 3**).
2. STD NMR (**Fig. 3**). A 1D saturation transfer difference pulse sequence with internal subtraction via phase cycling and a 3-9-19 WATERGATE pulse train for H_2O suppression was employed to record reference and difference STD spectra (*see* **Note 4**) **(*210*)**.

1. 90-degree high-power proton pulse widths, the offset for water suppression and on-resonance saturation (see below) were optimized for each sample.

2. Off-resonance irradiation was set to 34.8 ppm.

3. The irradiation power was (~ 2)B_1= 65 Hz, applied through a train of 50 ms eburp1 pulses with a 1 ms delay between the pulses. The relaxation delay was set to 0.1 s in all cases. A 30 ms spin-lock pulse with a strength of (~ 2)B_1= 1300 Hz was used to eliminate background antibody/ganglioside signals.

4. Spectra were recorded with 32000 points, a sweep width of 16 ppm, and 1024 to 2048 transients (*see* **Note 5**). A series of spectra with different saturation times (1, 2, 3 and 5s) and at different ligand: macromolecule ratios were recorded for each system studied. It is important to record an STD spectrum for ligand in the absence of macromolecule to ensure that on-resonance saturation does not perturb any of its signals.

5. Reference spectra were recorded using the same pulse sequence with saturation pulses applied at 34.8 ppm, and no internal subtraction.

5.1 Thiophenyl GD2. Reference STD and STD difference spectra (5s saturation) were recorded for thiophenyl GD2 in

the absence of mAb. On-resonance saturation at 0 ppm did not result in any signal in the difference spectrum, indicating that, as expected, the saturation pulse train was far enough away from the ligand resonances, and was not exciting a broader spectral region than it was supposed to. STD difference spectra recorded using the same experimental set-up with different saturation times for ligand:mAb ratios from 200:1 to 25:1 showed signals arising from specific protons, therefore saturation was being transferred from mAb 3F8 to the carbohydrate.

5.2 GD2-DPC micelles. Reference STD and STD difference spectra (5s saturation) were recorded for GD2-DPC micelles in the absence of mAb. On-resonance saturation at -1 ppm showed some signal at 1.25 ppm, resulting from saturation of the DPC micelles. Upon addition of mAb a series of STD difference spectra with on–resonance saturation at 9.3, 1, -1 and -2 ppm were recorded. Saturation at 9.3 ppm (where only mAb 3F8 signals were expected) and -2 ppm gave very similar results; spectra recorded with on-resonance saturation at 1 ppm and -1 ppm exhibited strong enhancement of ceramide signals, indicating that the transmitter was too close to the residual proton signals of the DPC micelles. Therefore -2 ppm was

used as on-resonance saturation to record a series of STD spectra at different saturation times and ratios of mAb to GD2.

3.3 Structure calculations of two types of GD2

1. Distance restraints derived from NOE or ROE data were produced by the software Felix 2004. The S-M-W bins method, which categorizes connectivities based on distance as strong (2.5 Å), medium (3.5 Å), and weak (6.0 Å), was used to convert the calculated distances to restraints and generate qualitative upper-bound restraints (*see* **Note 6)**.
2. The intra-residue distance of 1.78 Å between the H3ax and H3eq of N-acetyl neuraminic acid was used as a reference for distance calibration **(*34*)**.
3. In the simulation, the lipid portion of molecular was replaced by a truncated ceramide (**Fig. 1**). The topology file of the truncated ceramide was produced by ANTECHAMBER.
4. The energy minimization and simulation with distance restraints used the SANDER module of the AMBER 9 program with the AMBER force field (Glycam_04.dat and GAFF) with a dielectric constant of 80. After minimization, the system was heated up to 350 K from 5 K, and then was cooled down to 5 K. Total simulation time was 1 ns.

5. The simulated annealing was repeated (five times) until there was no change on potential energy. This final NMR structure was used as a starting input into 1ns restrained molecular dynamics simulations (rMD) to produce 8 families of conformers according to the combinations of dihedral angles of glycosidic bonds.
6. One conformer from each family was then used as a starting structure for an additional simulated annealing step with NMR refinement.
7. The AMBER 9 suite of programs together with the AMBER force field (Glycam_04.dat and GAFF) was used to perform 10ns MD simulations for the two types of GD2. Each GD2 conformation was solvated in a truncated octahedron TIP3P water box. Sodium counterions were added to maintain electroneutrality of the system.
8. The system was minimized first, followed by heating from 100 K to 303 K over 10 ps in the canonical ensemble (NVT), and by equilibrating to adjust the solvent density under 1 atm pressure over 10 ps in the isothermal isobaric ensemble (NPT) simulation. After an additional 100 ps simulation, a 1 ns production NPT run was obtained with snapshots collected every 1 ps. Langevin dynamics was used for temperature control. Bond lengths involving bonds to hydrogen atoms were constrained by SHAKE.

3.4 Molecular Modeling and calculation of STD signals

1. GD2 docking in the putative binding site of Fab fragment of 3F8 was performed with in-house docking software (*see* **Note 7**). A box around the 6 CDRs of the heavy and light chain of 3F8 (*see* **Note 8**) was constructed and defined the binding region to be searched.
2. In order to sample various conformations, 12000 conformers of GD2 were generated from snapshots taken from an MD simulation (12-ns) in explicit water using AMBER ff03 and GAFF force fields starting from the NMR structures. Partial charges of the conformers were calculated by the AM1-BCC method **(*219*)**.
3. Each of the docked conformers of GD2 was exhaustively docked into the 3F8 Fab and scored. The top-scoring 100 poses were clustered. The most populated cluster was taken to be representative of the true GD2 binding mode in the Fab of 3F8 antibody. The best-scored pose from this cluster was selected to represent the binding model. This pose was subjected to minimization followed by a 5-ns MD simulation.
4. The MD trajectory was used to calculate a predicted binding free energy of the complex using a Solvated Interaction Energy (SIE) approach **(*220*).**
5. Theoretical STD values were predicted by the CORCEMA-ST protocol based on the binding mode (**Fig. 4**) generated from MD

simulations for interactions of thiophenyl GD2 and a 3F8 Fab fragment. Spectral densities were calculated only for proton pairs having a distance of 6 Å or less. In the calculations, thiophenyl-GD2 and the 13 amino acid residues within the binding pocket were included (*see* **Note 9**).

6. The order parameters S^2 was set to 0.25 for intra-methyl relaxation, while S^2 of 0.85 was used for methyl–X relaxation.
7. The concentration of ligand was 500 µM and the ratio of ligand: protein was 50:1.
8. k_{on} was set to $5x10^7$ s^{-1} M^{-1} for the best fitting results. The value of the dissociation constant (K_D) for thiophenyl-GD2 that was used in the calculation was 10^{-6} M, calculated from a long-term MD simulation.
9. The final optimized values of the correlation times (τ) were 1.2 ns and 80 ns for the ligand in the free and bound states respectively.
10. STD values were calculated as [($I(t)(k)$- ($I0(k)$/I0(k))x100], with $I0(k)$ being the intensity of the signal of proton k without saturation transfer at time t=0, and $I(t)(k)$ being the intensity of proton k after saturation transfer during the saturation time t. For the comparison to the experimental STD values, an NOE R-factor is defined as (*see* **Note 10**) (**Table 1**):

$$\text{R-factor} = \sqrt{\frac{\sum (S_{expt,\,k} - S_{calk,\,k})^2}{\sum (S_{expt,\,k})^2}}$$

3.5 Sample preparation for STD NMR experiments to study the interaction of peptides and glycolipid micelles

1. Ganglioside GD2 was subjected to three cycles of freeze-drying with D_2O to remove traces of water and to prepare a stock solution with a final concentration of 3 mM in 50 mM deuterated phosphate buffer, pD 6.2. Dilution effects from addition of this GD2 stock solution to peptide ligand solution to make different ratios were minimal (*see* **Note 11**).

2. Stock solutions of peptide ligands, 2 to 3 mM each, were prepared by dissolving them in 50 mM deuterated phosphate buffer (*see* **Note 12**). The concentrations of the peptides were determined by UV (Nano-drop 1000) at 280 nM. 1D STD NMR spectra were acquired at 298 K for a variety of peptide to GD2 ratios.

3.6 STD NMR experiments to study the interaction of peptides and glycolipid micelles

1. NMR assignments. 1D proton spectra, as well as 2D TOCSY, COSY, NOESY and ROESY experiments in 90% H_2O/10% D_2O and 100% D_2O were recorded using the spectrometer's standard pulse sequences (with presaturation for water suppression) (*see* **Note 13**) at 25°C. Complete ^1H assignments were obtained for the

peptide. T1 relaxation times were recorded using the standard inversion recovery setup.

2. STD spectra (**Fig. 5**) for the peptide were recorded in 100% D_2O and 90% H_2O/10% D_2O. As described above for the ganglioside, an STD difference spectrum was recorded for the peptide in the absence of ganglioside GD2 to confirm that there was no saturation of the peptide at the chosen on-resonance frequency (0 ppm). Reference spectra and a series of STD difference spectra were recorded for different saturation times and peptide-ganglioside concentrations.

3.7 Transferred NOE experiments (Fig. 6)

1. Control spectrum. 200 ms NOESY of peptide alone. The standard NOESY pulse sequence, with presaturation for suppression of H_2O signal was used. The relaxation delay was 1.2s, sweep width 16 ppm, 2000 points were collected in the direct dimension and 256 complex points in the indirect dimension with a mixing time of 200 ms and 16 transients. If the peptide is unstructured in the absence of binding partner there will be very few cross peaks in this spectrum, and they may be of opposite sign from the diagonal.

2. Transferred NOEs. Similar to the STD experiment, in a weakly binding system, as the ligand is transiently bound to a macromolecule, NOEs between ligand atoms in the bound form develop and this information is maintained in the signal of the free peptide when the peptide dissociates. The same experimental setup is used as for the NOESY of the free ligand. If the peptide

becomes structured upon binding macromolecule, there will be many more NOEs visible. The same conditions as described above were used to record a NOESY for the peptide in the presence of ganglioside GD2. The ganglioside resonances are broad enough that there was no need to suppress their signal. A short spin-lock as in the STD experiment can be used to suppress macromolecule signal if it interferes with the 2D spectrum. Additional NOESY spectra with mixing times of 50 and 100 ms were also recorded to assess signal build-up to ensure that correct intensities were used in subsequent structure calculations.

3.8 Structure calculations of unbound and bound peptide ligands.

1. Cross-peaks from NOESY spectra with mixing times of 100 and 200 ms, which lie within the initial build-up of the NOE curve, were measured with SPARKY.

2. Coupling constants (^3JH_N-H_α) measured from 1D proton and 2D COSY spectra were used to constrain the backbone ϕ angles.

3. The conformations of the peptides are constrained by an intra-chain disulfide between two cysteines.

4. 3D structures of peptide ligands were calculated by the software ARIA 2.2/CNS 1.2 with the network anchoring approach.

5. From the 200 structures calculated for each peptide, the 20 lowest energy ones were chosen and clustered by MMTSB.

6. Structures were visualized using Discovery Studio 1.7, PyMOL and VMD-Xplor on Mac OS X.

4. Notes

1. Ganglisoides, as amphiphilic compounds, spontaneously form micelles (aggregates of high molecular weight) when present in water. Therefore a ganglioside GD2 sugar analogue, lacking the lipophilic ceramide functionality, was designed in order to study its conformations and interactions with the antibody in aqueous solution.

2. Intact ganglioside GD2 can be studied through NMR by inserting the whole molecule into DPC or SDS micelles in an appropriate ratio. The sugar head group is solvent exposed and exhibits sharp line-widths in NMR spectra.

3. Prior to recording any NMR spectra, the probe was tuned to the appropriate nuclei, samples were shimmed using automatic gradient shimming and the deuterium lock was adjusted to be exactly on resonance. 90-degree proton pulse-widths were measured for each sample, and the transmitter offset for H_2O suppression was optimized.

4. It has been observed that STD intensities can be influenced by the ligand proton's T1 relaxation rate **(*202*)**. At longer saturation times signals with longer T1s will appear enhanced with respect to signals arising from protons with shorter T1s. Therefore knowledge

of the T1 relaxation rates of the individual protons in a ligand is important in order to assess the relative importance of different signals in an STD spectrum. It has been proposed that the rate at which the STD signal builds up at short relaxation times may be a more accurate indication of a binding epitope. In practice it may not always be possible to obtain good signal to noise in spectra recorded with very short saturation times.

5. The pulse sequence used for this study was kindly shared by Albin Otter, University of Alberta. Since this time a version of the STD pulse sequence has been included in the VNMR BioPack Pulse sequence library. It is very similar to the one used in this study, with DPFGSE solvent suppression instead of WATERGATE.

6. Different mixing times of NOESY spectra were used to evaluate the linear build-up of NOEs.

7. There are many other docking programs such as AUTODOCK that can be used.

8. The homology structure of Fab fragment of 3F8 was built up based on crystal structure of malaria antigen AMA1 antibody Fab (pdb code 2q8a) **(*217*)** and 13G5 antibody Fab (pdb code 2gjz) **(*218*)** selected as templates for light chain (84%) and heavy chain (84%) of 3F8 respectively. If there are crystal or NMR structures of the protein of interest available, they can be directly input into the docking programs.

9. Software such as DiscoveryStudio can be used to determine amino acid residues within the binding pocket.

10. R-factor can be used as quality control of docking model. The smaller the R-factor (<0.5), the more reflective of the true binding mode, providing more accurate information for drug design.

11. The 1D spectrum of ganglioside GD2 showed that it formed micelles at the concentrations used in the STD and trNOE experiments. Linewidths were very broad in comparison to thiophenyl GD2 or the sugar resonances from ganglioside GD2 embedded in DPC micelles. The cmc for ganglioside GD2 has not been reported, however values for related gangliosides range from 3.9×10^{-8} M to 3.4×10^{-9} M **(*204*)**, well below the lowest concentration of GD2 used in this study.

12. Solubility and pH of peptide solution are very important for NMR experiments. The pH of the final peptide solution in water should be checked, as it is difficult to remove traces of trifluoroacetic acid (TFA) after reverse-phase HPLC (a common step in peptide purification). Presence of TFA may result in lower than expected pH upon dissolution of the peptide. It is important to ensure that the peptide is completely soluble. If needed, the pH or the concentration may be changed to improve solubility.

13. Solvent presaturation was used for 2D spectra, in general watergate should provide equivalent or superior solvent

suppression, however on our system we find that due to longer gradient recovery times on the cryogenic probe, presaturation provides better solvent suppression despite lower signal intensity of exchangeable protons.

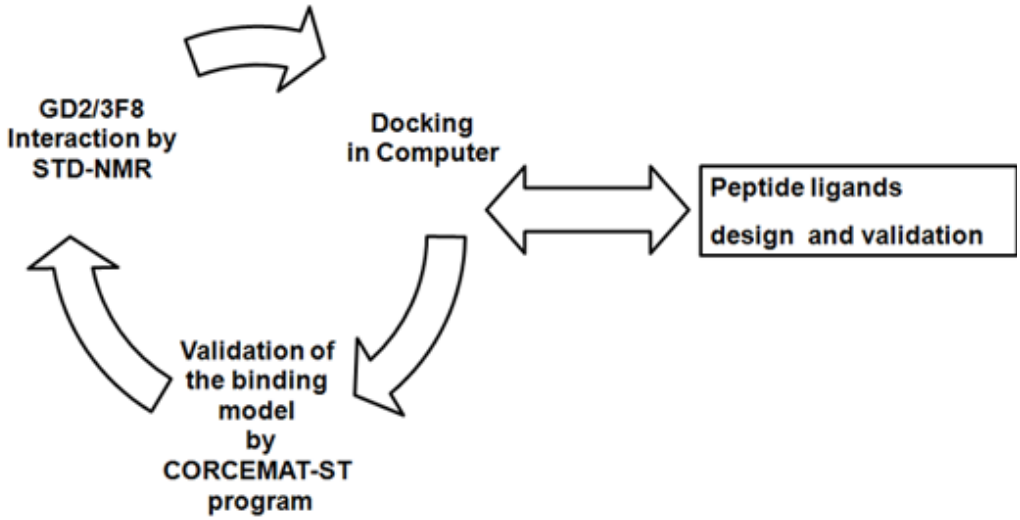

Fig. 1 Structure-based drug design by NMR.

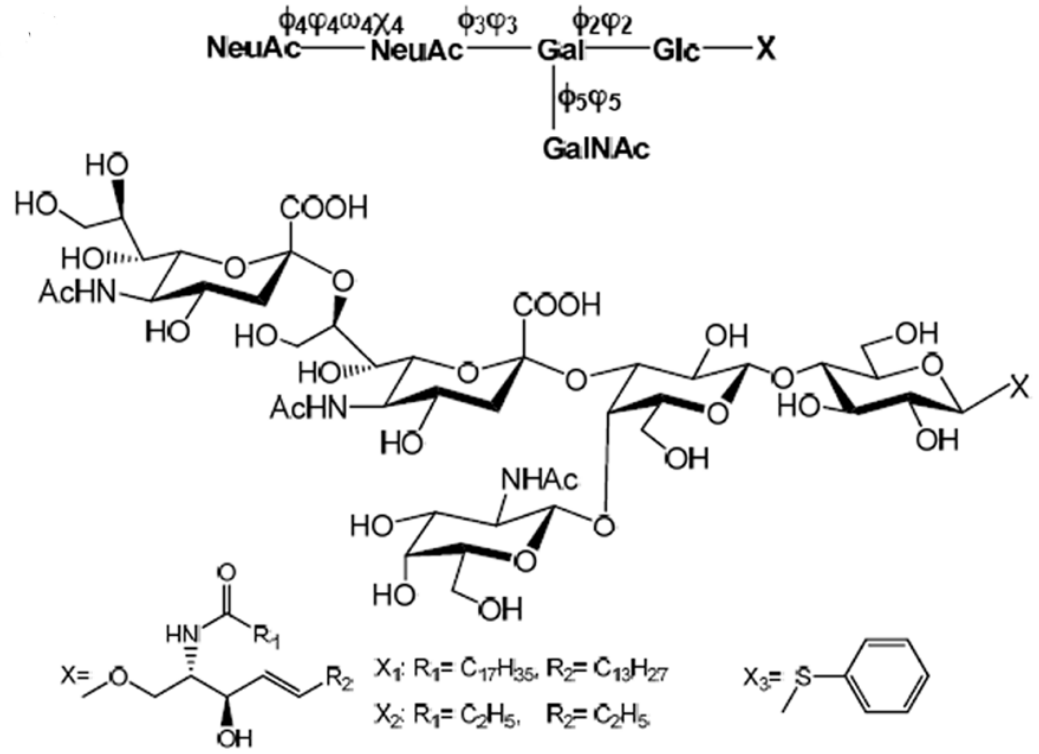

Fig. 2 Structures of ganglioside GD2 and its derivatives. The carbohydrate “head” of GD2 is shown, to which can be attached either a ceramide or lipid tail (X1), this is herein referred to as ganglioside GD2. The ceramide tail of ganglioside GD2 can be truncated (X2) for the purpose of modeling. X3 is a synthetic water-soluble thiophenyl GD2, lacking the ceramide and lipid tail, as an analog of ganglioside GD2. Residues and torsion angles are shown.

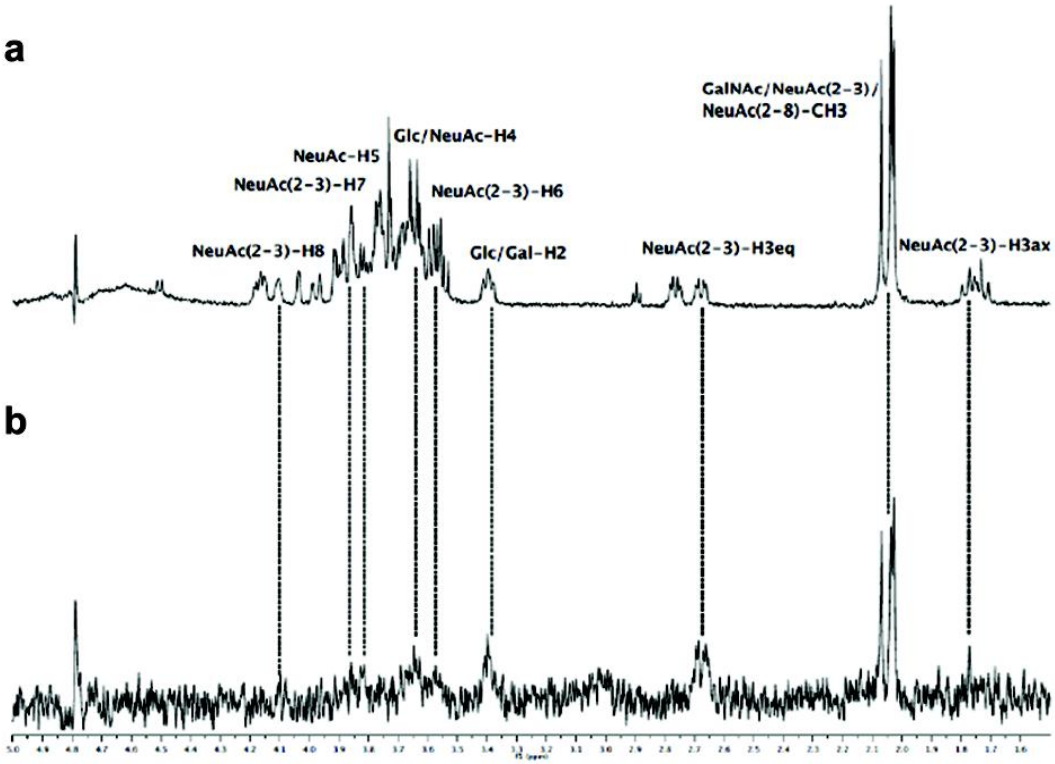

Fig. 3 STD NMR spectra, STD amplification factor and structure model of thiophenyl GD2 binding to mAb 3F8. (A) Reference spectrum of a mixture of thiophenyl GD2 (500 µM) and 3F8 (10 µM binding sites) at a 50:1 ratio. (B) STD NMR spectrum of the same sample (T_{sat}= 5 s).

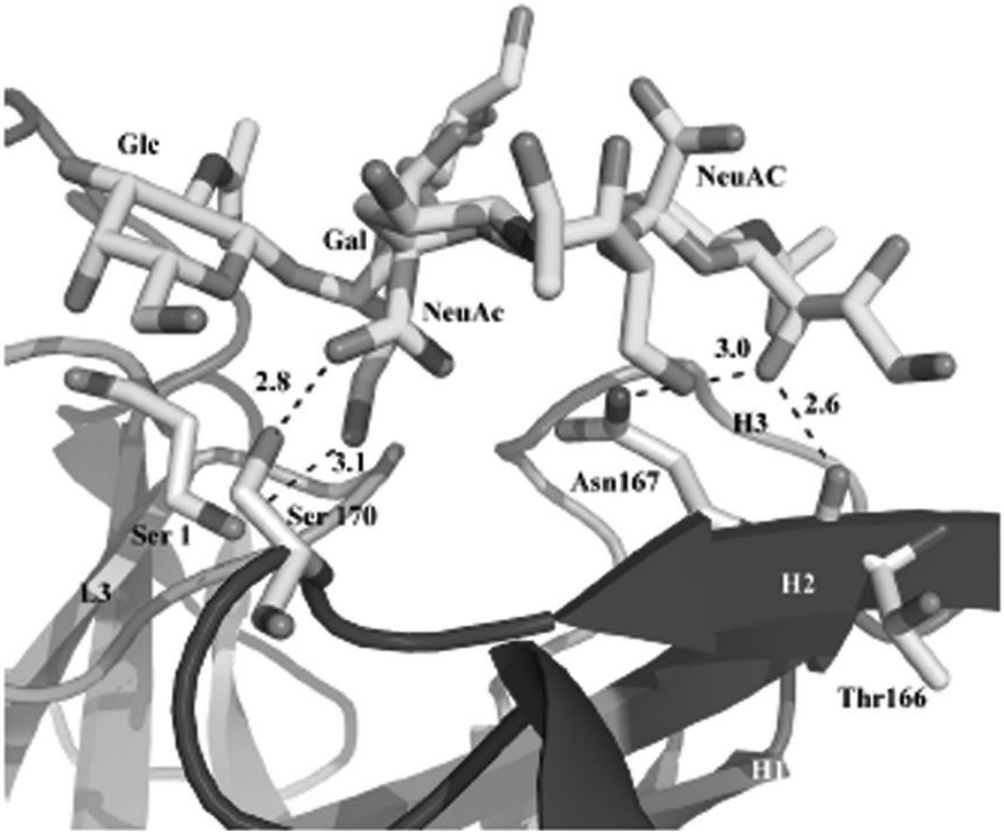

Fig. 4 The predicted binding mode of GD2 in the antigen binding surface of a Fab fragment of 3F8 antibody. The Fab of 3F8 VL and VH is displayed as a ribbon structure. Selected residues of 3F8 are represented as thick capped sticks with carbon, nitrogen and oxygen in gray, blue and red, respectively. GD2 is shown as capped sticks, color-coded as in panel A. Black dashed lines are H-bonds. Distances are measured between the heavy atoms. Ser1 (framework), Thr 166, Asn 167 and Ser170 (H2) form H-bonds with the GD2 molecule.

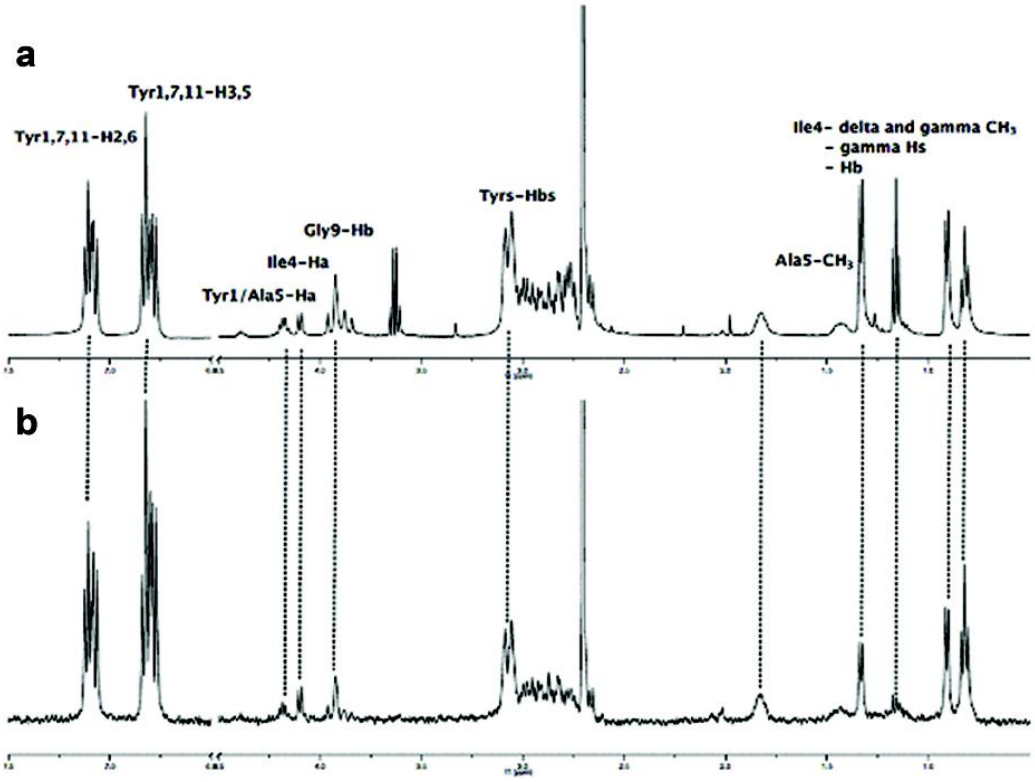

Fig. 5 STD NMR spectra and STD amplification factor for a mixture of ganglioside GD2 micelles and M50B. (A) Reference spectrum of a mixture of ganglioside GD2 micelles (200 μM) and peptide ligand M50B (1 mM) in a ratio of 1:5. (B) STD NMR spectrum of the same sample at 298 K (T_{sat}= 5 s).

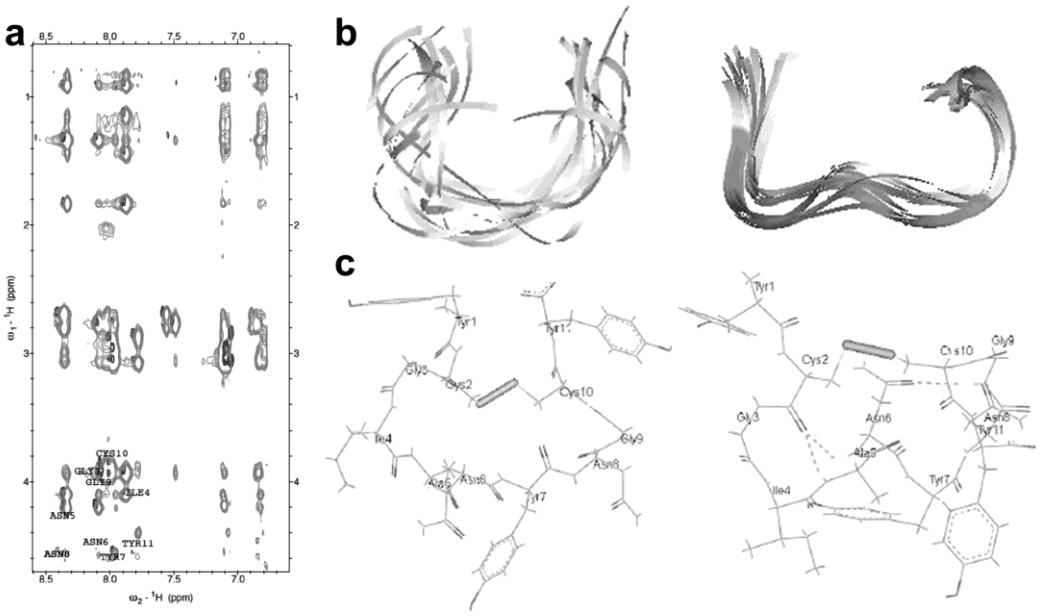

Fig. 6 Ensemble of 12 and 19 lowest-energy structures calculated for the M50B in the free and bound state in water respectively. (A) Overlay of ROESY spectrum (gray) of M50B in the free state and trans-NOESY spectrum (black) of M50B in the bound state. The mixing times used to record these spectra are 200 and 100ms respectively. (B) The ensembles of structures are in flat ribbon representation and the β turn is in green. (C) The average structure is in line representation (water molecules are removed). There are three hydrogen bonds between carbonyl group and amide of Cys2 and Ala5, Cys2 and Asn6 and Asn6 and Gly9.

Appendix III Supporting information for Chapter 4

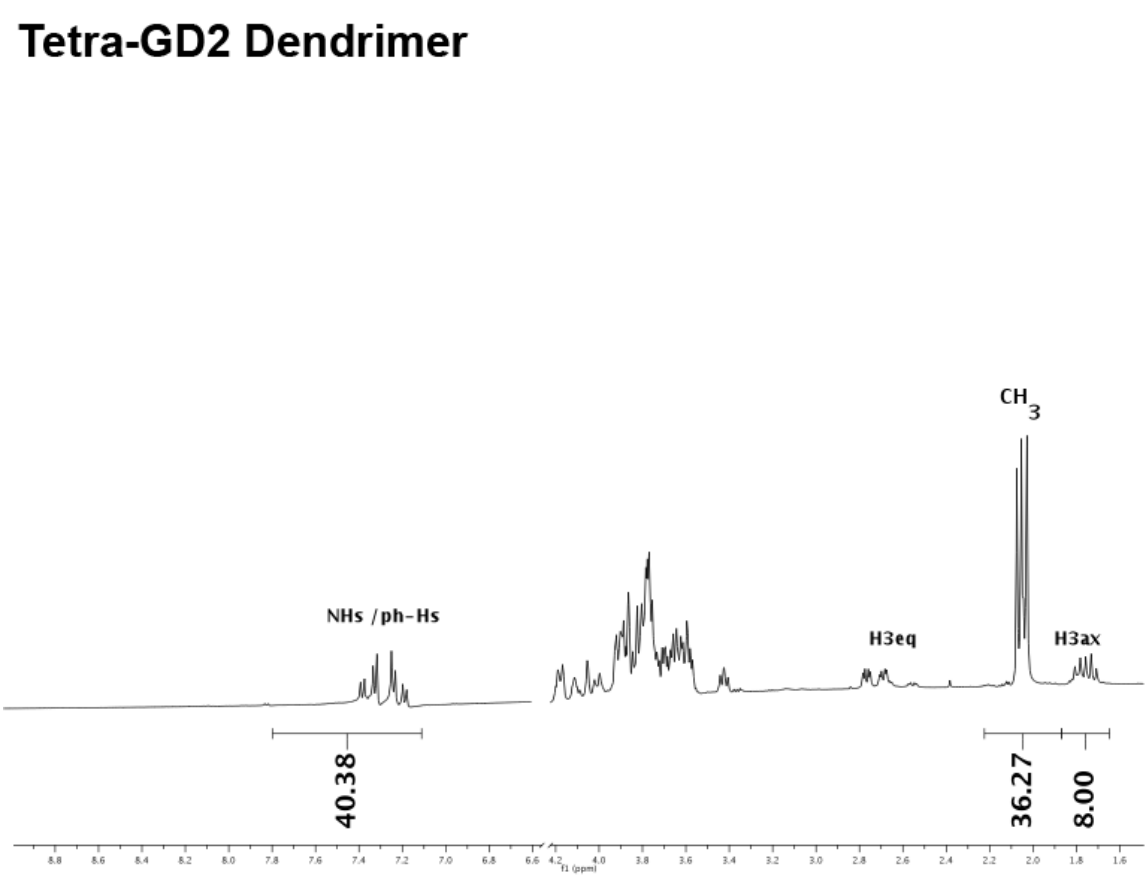

Figure S1. ^{1}H-NMR spectrum of tetra-GD2 dendrimer in deuterated water.

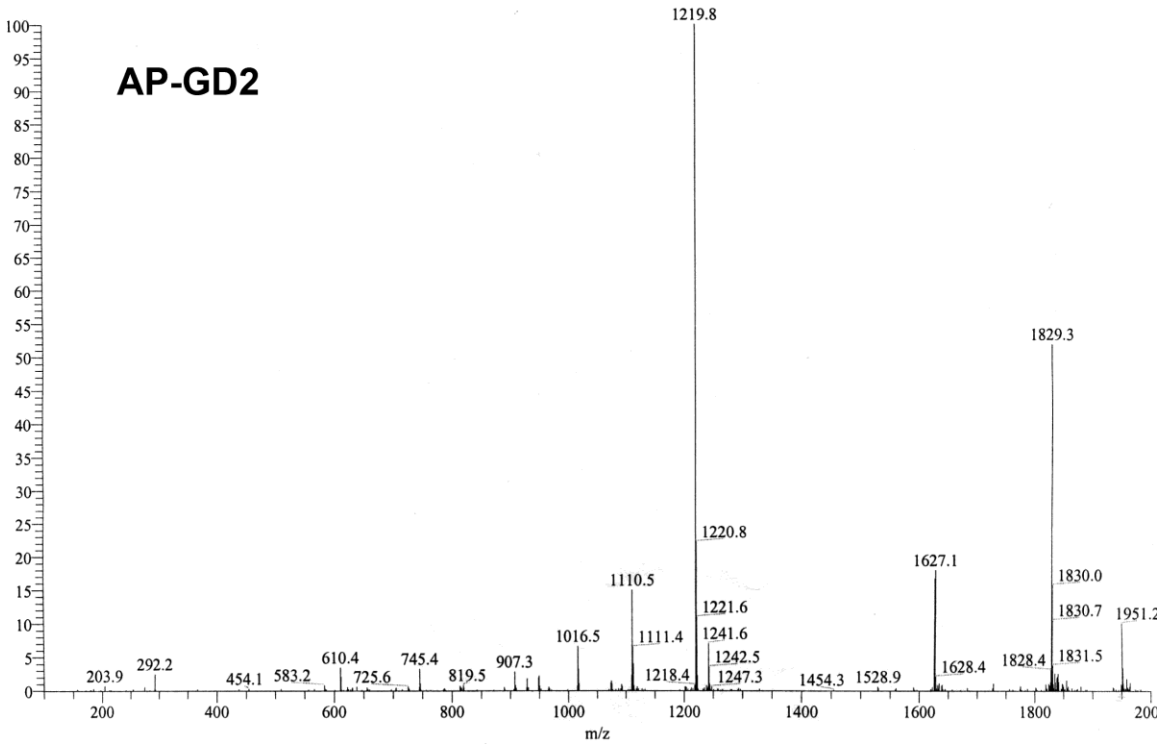

Figure S2. Mass spectrum of amino phenyl ether-analog of GD2 (AP-GD2)

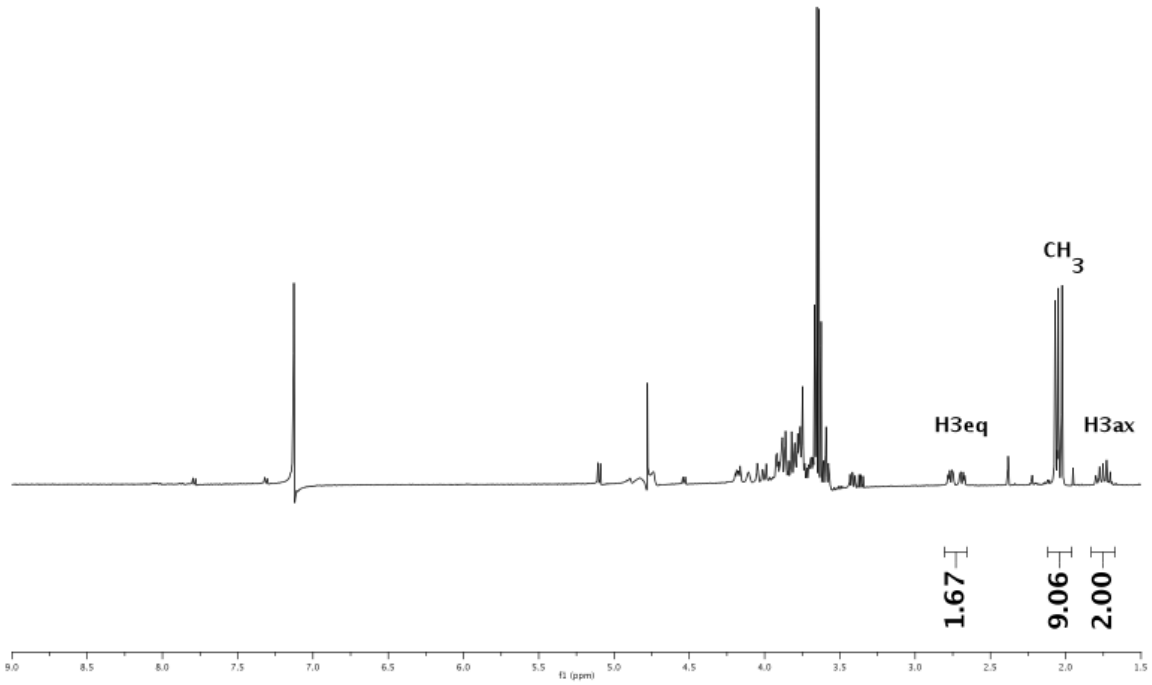

Figure S3. ^{1}H-NMR spectrum of amino phenyl ether-analog of GD2 (AP-GD2) in deuterated water.

Appendix IV Copyright statement

Chapter 2 reproduces material published in Tong W, Gagnon M, and Sprules T, et al. Small-molecule ligands of GD2 ganglioside, designed from NMR studies, exhibit induced-fit binding and bioactivity. Chem Biol 2010; 17(2): 183-94.

Elsevier grants for the author to use this work in his dissertation, as described at the following URL:

http://s100.copyright.com/CustomerAdmin/PLF.jsp?lID=2011091_1316545587791

References

1. Svennerholm, L., Bostrom, K., Fredman, P., Jungbjer, B., Lekman, A., Mansson, J. E., and Rynmark, B. M. (1994) Gangliosides and allied glycosphingolipids in human peripheral nerve and spinal cord, *Biochimica et Biophysica Acta 1214*, 115-123.
2. Rapport, M. M., Donnenfeld, H., Brunner, W., Hungund, B., and Bartfeld, H. (1985) Ganglioside patterns in amyotrophic lateral sclerosis brain regions, *Annals of Neurology 18*, 60-67.
3. Zhang, S., Cordon-Cardo, C., Zhang, H. S., Reuter, V. E., Adluri, S., Hamilton, W. B., Lloyd, K. O., and Livingston, P. O. (1997) Selection of tumor antigens as targets for immune attack using immunohistochemistry: I. Focus on gangliosides, *International Journal of Cancer 73*, 42-49.
4. Cahan, L. D., Irie, R. F., Singh, R., Cassidenti, A., and Paulson, J. C. (1982) Identification of a Human Neuroectodermal Tumor Antigen (OFA-I-2) as Ganglioside GD2, *Proc Natl Acad Sci U S A 79*, 7629-7633.
5. Cheresh, D. A., Rosenberg, J., Mujoo, K., Hirschowitz, L., and Reisfeld, R. A. (1986) Biosynthesis and Expression of the Disialoganglioside GD2, a Relevant Target Antigen on Small Cell Lung Carcinoma for Monoclonal Antibody-mediated Cytolysis, *Cancer Research 46*, 5112-5118.

6. Cheresh, D. A., Pierschbacher, M. D., Herzig, M. A., and Mujoo, K. (1986) Disialogangliosides GD2 and GD3 are involved in the attachment of human melanoma and neuroblastoma cells to extracellular matrix proteins, *J. Cell Biol. 102*, 688-696.

7. Schulz, G., Cheresh, D. A., Varki, N. M., Yu, A., Staffileno, L. K., and Reisfeld, R. A. (1984) Detection of ganglioside GD2 in tumor tissues and sera of neuroblastoma patients, *Cancer Research 44*, 5914-5920.

8. Astronomo, R. D., and Burton, D. R. (2010) Carbohydrate vaccines: developing sweet solutions to sticky situations?, *Nat Rev Drug Discov 9*, 308-324.

9. Gagnon, M., and Saragovi, H. U. (2002) Gangliosides: therapeutic agents or therapeutic targets?, *Expert Opinion on Therapeutic Patents 12*, 1215-1223.

10. Yamashita, T., Wada, R., Sasaki, T., Deng, C., Bierfreund, U., Sandhoff, K., and Proia, R. L. (1999) A vital role for glycosphingolipid synthesis during development and differentiation, *Proc Natl Acad Sci U S A 96*, 9142-9147.

11. Sabel, B. A., Slavin, M. D., and Stein, D. G. (1984) GM1 ganglioside treatment facilitates behavioral recovery from bilateral brain damage, *Science 225*, 340-342.

12. Dreyfus, H., Sahel, J., Heidinger, V., Mohand-Said, S., Guerold, B., Meuillet, E., Fontaine, V., and Hicks, D. (1998) Gangliosides and

neurotrophic growth factors in the retina. Molecular interactions and applications as neuroprotective agents, *Annals of the New York Academy of Sciences 845*, 240-252.

13. Birkle, S., Zeng, G., Gao, L., Yu, R. K., and Aubry, J. (2003) Role of tumor-associated gangliosides in cancer progression, *Biochimie 85*, 455-463.

14. Regina Todeschini, A., and Hakomori, S. I. (2008) Functional role of glycosphingolipids and gangliosides in control of cell adhesion, motility, and growth, through glycosynaptic microdomains, *Biochimica et Biophysica Acta 1780*, 421-433.

15. Svennerholm, L. (1970) Classification of lipidoses, *Riv Patol Nerv Ment 91*, 277-278.

16. Ando, H., Ishida, H., and Kiso, M. (2010) Renewed synthetic approach to gangliosides exploiting versatile and powerful synthetic units, *Methods in Enzymology 478*, 521-540.

17. Nores, G. A., Hanai, N., Levery, S. B., Eaton, H. L., Salyan, E. K., and Hakomori, S. (1988) Synthesis and characterization of lyso-GM3 (II3Neu5Ac Lactosyl sphingosine), de-N-acetyl-GM3 (II3NeuNH2 lactosyl Cer), and related compounds, *Carbohydrate Research 179*, 393-410.

18. Sugimoto, M., Numata, M., Koike, K., Nakahara, Y., and Ogawa, T. (1986) Total synthesis of gangliosides GM1 and GM2, *Carbohydrate Research 156*, C1-5.

19. Ishida, H. K., Ishida, H., Kiso, M., and Hasegawa, A. (1994) Total synthesis of ganglioside GQ1b, *Carbohydrate Research 260*, C1-6.

20. Ishida, H., Ohta, Y., Tsukada, Y., Isogai, Y., Kiso, M., and Hasegawa, A. (1994) A facile total synthesis of ganglioside GD2, *Carbohydrate Research 252*, 283-290.

21. Imamura, A., Ando, H., Ishida, H., and Kiso, M. (2009) Ganglioside GQ1b: efficient total synthesis and the expansion to synthetic derivatives to elucidate its biological roles, *Journal of Organic Chemistry 74*, 3009-3023.

22. Zeng, G., and Yu, R. K. (2008) Cloning and transcriptional regulation of genes responsible for synthesis of gangliosides, *Curr Drug Targets 9*, 317-324.

23. Gilbert, M., Brisson, J. R., Karwaski, M. F., Michniewicz, J., Cunningham, A. M., Wu, Y., Young, N. M., and Wakarchuk, W. W. (2000) Biosynthesis of ganglioside mimics in Campylobacter jejuni OH4384. Identification of the glycosyltransferase genes, enzymatic synthesis of model compounds, and characterization of nanomole amounts by 600-mhz (1)h and (13)c NMR analysis, *J. Biol. Chem. 275*, 3896-3906.

24. Gilbert, M., Karwaski, M. F., Bernatchez, S., Young, N. M., Taboada, E., Michniewicz, J., Cunningham, A. M., and Wakarchuk, W. W. (2002) The genetic bases for the variation in the lipo-oligosaccharide of the mucosal pathogen, Campylobacter jejuni.

Biosynthesis of sialylated ganglioside mimics in the core oligosaccharide, *J. Biol. Chem. 277*, 327-337.

25. Chiu, C. P., Watts, A. G., Lairson, L. L., Gilbert, M., Lim, D., Wakarchuk, W. W., Withers, S. G., and Strynadka, N. C. (2004) Structural analysis of the sialyltransferase CstII from Campylobacter jejuni in complex with a substrate analog, *Nat Struct Mol Biol 11*, 163-170.

26. Blixt, O., Vasiliu, D., Allin, K., Jacobsen, N., Warnock, D., Razi, N., Paulson, J. C., Bernatchez, S., Gilbert, M., and Wakarchuk, W. (2005) Chemoenzymatic synthesis of 2-azidoethyl-ganglio-oligosaccharides GD3, GT3, GM2, GD2, GT2, GM1, and GD1a, *Carbohydrate Research 340*, 1963-1972.

27. Pukin, A. V., Weijers, C. A., van Lagen, B., Wechselberger, R., Sun, B., Gilbert, M., Karwaski, M. F., Florack, D. E., Jacobs, B. C., Tio-Gillen, A. P., van Belkum, A., Endtz, H. P., Visser, G. M., and Zuilhof, H. (2008) GM3, GM2 and GM1 mimics designed for biosensing: chemoenzymatic synthesis, target affinities and 900 MHz NMR analysis, *Carbohydrate Research 343*, 636-650.

28. Jacques, S., Rich, J. R., Ling, C. C., and Bundle, D. R. (2006) Chemoenzymatic synthesis of GM3 and GM2 gangliosides containing a truncated ceramide functionalized for glycoconjugate synthesis and solid phase applications, *Organic & Biomolecular Chemistry 4*, 142-154.

29. Yu, H., Cheng, J., Ding, L., Khedri, Z., Chen, Y., Chin, S., Lau, K., Tiwari, V. K., and Chen, X. (2009) Chemoenzymatic synthesis of GD3 oligosaccharides and other disialyl glycans containing natural and non-natural sialic acids, *J. Am. Chem. Soc. 131*, 18467-18477.

30. Scarsdale, J. N., Prestegard, J. H., and Yu, R. K. (1990) NMR and computational studies of interactions between remote residues in gangliosides, *Biochemistry 29*, 9843-9855.

31. PAOLA BROCCA, D. A. a. S. S. (1996) Nuclear Overhauser effect investigation on GM1 ganglioside containing N-glycolyl-neuraminic acid (ll3Neu5GcGgOse4Cer), *Glycoconjugate Journal 13*, 57-62.

32. Brocca, P., Berthault, P., and Sonnino, S. (1998) Conformation of the oligosaccharide chain of G(M1) ganglioside in a carbohydrate-enriched surface, *Biophys. J. 74*, 309-318.

33. Acquotti, D., Poppe, L., Dabrowski, J., Von der Lieth, C., Sonnino, S., and Tettamanti, G. (1990) Three-dimensional structure of the oligosaccharide chain of GM1 ganglioside revealed by a distance-mapping procedure: a rotating and laboratory frame nuclear overhauser enhancement investigation of native glycolipid in dimethyl sulfoxide and in water-odecylphosphocholine solutions *J. Am. Chem. Soc. 112*, 7772-7778.

34. Siebert, H. C., Reuter, G., Schauer, R., Von der Lieth, C. W., and Dabrowski, J. (1992) Solution conformations of GM3 ganglioside containing different sialic acid residues as revealed by NOE-based

distance mapping, molecular mechanics, and molecular dynamics calculations, *Biochemistry 31*, 6962-6971.

35. Houliston, R. S., Yuki, N., Hirama, T., Khieu, N. H., Brisson, J.-R., Gilbert, M., and Jarrell, H. C. (2007) Recognition characteristics of monoclonal antibodies that are cross-reactive with gangliosides and lipooligosaccharide from Campylobacter jejuni strains associated with Guillain-Barre and Fisher syndromes, *Biochemistry 46*, 36-44.
36. Tong, W., Gagnon, M., Sprules, T., Gilbert, M., Chowdhury, S., Meerovitch, K., Hansford, K., Purisima, E. O., Blankenship, J. W., Cheung, N. K., Gehring, K., Lubell, W. D., and Saragovi, H. U. (2010) Small-molecule ligands of GD2 ganglioside, designed from NMR studies, exhibit induced-fit binding and bioactivity, *Chem Biol 17*, 183-194.
37. Brocca, P., Bernardi, A., Raimondi, L., and Sonnino, S. (2000) Modeling ganglioside headgroups by conformational analysis and molecular dynamics, *Glycoconjugate Journal 17*, 283-299.
38. Vasudevan, S. V., and Balaji, P. V. (2002) Comparative analysis of ganglioside conformations by MD simulations: implications for specific recognition by proteins, *Journal of Molecular Structure: THEOCHEM 583*, 215-232.
39. Malorni, W., Giammarioli, A. M., Garofalo, T., and Sorice, M. (2007) Dynamics of lipid raft components during lymphocyte apoptosis: the paradigmatic role of GD3, *Apoptosis 12*, 941-949.

40. Li, R., Liu, Y., and Ladisch, S. (2001) Enhancement of epidermal growth factor signaling and activation of SRC kinase by gangliosides, *J. Biol. Chem. 276*, 42782-42792.

41. Liu, Y., Li, R., and Ladisch, S. (2004) Exogenous ganglioside GD1a enhances epidermal growth factor receptor binding and dimerization, *J. Biol. Chem. 279*, 36481-36489.

42. Liu, Y., McCarthy, J., and Ladisch, S. (2006) Membrane ganglioside enrichment lowers the threshold for vascular endothelial cell angiogenic signaling, *Cancer Research 66*, 10408-10414.

43. Choi, H. J., Chung, T. W., Kang, S. K., Lee, Y. C., Ko, J. H., Kim, J. G., and Kim, C. H. (2006) Ganglioside GM3 modulates tumor suppressor PTEN-mediated cell cycle progression--transcriptional induction of p21(WAF1) and p27(kip1) by inhibition of PI-3K/AKT pathway, *Glycobiology 16*, 573-583.

44. Cazet, A., Groux-Degroote, S., Teylaert, B., Kwon, K. M., Lehoux, S., Slomianny, C., Kim, C. H., Le Bourhis, X., and Delannoy, P. (2009) GD3 synthase overexpression enhances proliferation and migration of MDA-MB-231 breast cancer cells, *Biol Chem 390*, 601-609.

45. Cazet, A., Lefebvre, J., Adriaenssens, E., Julien, S., Bobowski, M., Grigoriadis, A., Tutt, A., Tulasne, D., Le Bourhis, X., and Delannoy, P. (2010) GD synthase expression enhances proliferation and

tumor growth of MDA-MB-231 breast cancer cells through c-Met activation, *Molecular Cancer Research 8*, 1526-1535.

46. Liu, Y., Yan, S., Wondimu, A., Bob, D., Weiss, M., Sliwinski, K., Villar, J., Notario, V., Sutherland, M., Colberg-Poley, A. M., and Ladisch, S. (2010) Ganglioside synthase knockout in oncogene-transformed fibroblasts depletes gangliosides and impairs tumor growth, *Oncogene 29*, 3297-3306.

47. Bjerkvig, R., Engebraaten, O., Laerum, O. D., Fredman, P., Svennerholm, L., Vrionis, F. D., Wikstrand, C. J., and Bigner, D. D. (1991) Anti-GM2 monoclonal antibodies induce necrosis in GM2-rich cultures of a human glioma cell line, *Cancer Research 51*, 4643-4648.

48. Hanibuchi, M., Yano, S., Nishioka, Y., Yanagawa, H., Miki, T., and Sone, S. (2000) Immunological circumvention of multiple organ metastases of multidrug resistant human small cell lung cancer cells by mouse-human chimeric anti-ganglioside GM2 antibody KM966, *Clinical & Experimental Metastasis 18*, 353-360.

49. Dippold, W. G., Knuth, A., and Meyer zum Buschenfelde, K. H. (1984) Inhibition of human melanoma cell growth in vitro by monoclonal anti-GD3-ganglioside antibody, *Cancer Research 44*, 806-810.

50. Liu, Z., Lee, F. T., Hanai, N., Smyth, F. E., Burgess, A. W., Old, L. J., and Scott, A. M. (2002) Cytokine enhancement of in vitro

antibody-dependent cellular cytotoxicity mediated by chimeric anti-GD3 monoclonal antibody KM871, *Cancer Immunity 2*, 13.

51. Kirkwood, J. M., Mascari, R. A., Edington, H. D., Rabkin, M. S., Day, R. S., Whiteside, T. L., Vlock, D. R., and Shipe-Spotloe, J. M. (2000) Analysis of therapeutic and immunologic effects of R(24) anti-GD3 monoclonal antibody in 37 patients with metastatic melanoma, *Cancer 88*, 2693-2702.

52. Hedberg, K. M., Dellheden, B., Wikstrand, C. J., and Fredman, P. (2000) Monoclonal anti-GD3 antibodies selectively inhibit the proliferation of human malignant glioma cells in vitro, *Glycoconjugate Journal 17*, 717-726.

53. Yoshida, S., Fukumoto, S., Kawaguchi, H., Sato, S., Ueda, R., and Furukawa, K. (2001) Ganglioside G(D2) in small cell lung cancer cell lines: enhancement of cell proliferation and mediation of apoptosis, *Cancer Research 61*, 4244-4252.

54. Aixinjueluo, W., Furukawa, K., Zhang, Q., Hamamura, K., Tokuda, N., Yoshida, S., and Ueda, R. (2005) Mechanisms for the apoptosis of small cell lung cancer cells induced by anti-GD2 monoclonal antibodies: roles of anoikis, *J. Biol. Chem. 280*, 29828-29836.

55. Kowalczyk, A., Gil, M., Horwacik, I., Odrowaz, Z., Kozbor, D., and Rokita, H. (2009) The GD2-specific 14G2a monoclonal antibody induces apoptosis and enhances cytotoxicity of chemotherapeutic

drugs in IMR-32 human neuroblastoma cells, *Cancer Letters 281*, 171-182.

56. Lovat, P. E., Corazzari, M., Di Sano, F., Piacentini, M., and Redfern, C. P. (2005) The role of gangliosides in fenretinide-induced apoptosis of neuroblastoma, *Cancer Letters 228*, 105-110.

57. Wang, X., Sun, P., Al-Qamari, A., Tai, T., Kawashima, I., and Paller, A. S. (2001) Carbohydrate-carbohydrate binding of ganglioside to integrin alpha(5) modulates alpha(5)beta(1) function, *J. Biol. Chem. 276*, 8436-8444.

58. Shirure, V. S., Henson, K. A., Schnaar, R. L., Nimrichter, L., and Burdick, M. M. (2011) Gangliosides expressed on breast cancer cells are E-selectin ligands, *Biochemical & Biophysical Research Communications 406*, 423-429.

59. Ben-David, T., Sagi-Assif, O., Meshel, T., Lifshitz, V., Yron, I., and Witz, I. P. (2008) The involvement of the sLe-a selectin ligand in the extravasation of human colorectal carcinoma cells, *Immunol Lett 116*, 218-224.

60. Ito, A., Handa, K., Withers, D. A., Satoh, M., and Hakomori, S. (2001) Binding specificity of siglec7 to disialogangliosides of renal cell carcinoma: possible role of disialogangliosides in tumor progression, *FEBS Letters 504*, 82-86.

61. Probstmeier, R., Michels, M., Franz, T., Chan, B. M. C., and Pesheva, P. (1999) Tenascin-R interferes with integrin-dependent

oligodendrocyte precursor cell adhesion by a ganglioside-mediated signalling mechanism, *European Journal of Neuroscience 11*, 2474-2488.

62. Toledo, M. S., Suzuki, E., Handa, K., and Hakomori, S. (2004) Cell growth regulation through GM3-enriched microdomain (glycosynapse) in human lung embryonal fibroblast WI38 and its oncogenic transformant VA13, *J. Biol. Chem. 279*, 34655-34664.

63. Miura, Y., Kainuma, M., Jiang, H., Velasco, H., Vogt, P. K., and Hakomori, S. (2004) Reversion of the Jun-induced oncogenic phenotype by enhanced synthesis of sialosyllactosylceramide (GM3 ganglioside), *Proc Natl Acad Sci U S A 101*, 16204-16209.

64. Ono, M., Handa, K., Sonnino, S., Withers, D. A., Nagai, H., and Hakomori, S. (2001) GM3 ganglioside inhibits CD9-facilitated haptotactic cell motility: coexpression of GM3 and CD9 is essential in the downregulation of tumor cell motility and malignancy, *Biochemistry 40*, 6414-6421.

65. Mitsuzuka, K., Handa, K., Satoh, M., Arai, Y., and Hakomori, S. (2005) A specific microdomain ("glycosynapse 3") controls phenotypic conversion and reversion of bladder cancer cells through GM3-mediated interaction of alpha3beta1 integrin with CD9, *J. Biol. Chem. 280*, 35545-35553.

66. Todeschini, A. R., Dos Santos, J. N., Handa, K., and Hakomori, S. I. (2007) Ganglioside GM2-tetraspanin CD82 complex inhibits met

and its cross-talk with integrins, providing a basis for control of cell motility through glycosynapse, *J. Biol. Chem. 282*, 8123-8133.

67. Todeschini, A. R., Dos Santos, J. N., Handa, K., and Hakomori, S. I. (2008) Ganglioside GM2/GM3 complex affixed on silica nanospheres strongly inhibits cell motility through CD82/cMet-mediated pathway, *Proc Natl Acad Sci U S A 105*, 1925-1930.

68. Kroes, R. A., He, H., Emmett, M. R., Nilsson, C. L., Leach, F. E., 3rd, Amster, I. J., Marshall, A. G., and Moskal, J. R. (2010) Overexpression of ST6GalNAcV, a ganglioside-specific alpha2,6-sialyltransferase, inhibits glioma growth in vivo, *Proc Natl Acad Sci U S A 107*, 12646-12651.

69. Ziche, M., Morbidelli, L., Alessandri, G., and Gullino, P. M. (1992) Angiogenesis can be stimulated or repressed in vivo by a change in GM3:GD3 ganglioside ratio, *Laboratory Investigation 67*, 711-715.

70. Deng, W., Li, R., Guerrera, M., Liu, Y., and Ladisch, S. (2002) Transfection of glucosylceramide synthase antisense inhibits mouse melanoma formation, *Glycobiology 12*, 145-152.

71. Zeng, G., Gao, L., Birkle, S., and Yu, R. K. (2000) Suppression of ganglioside GD3 expression in a rat F-11 tumor cell line reduces tumor growth, angiogenesis, and vascular endothelial growth factor production, *Cancer Research 60*, 6670-6676.

72. Lluis, J. M., Llacuna, L., von Montfort, C., Barcena, C., Enrich, C., Morales, A., and Fernandez-Checa, J. C. (2009) GD3 synthase

overexpression sensitizes hepatocarcinoma cells to hypoxia and reduces tumor growth by suppressing the cSrc/NF-kappaB survival pathway, *PLoS One 4*, e8059.

73. Chung, T. W., Kim, S. J., Choi, H. J., Kim, K. J., Kim, M. J., Kim, S. H., Lee, H. J., Ko, J. H., Lee, Y. C., Suzuki, A., and Kim, C. H. (2009) Ganglioside GM3 inhibits VEGF/VEGFR-2-mediated angiogenesis: direct interaction of GM3 with VEGFR-2, *Glycobiology 19*, 229-239.

74. Mukherjee, P., Faber, A. C., Shelton, L. M., Baek, R. C., Chiles, T. C., and Seyfried, T. N. (2008) Ganglioside GM3 suppresses the pro-angiogenic effects of vascular endothelial growth factor and ganglioside GD1A, *Journal of Lipid Research*.

75. Mukherjee, P., Faber, A. C., Shelton, L. M., Baek, R. C., Chiles, T. C., and Seyfried, T. N. (2008) Thematic review series: sphingolipids. Ganglioside GM3 suppresses the proangiogenic effects of vascular endothelial growth factor and ganglioside GD1a, *Journal of Lipid Research 49*, 929-938.

76. Offner, H., Thieme, T., and Vandenbark, A. A. (1987) Gangliosides induce selective modulation of CD4 from helper T lymphocytes, *Journal of Immunology 139*, 3295-3305.

77. Chu, J. W., and Sharom, F. J. (1995) Gangliosides interact with interleukin-4 and inhibit interleukin-4-stimulated helper T-cell proliferation, *Immunology 84*, 396-403.

78. Biswas, S., Biswas, K., Richmond, A., Ko, J., Ghosh, S., Simmons, M., Rayman, P., Rini, B., Gill, I., Tannenbaum, C. S., and Finke, J. H. (2009) Elevated levels of select gangliosides in T cells from renal cell carcinoma patients is associated with T cell dysfunction, *Journal of Immunology 183*, 5050-5058.

79. Park, J. E., Wu, D. Y., Prendes, M., Lu, S. X., Ragupathi, G., Schrantz, N., and Chapman, P. B. (2008) Fine specificity of natural killer T cells against GD3 ganglioside and identification of GM3 as an inhibitory natural killer T-cell ligand, *Immunology 123*, 145-155.

80. Grayson, G., and Ladisch, S. (1992) Immunosuppression by human gangliosides. II. Carbohydrate structure and inhibition of human NK activity, *Cellular Immunology 139*, 18-29.

81. Sriram, V., Cho, S., Li, P., O'Donnell, P. W., Dunn, C., Hayakawa, K., Blum, J. S., and Brutkiewicz, R. R. (2002) Inhibition of glycolipid shedding rescues recognition of a CD1+ T cell lymphoma by natural killer T (NKT) cells, *Proc Natl Acad Sci U S A 99*, 8197-8202.

82. Dumontet, C., Rebbaa, A., Bienvenu, J., and Portoukalian, J. (1994) Inhibition of immune cell proliferation and cytokine production by lipoprotein-bound gangliosides, *Cancer Immunology, Immunotherapy 38*, 311-316.

83. Shurin, G. V., Shurin, M. R., Bykovskaia, S., Shogan, J., Lotze, M. T., and Barksdale, E. M., Jr. (2001) Neuroblastoma-derived

gangliosides inhibit dendritic cell generation and function, *Cancer Research 61*, 363-369.

84. Bennaceur, K., Popa, I., Chapman, J. A., Migdal, C., Peguet-Navarro, J., Touraine, J. L., and Portoukalian, J. (2009) Different mechanisms are involved in apoptosis induced by melanoma gangliosides on human monocyte-derived dendritic cells, *Glycobiology 19*, 576-582.

85. Ladisch, S., Li, R., and Olson, E. (1994) Ceramide structure predicts tumor ganglioside immunosuppressive activity, *Proc Natl Acad Sci U S A 91*, 1974-1978.

86. Sorice, M., Matarrese, P., Manganelli, V., Tinari, A., Giammarioli, A. M., Mattei, V., Misasi, R., Garofalo, T., and Malorni, W. (2010) Role of GD3-CLIPR-59 association in lymphoblastoid T cell apoptosis triggered by CD95/Fas, *PLoS One 5*, e8567.

87. Garofalo, T., Misasi, R., Mattei, V., Giammarioli, A. M., Malorni, W., Pontieri, G. M., Pavan, A., and Sorice, M. (2003) Association of the death-inducing signaling complex with microdomains after triggering through CD95/Fas. Evidence for caspase-8-ganglioside interaction in T cells, *J. Biol. Chem. 278*.

88. Chahlavi, A., Rayman, P., Richmond, A. L., Biswas, K., Zhang, R., Vogelbaum, M., Tannenbaum, C., Barnett, G., and Finke, J. H. (2005) Glioblastomas induce T-lymphocyte death by two distinct

pathways involving gangliosides and CD70, *Cancer Research 65*, 5428-5438.

89. Crespo, F. A., Sun, X., Cripps, J. G., and Fernandez-Botran, R. (2006) The immunoregulatory effects of gangliosides involve immune deviation favoring type-2 T cell responses, *J Leukoc Biol 79*, 586-595.

90. Caldwell, S., Heitger, A., Shen, W., Liu, Y., Taylor, B., and Ladisch, S. (2003) Mechanisms of ganglioside inhibition of APC function, *Journal of Immunology 171*, 1676-1683.

91. Shen, W., Stone, K., Jales, A., Leitenberg, D., and Ladisch, S. (2008) Inhibition of TLR activation and up-regulation of IL-1R-associated kinase-M expression by exogenous gangliosides, *Journal of Immunology 180*, 4425-4432.

92. Frost, J. D., Hank, J. A., Reaman, G. H., Frierdich, S., Seeger, R. C., Gan, J., Anderson, P. M., Ettinger, L. J., Cairo, M. S., Blazar, B. R., Krailo, M. D., Matthay, K. K., Reisfeld, R. A., and Sondel, P. M. (1997) A phase I/IB trial of murine monoclonal anti-GD2 antibody 14.G2a plus interleukin-2 in children with refractory neuroblastoma: a report of the Children's Cancer Group, *Cancer 80*, 317-333.

93. Kushner, B. H., Kramer, K., and Cheung, N. K. (2001) Phase II trial of the anti-G(D2) monoclonal antibody 3F8 and granulocyte-macrophage colony-stimulating factor for neuroblastoma, *Journal of Clinical Oncology 19*, 4189-4194.

94. Albertini, M. R., Hank, J. A., Schiller, J. H., Khorsand, M., Borchert, A. A., Gan, J., Bechhofer, R., Storer, B., Reisfeld, R. A., and Sondel, P. M. (1997) Phase IB trial of chimeric antidisialoganglioside antibody plus interleukin 2 for melanoma patients, *Clinical Cancer Research 3*, 1277-1288.

95. Gilman, A. L., Ozkaynak, M. F., Matthay, K. K., Krailo, M., Yu, A. L., Gan, J., Sternberg, A., Hank, J. A., Seeger, R., Reaman, G. H., and Sondel, P. M. (2009) Phase I study of ch14.18 with granulocyte-macrophage colony-stimulating factor and interleukin-2 in children with neuroblastoma after autologous bone marrow transplantation or stem-cell rescue: a report from the Children's Oncology Group, *Journal of Clinical Oncology 27*, 85-91.

96. Shusterman, S., London, W. B., Gillies, S. D., Hank, J. A., Voss, S. D., Seeger, R. C., Reynolds, C. P., Kimball, J., Albertini, M. R., Wagner, B., Gan, J., Eickhoff, J., DeSantes, K. B., Cohn, S. L., Hecht, T., Gadbaw, B., Reisfeld, R. A., Maris, J. M., and Sondel, P. M. (2010) Antitumor activity of hu14.18-IL2 in patients with relapsed/refractory neuroblastoma: a Children's Oncology Group (COG) phase II study, *Journal of Clinical Oncology 28*, 4969-4975.

97. Yu, A. L., Gilman, A. L., Ozkaynak, M. F., London, W. B., Kreissman, S. G., Chen, H. X., Smith, M., Anderson, B., Villablanca, J. G., Matthay, K. K., Shimada, H., Grupp, S. A., Seeger, R., Reynolds, C. P., Buxton, A., Reisfeld, R. A., Gillies, S. D., Cohn, S.

L., Maris, J. M., and Sondel, P. M. (2010) Anti-GD2 antibody with GM-CSF, interleukin-2, and isotretinoin for neuroblastoma, *The New England journal of medicine 363*, 1324-1334.

98. Carter, P. (2001) Improving the efficacy of antibody-based cancer therapies, *Nat Rev Cancer 1*, 118-129.

99. Mujoo, K., Cheresh, D. A., Yang, H. M., and Reisfeld, R. A. (1987) Disialoganglioside GD2 on human neuroblastoma cells: target antigen for monoclonal antibody-mediated cytolysis and suppression of tumor growth, *Cancer Research 47*, 1098-1104.

100. Tsuchida, T., Saxton, R. E., Morton, D. L., and Irie, R. F. (1987) Gangliosides of human melanoma, *Journal of the National Cancer Institute 78*, 45-54.

101. Lipinski, M., Braham, K., Philip, I., Wiels, J., Philip, T., Goridis, C., Lenoir, G. M., and Tursz, T. (1987) Neuroectoderm-associated antigens on Ewing's sarcoma cell lines, *Cancer Research 47*, 183-187.

102. Seyfried, T. N., Yu, R. K., Saito, M., and Albert, M. (1987) Ganglioside composition of an experimental mouse brain tumor, *Cancer Research 47*, 3538-3542.

103. Mennel, H. D., Bosslet, K., Wiegandt, H., Sedlacek, H. H., Bauer, B. L., and Rodden, A. F. (1992) Expression of GD2-epitopes in human intracranial tumors and normal brain, *Experimental and Toxicologic Pathology 44*, 317-324.

104. Navid, F., Santana, V. M., and Barfield, R. C. (2010) Anti-GD2 antibody therapy for GD2-expressing tumors, *Current Cancer Drug Dargets 10*, 200-209.

105. Cheung, N. K., Saarinen, U. M., Neely, J. E., Landmeier, B., Donovan, D., and Coccia, P. F. (1985) Monoclonal antibodies to a glycolipid antigen on human neuroblastoma cells, *Cancer Research 45*, 2642-2649.

106. Saleh, M. N., Khazaeli, M. B., Wheeler, R. H., Dropcho, E., Liu, T., Urist, M., Miller, D. M., Lawson, S., Dixon, P., Russell, C. H., and et al. (1992) Phase I trial of the murine monoclonal anti-GD2 antibody 14G2a in metastatic melanoma, *Cancer Res 52*, 4342-4347.

107. Handgretinger, R., Anderson, K., Lang, P., Dopfer, R., Klingebiel, T., Schrappe, M., Reuland, P., Gillies, S. D., Reisfeld, R. A., and Neithammer, D. (1995) A phase I study of human/mouse chimeric antiganglioside GD2 antibody ch14.18 in patients with neuroblastoma, *Eur J Cancer 31A*, 261-267.

108. Murray, J. L., Cunningham, J. E., Brewer, H., Mujoo, K., Zukiwski, A. A., Podoloff, D. A., Kasi, L. P., Bhadkamkar, V., Fritsche, H. A., Benjamin, R. S., and et al. (1994) Phase I trial of murine monoclonal antibody 14G2a administered by prolonged intravenous infusion in patients with neuroectodermal tumors, *Journal of Clinical Oncology 12*, 184-193.

109. Cheung, N. K., Lazarus, H., Miraldi, F. D., Abramowsky, C. R., Kallick, S., Saarinen, U. M., Spitzer, T., Strandjord, S. E., Coccia, P. F., and Berger, N. A. (1987) Ganglioside GD2 specific monoclonal antibody 3F8: a phase I study in patients with neuroblastoma and malignant melanoma, *J Clin Oncol 5*, 1430-1440.

110. Cheung, N. K., Kushner, B. H., Cheung, I. Y., Kramer, K., Canete, A., Gerald, W., Bonilla, M. A., Finn, R., Yeh, S. J., and Larson, S. M. (1998) Anti-G(D2) antibody treatment of minimal residual stage 4 neuroblastoma diagnosed at more than 1 year of age, *J Clin Oncol 16*, 3053-3060.

111. Brodeur, G. M., Pritchard, J., Berthold, F., Carlsen, N. L., Castel, V., Castelberry, R. P., De Bernardi, B., Evans, A. E., Favrot, M., Hedborg, F., and et al. (1993) Revisions of the international criteria for neuroblastoma diagnosis, staging, and response to treatment, *Journal of Clinical Oncology 11*, 1466-1477.

112. Cheung, N. K., Kushner, B. H., Yeh, S. D., and Larson, S. M. (1998) 3F8 monoclonal antibody treatment of patients with stage 4 neuroblastoma: a phase II study, *Int J Oncol 12*, 1299-1306.

113. Munn, D. H., and Cheung, N. K. (1987) Interleukin-2 enhancement of monoclonal antibody-mediated cellular cytotoxicity against human melanoma, *Cancer Research 47*, 6600-6605.

114. Kushner, B. H., and Cheung, N. K. (1989) GM-CSF enhances 3F8 monoclonal antibody-dependent cellular cytotoxicity against human melanoma and neuroblastoma, *Blood 73*, 1936-1941.

115. Munn, D. H., Garnick, M. B., and Cheung, N. K. (1990) Effects of parenteral recombinant human macrophage colony-stimulating factor on monocyte number, phenotype, and antitumor cytotoxicity in nonhuman primates, *Blood 75*, 2042-2048.

116. Cheung, N. K., Sowers, R., Vickers, A. J., Cheung, I. Y., Kushner, B. H., and Gorlick, R. (2006) FCGR2A polymorphism is correlated with clinical outcome after immunotherapy of neuroblastoma with anti-GD2 antibody and granulocyte macrophage colony-stimulating factor, *Journal of Clinical Oncology 24*, 2885-2890.

117. Gillies, S. D., Lo, K. M., and Wesolowski, J. (1989) High-level expression of chimeric antibodies using adapted cDNA variable region cassettes, *J Immunol Methods 125*, 191-202.

118. Saleh, M. N., Khazaeli, M. B., Wheeler, R. H., Allen, L., Tilden, A. B., Grizzle, W., Reisfeld, R. A., Yu, A. L., Gillies, S. D., and LoBuglio, A. F. (1992) Phase I trial of the chimeric anti-GD2 monoclonal antibody ch14.18 in patients with malignant melanoma, *Hum Antibodies Hybridomas 3*, 19-24.

119. Ozkaynak, M. F., Sondel, P. M., Krailo, M. D., Gan, J., Javorsky, B., Reisfeld, R. A., Matthay, K. K., Reaman, G. H., and Seeger, R. C. (2000) Phase I study of chimeric human/murine anti-ganglioside

G(D2) monoclonal antibody (ch14.18) with granulocyte-macrophage colony-stimulating factor in children with neuroblastoma immediately after hematopoietic stem-cell transplantation: a Children's Cancer Group Study, *Journal of Clinical Oncology 18*, 4077-4085.

120. Sorkin, L. S., Otto, M., Baldwin, W. M., 3rd, Vail, E., Gillies, S. D., Handgretinger, R., Barfield, R. C., Ming Yu, H., and Yu, A. L. (2010) Anti-GD(2) with an FC point mutation reduces complement fixation and decreases antibody-induced allodynia, *Pain 149*, 135-142.

121. Kushner, B. H., Kramer, K., Modak, S., and Cheung, N. K. (2011) Successful multifold dose escalation of anti-GD2 monoclonal antibody 3F8 in patients with neuroblastoma: a phase I study, *Journal of Clinical Oncology 29*, 1168-1174.

122. Portoukalian, J., Zwingelstein, G., and Dore, J. F. (1979) Lipid composition of human malignant melanoma tumors at various levels of malignant growth, *Eur J Biochem 94*, 19-23.

123. Carubia, J. M., Yu, R. K., Macala, L. J., Kirkwood, J. M., and Varga, J. M. (1984) Gangliosides of normal and neoplastic human melanocytes, *Biochemical & Biophysical Research Communications 120*, 500-504.

124. Welt, S., Carswell, E. A., Vogel, C. W., Oettgen, H. F., and Old, L. J. (1987) Immune and nonimmune effector functions of IgG3 mouse monoclonal antibody R24 detecting the disialoganglioside GD3 on

the surface of melanoma cells, *Clin Immunol Immunopathol 45*, 214-229.

125. Houghton, A. N., Mintzer, D., Cordon-Cardo, C., Welt, S., Fliegel, B., Vadhan, S., Carswell, E., Melamed, M. R., Oettgen, H. F., and Old, L. J. (1985) Mouse monoclonal IgG3 antibody detecting GD3 ganglioside: a phase I trial in patients with malignant melanoma, *Proc Natl Acad Sci U S A 82*, 1242-1246.

126. Vadhan-Raj, S., Cordon-Cardo, C., Carswell, E., Mintzer, D., Dantis, L., Duteau, C., Templeton, M. A., Oettgen, H. F., Old, L. J., and Houghton, A. N. (1988) Phase I trial of a mouse monoclonal antibody against GD3 ganglioside in patients with melanoma: induction of inflammatory responses at tumor sites, *Journal of Clinical Oncology 6*, 1636-1648.

127. Bajorin, D. F., Chapman, P. B., Wong, G., Coit, D. G., Kunicka, J., Dimaggio, J., Cordon-Cardo, C., Urmacher, C., Dantes, L., Templeton, M. A., and et al. (1990) Phase I evaluation of a combination of monoclonal antibody R24 and interleukin 2 in patients with metastatic melanoma, *Cancer Research 50*, 7490-7495.

128. Minasian, L. M., Szatrowski, T. P., Rosenblum, M., Steffens, T., Morrison, M. E., Chapman, P. B., Williams, L., Nathan, C. F., and Houghton, A. N. (1994) Hemorrhagic tumor necrosis during a pilot trial of tumor necrosis factor-alpha and anti-GD3 ganglioside

monoclonal antibody in patients with metastatic melanoma, *Blood 83*, 56-64.

129. Minasian, L. M., Yao, T. J., Steffens, T. A., Scheinberg, D. A., Williams, L., Riedel, E., Houghton, A. N., and Chapman, P. B. (1995) A phase I study of anti-GD3 ganglioside monoclonal antibody R24 and recombinant human macrophage-colony stimulating factor in patients with metastatic melanoma, *Cancer 75*, 2251-2257.

130. Scott, A. M., Liu, Z., Murone, C., Johns, T. G., MacGregor, D., Smyth, F. E., Lee, F. T., Cebon, J., Davis, I. D., Hopkins, W., Mountain, A. J., Rigopoulos, A., Hanai, N., and Old, L. J. (2005) Immunological effects of chimeric anti-GD3 monoclonal antibody KM871 in patients with metastatic melanoma, *Cancer Immunity 5*, 3.

131. Fredman, P., Hedberg, K., and Brezicka, T. (2003) Gangliosides as therapeutic targets for cancer, *Biodrugs 17*, 155-167.

132. Fernandez, L. E., Alonso, D. F., Gomez, D. E., and Vazquez, A. M. (2003) Ganglioside-based vaccines and anti-idiotype antibodies for active immunotherapy against cancer, *Expert Review of Vaccines 2*, 817-823.

133. Krug, L. M. (2004) Vaccine therapy for small cell lung cancer, *Seminars in Oncology 31*, 112-116.

134. Chapman, P. B. (2007) Melanoma vaccines, *Seminars in Oncology 34*, 516-523.

135. Lens, M. (2008) The role of vaccine therapy in the treatment of melanoma, *Expert Opin Biol Ther 8*, 315-323.

136. Mond, J. J., Lees, A., and Snapper, C. M. (1995) T cell-independent antigens type 2, *Annu Rev Immunol 13*, 655-692.

137. Danishefsky, S. J., and Allen, J. R. (2000) From the Laboratory to the Clinic: A Retrospective on Fully Synthetic Carbohydrate-Based Anticancer Vaccines, *Angew Chem Int Ed 39*, 836-863.

138. Nagorny, P., Kim, W. H., Wan, Q., Lee, D., and Danishefsky, S. J. (2009) On the emerging role of chemistry in the fashioning of biologics: synthesis of a bidomainal fucosyl GM1-based vaccine for the treatment of small cell lung cancer, *Journal of Organic Chemistry 74*, 5157-5162.

139. Vangsted, A. J., Clausen, H., Kjeldsen, T. B., White, T., Sweeney, B., Hakomori, S., Drivsholm, L., and Zeuthen, J. (1991) Immunochemical detection of a small cell lung cancer-associated ganglioside (FucGM1) antigen in serum, *Cancer Research 51*, 2879-2884.

140. Brezicka, T., Bergman, B., Olling, S., and Fredman, P. (2000) Reactivity of monoclonal antibodies with ganglioside antigens in human small cell lung cancer tissues, *Lung Cancer 28*, 29-36.

141. Neninger, E., Diaz, R. M., de la Torre, A., Rives, R., Diaz, A., Saurez, G., Gabri, M. R., Alonso, D. F., Wilkinson, B., Alfonso, A. M., Combet, T., Perez, R., and Vazquez, A. M. (2007) Active

immunotherapy with 1E10 anti-idiotype vaccine in patients with small cell lung cancer: report of a phase I trial, *Cancer Biol Ther 6*, 145-150.

142. Hamilton, W. B., Helling, F., Lloyd, K. O., and Livingston, P. O. (1993) Ganglioside expression on human malignant melanoma assessed by quantitative immune thin-layer chromatography, *International Journal of Cancer 53*, 566-573.

143. Livingston, P. (1998) Ganglioside vaccines with emphasis on GM2, *Seminars in Oncology 25*, 636-645.

144. Nakarai, H., Chandler, P. J., Kano, K., Morton, D. L., and Irie, R. F. (1990) Hanganutziu-Deicher antigen as a possible target for immunotherapy of melanoma, *Int Arch Allergy Appl Immunol 91*, 323-328.

145. Marquina, G., Waki, H., Fernandez, L. E., Kon, K., Carr, A., Valiente, O., Perez, R., and Ando, S. (1996) Gangliosides expressed in human breast cancer, *Cancer Research 56*, 5165-5171.

146. Senn, H. J., Orth, M., Fitzke, E., Wieland, H., and Gerok, W. (1989) Gangliosides in normal human serum. Concentration, pattern and transport by lipoproteins, *Eur J Biochem 181*, 657-662.

147. Sorice, M., Longo, A., Garofalo, T., Mattei, V., Misasi, R., and Pavan, A. (2004) Role of GM3-enriched microdomains in signal

transduction regulation in T lymphocytes, *Glycoconjugate Journal 20*, 63-70.

148. Dickler, M. N., Ragupathi, G., Liu, N. X., Musselli, C., Martino, D. J., Miller, V. A., Kris, M. G., Brezicka, F. T., Livingston, P. O., and Grant, S. C. (1999) Immunogenicity of a fucosyl-GM1-keyhole limpet hemocyanin conjugate vaccine in patients with small cell lung cancer, *Clinical Cancer Research 5*, 2773-2779.

149. Krug, L. M., Ragupathi, G., Hood, C., Kris, M. G., Miller, V. A., Allen, J. R., Keding, S. J., Danishefsky, S. J., Gomez, J., Tyson, L., Pizzo, B., Baez, V., and Livingston, P. O. (2004) Vaccination of patients with small-cell lung cancer with synthetic fucosyl GM-1 conjugated to keyhole limpet hemocyanin, *Clinical Cancer Research 10*, 6094-6100.

150. Kim, S. K., Wu, X., Ragupathi, G., Gathuru, J., Koide, F., Cheung, N. K., Panageas, K., and Livingston, P. O. (2011) Impact of minimal tumor burden on antibody response to vaccination, *Cancer Immunology, Immunotherapy 60*, 621-627.

151. Ragupathi, G., Livingston, P. O., Hood, C., Gathuru, J., Krown, S. E., Chapman, P. B., Wolchok, J. D., Williams, L. J., Oldfield, R. C., and Hwu, W. J. (2003) Consistent antibody response against ganglioside GD2 induced in patients with melanoma by a GD2 lactone-keyhole limpet hemocyanin conjugate vaccine plus

immunological adjuvant QS-21, *Clinical Cancer Research 9*, 5214-5220.

152. Kirkwood, J. M., Ibrahim, J. G., Sosman, J. A., Sondak, V. K., Agarwala, S. S., Ernstoff, M. S., and Rao, U. (2001) High-dose interferon alfa-2b significantly prolongs relapse-free and overall survival compared with the GM2-KLH/QS-21 vaccine in patients with resected stage IIB-III melanoma: results of intergroup trial E1694/S9512/C509801, *Journal of Clinical Oncology 19*, 2370-2380.

153. Foon, K. A., Lutzky, J., Baral, R. N., Yannelli, J. R., Hutchins, L., Teitelbaum, A., Kashala, O. L., Das, R., Garrison, J., Reisfeld, R. A., and Bhattacharya-Chatterjee, M. (2000) Clinical and immune responses in advanced melanoma patients immunized with an anti-idiotype antibody mimicking disialoganglioside GD2, *Journal of Clinical Oncology 18*, 376-384.

154. Chapman, P. B., Wu, D., Ragupathi, G., Lu, S., Williams, L., Hwu, W. J., Johnson, D., and Livingston, P. O. (2004) Sequential immunization of melanoma patients with GD3 ganglioside vaccine and anti-idiotypic monoclonal antibody that mimics GD3 ganglioside, *Clinical Cancer Research 10*, 4717-4723.

155. Bolesta, E., Kowalczyk, A., Wierzbicki, A., Rotkiewicz, P., Bambach, B., Tsao, C. Y., Horwacik, I., Kolinski, A., Rokita, H., Brecher, M., Wang, X., Ferrone, S., and Kozbor, D. (2005) DNA vaccine

expressing the mimotope of GD2 ganglioside induces protective GD2 cross-reactive antibody responses, *Cancer Research 65*, 3410-3418.

156. Fest, S., Huebener, N., Weixler, S., Bleeke, M., Zeng, Y., Strandsby, A., Volkmer-Engert, R., Landgraf, C., Gaedicke, G., Riemer, A. B., Michalsky, E., Jaeger, I. S., Preissner, R., Forster-Wald, E., Jensen-Jarolim, E., and Lode, H. N. (2006) Characterization of GD2 peptide mimotope DNA vaccines effective against spontaneous neuroblastoma metastases, *Cancer Research 66*, 10567-10575.

157. Zeytin, H. E., Tripathi, P. K., Bhattacharya-Chatterjee, M., Foon, K. A., and Chatterjee, S. K. (2000) Construction and characterization of DNA vaccines encoding the single-chain variable fragment of the anti-idiotype antibody 1A7 mimicking the tumor-associated antigen disialoganglioside GD2, *Cancer Gene Therapy 7*, 1426-1436.

158. Carr, A., Rodriguez, E., Arango Mdel, C., Camacho, R., Osorio, M., Gabri, M., Carrillo, G., Valdes, Z., Bebelagua, Y., Perez, R., and Fernandez, L. E. (2003) Immunotherapy of advanced breast cancer with a heterophilic ganglioside (NeuGcGM3) cancer vaccine, *Journal of Clinical Oncology 21*, 1015-1021.

159. Osorio, M., Gracia, E., Rodriguez, E., Saurez, G., Arango Mdel, C., Noris, E., Torriella, A., Joan, A., Gomez, E., Anasagasti, L., Gonzalez, J. L., Melgares Mde, L., Torres, I., Gonzalez, J., Alonso,

D., Rengifo, E., Carr, A., Perez, R., and Fernandez, L. E. (2008) Heterophilic NeuGcGM3 ganglioside cancer vaccine in advanced melanoma patients: results of a Phase Ib/IIa study, *Cancer Biol Ther 7*, 488-495.

160. Chapman, P. B., Morrisey, D., Panageas, K. S., Williams, L., Lewis, J. J., Israel, R. J., Hamilton, W. B., and Livingston, P. O. (2000) Vaccination with a bivalent G(M2) and G(D2) ganglioside conjugate vaccine: a trial comparing doses of G(D2)-keyhole limpet hemocyanin, *Clinical Cancer Research 6*, 4658-4662.

161. Ragupathi, G., Meyers, M., Adluri, S., Howard, L., Musselli, C., and Livingston, P. O. (2000) Induction of antibodies against GD3 ganglioside in melanoma patients by vaccination with GD3-lactone-KLH conjugate plus immunological adjuvant QS-21, *International Journal of Cancer 85*, 659-666.

162. Park, J. E., Lu, S. X., Wu, D. Y., Prendes, M., and Chapman, P. B. (2008) Antibody response to GD3 ganglioside is independent of NKT cells, *Cytotherapy 10*, 38-44.

163. Deng, K., Adams, M. M., Damani, P., Livingston, P. O., Ragupathi, G., and Gin, D. Y. (2008) Synthesis of QS-21-xylose: establishment of the immunopotentiating activity of synthetic QS-21 adjuvant with a melanoma vaccine, *Angew Chem Int Ed 47*, 6395-6398.

164. Ragupathi, G., Damani, P., Deng, K., Adams, M. M., Hang, J., George, C., Livingston, P. O., and Gin, D. Y. (2010) Preclinical

evaluation of the synthetic adjuvant SQS-21 and its constituent isomeric saponins, *Vaccine 28*, 4260-4267.

165. Helling, F., Zhang, S., Shang, A., Adluri, S., Calves, M., Koganty, R., Longenecker, B. M., Yao, T. J., Oettgen, H. F., and Livingston, P. O. (1995) GM2-KLH conjugate vaccine: increased immunogenicity in melanoma patients after administration with immunological adjuvant QS-21, *Cancer Research 55*, 2783-2788.

166. Chapman, P. B., Morrissey, D. M., Panageas, K. S., Hamilton, W. B., Zhan, C., Destro, A. N., Williams, L., Israel, R. J., and Livingston, P. O. (2000) Induction of antibodies against GM2 ganglioside by immunizing melanoma patients using GM2-keyhole limpet hemocyanin + QS21 vaccine: a dose-response study, *Clinical Cancer Research 6*, 874-879.

167. Kirkwood, J. M., Ibrahim, J., Lawson, D. H., Atkins, M. B., Agarwala, S. S., Collins, K., Mascari, R., Morrissey, D. M., and Chapman, P. B. (2001) High-dose interferon alfa-2b does not diminish antibody response to GM2 vaccination in patients with resected melanoma: results of the Multicenter Eastern Cooperative Oncology Group Phase II Trial E2696, *Journal of Clinical Oncology 19*, 1430-1436.

168. Livingston, P. O., Hood, C., Krug, L. M., Warren, N., Kris, M. G., Brezicka, T., and Ragupathi, G. (2005) Selection of GM2, fucosyl GM1, globo H and polysialic acid as targets on small cell lung

cancers for antibody mediated immunotherapy, *Cancer Immunology, Immunotherapy 54*, 1018-1025.

169. Ragupathi, G., Gathuru, J., and Livingston, P. (2005) Antibody inducing polyvalent cancer vaccines, *Cancer Treat Res 123*, 157-180.

170. Cheung, N. K., Canete, A., Cheung, I. Y., Ye, J. N., and Liu, C. (1993) Disialoganglioside GD2 anti-idiotypic monoclonal antibodies, *International Journal of Cancer 54*, 499-505.

171. Chapman, P. B., and Houghton, A. N. (1991) Induction of IgG antibodies against GD3 ganglioside in rabbits by an anti-idiotypic monoclonal antibody, *Journal of Clinical Investigation 88*, 186-192.

172. Foon, K. A., Sen, G., Hutchins, L., Kashala, O. L., Baral, R., Banerjee, M., Chakraborty, M., Garrison, J., Reisfeld, R. A., and Bhattacharya-Chatterjee, M. (1998) Antibody responses in melanoma patients immunized with an anti-idiotype antibody mimicking disialoganglioside GD2, *Clinical Cancer Research 4*, 1117-1124.

173. Sen, G., Chakraborty, M., Foon, K. A., Reisfeld, R. A., and Bhattacharya-Chatterjee, M. (1997) Preclinical evaluation in nonhuman primates of murine monoclonal anti-idiotype antibody that mimics the disialoganglioside GD2, *Clinical Cancer Research 3*, 1969-1976.

174. McCaffery, M., Yao, T. J., Williams, L., Livingston, P. O., Houghton, A. N., and Chapman, P. B. (1996) Immunization of melanoma patients with BEC2 anti-idiotypic monoclonal antibody that mimics GD3 ganglioside: enhanced immunogenicity when combined with adjuvant, *Clinical Cancer Research 2*, 679-686.

175. Grant, S. C., Kris, M. G., Houghton, A. N., and Chapman, P. B. (1999) Long survival of patients with small cell lung cancer after adjuvant treatment with the anti-idiotypic antibody BEC2 plus Bacillus Calmette-Guerin, *Clinical Cancer Research 5*, 1319-1323.

176. Yao, T. J., Meyers, M., Livingston, P. O., Houghton, A. N., and Chapman, P. B. (1999) Immunization of melanoma patients with BEC2-keyhole limpet hemocyanin plus BCG intradermally followed by intravenous booster immunizations with BEC2 to induce anti-GD3 ganglioside antibodies, *Clinical Cancer Research 5*, 77-81.

177. Chapman, P. B., Williams, L., Salibi, N., Hwu, W. J., Krown, S. E., and Livingston, P. O. (2004) A phase II trial comparing five dose levels of BEC2 anti-idiotypic monoclonal antibody vaccine that mimics GD3 ganglioside, *Vaccine 22*, 2904-2909.

178. Cheung, N. K., Guo, H. F., Heller, G., and Cheung, I. Y. (2000) Induction of Ab3 and Ab3' antibody was associated with long-term survival after anti-G(D2) antibody therapy of stage 4 neuroblastoma, *Clinical Cancer Research 6*, 2653-2660.

179. Uttenreuther-Fischer, M. M., Kruger, J. A., and Fischer, P. (2006) Molecular characterization of the anti-idiotypic immune response of a relapse-free neuroblastoma patient following antibody therapy: a possible vaccine against tumors of neuroectodermal origin?, *Journal of Immunology 176*, 7775-7786.

180. Alfonso, M., Diaz, A., Hernandez, A. M., Perez, A., Rodriguez, E., Bitton, R., Perez, R., and Vazquez, A. M. (2002) An anti-idiotype vaccine elicits a specific response to N-glycolyl sialic acid residues of glycoconjugates in melanoma patients, *Journal of Immunology 168*, 2523-2529.

181. Diaz, A., Alfonso, M., Alonso, R., Saurez, G., Troche, M., Catala, M., Diaz, R. M., Perez, R., and Vazquez, A. M. (2003) Immune responses in breast cancer patients immunized with an anti-idiotype antibody mimicking NeuGc-containing gangliosides, *Clin Immunol 107*, 80-89.

182. Guthmann, M. D., Castro, M. A., Cinat, G., Venier, C., Koliren, L., Bitton, R. J., Vazquez, A. M., and Fainboim, L. (2006) Cellular and humoral immune response to N-Glycolyl-GM3 elicited by prolonged immunotherapy with an anti-idiotypic vaccine in high-risk and metastatic breast cancer patients, *J Immunother 29*, 215-223.

183. Wondimu, A., Zhang, T., Kieber-Emmons, T., Gimotty, P., Sproesser, K., Somasundaram, R., Ferrone, S., Tsao, C. Y., and Herlyn, D. (2008) Peptides mimicking GD2 ganglioside elicit cellular,

humoral and tumor-protective immune responses in mice, *Cancer Immunology, Immunotherapy 57*, 1079-1089.

184. Bleeke, M., Fest, S., Huebener, N., Landgraf, C., Schraven, B., Gaedicke, G., Volkmer, R., and Lode, H. N. (2009) Systematic amino acid substitutions improved efficiency of GD2-peptide mimotope vaccination against neuroblastoma, *European Journal of Cancer 45*, 2915-2921.

185. Kozbor, D. (2010) Cancer vaccine with mimotopes of tumor-associated carbohydrate antigens, *Immunol Res 46*, 23-31.

186. Horwacik, I., Kurcinski, M., Bzowska, M., Kowalczyk, A. K., Czaplicki, D., Kolinski, A., and Rokita, H. (2011) Analysis and optimization of interactions between peptides mimicking the GD2 ganglioside and the monoclonal antibody 14G2a, *International Journal of Molecular Medicine*.

187. Dube, D. H., and Bertozzi, C. R. (2005) Glycans in cancer and inflammation--potential for therapeutics and diagnostics, *Nat Rev Drug Discov 4*, 477-488.

188. Svennerholm, L., Bostrom, K., Jungbjer, B., and Olsson, L. (1994) Membrane lipids of adult human brain: lipid composition of frontal and temporal lobe in subjects of age 20 to 100 years, *J Neurochem 63*, 1802-1811.

189. Yuki, N., Yamada, M., Tagawa, Y., Takahashi, H., and Handa, S. (1997) Pathogenesis of the neurotoxicity caused by anti-GD2 antibody therapy, *J Neurol Sci 149*, 127-130.

190. Watanabe, T., Pukel, C. S., Takeyama, H., Lloyd, K. O., Shiku, H., Li, L. T., Travassos, L. R., Oettgen, H. F., and Old, L. J. (1982) Human melanoma antigen AH is an autoantigenic ganglioside related to GD2, *J. Exp. Med. 156*, 1884-1889.

191. Thurin, J., Thurin, M., Herlyn, M., Elder, D. E., Steplewski, Z., Clark, W. H., and Koprowski, H. (1986) GD2 ganglioside biosynthesis is a distinct biochemical event in human melanoma tumor progression, *FEBS Letters 208*, 17-22.

192. Modak, S., and Cheung, N. K. (2007) Disialoganglioside directed immunotherapy of neuroblastoma, *Cancer Invest 25*, 67-77.

193. Hakomori, S.-I., and Zhang, Y. (1997) Glycosphingolipid antigens and cancer therapy, *Chem Biol 4*, 97-104.

194. Gouy, H., Deterre, P., Debre, P., and Bismuth, G. (1994) Cell calcium signaling via GM1 cell surface gangliosides in the human Jurkat T cell line, *Journal of Immunology 152*, 3271-3281.

195. Golard, A. (1998) Anti-GM3 antibodies activate calcium inflow and inhibit platelet- derived growth factor beta receptors (PDGFbetar) in T51B rat liver epithelial cells, *Glycobiology 8*, 1221-1225.

196. Chatterjee, C., Majumder, B., and Mukhopadhyay, C. (2004) Pulsed-Field Gradient and Saturation Transfer Difference NMR

Study of Enkephalins in the Ganglioside GM1 Micelle, *J. Phys. Chem. B 108*, 7430-7436.

197. Mandal, P. K., and Pettegrew, J. W. (2004) Alzheimer's disease: NMR studies of asialo (GM1) and trisialo (GT1b) ganglioside interactions with Abeta(1-40) peptide in a membrane mimic environment, *Neurochem Res 29*, 447-453.

198. Chatterjee, C., and Mukhopadhyay, C. (2005) Interaction and structural study of kinin peptide bradykinin and ganglioside monosialylated 1 micelle, *Biopolymers 78*, 197-205.

199. Meyer, B., and Peters, T. (2003) NMR spectroscopy techniques for screening and identifying ligand binding to protein receptors, *Angew Chem Int Ed 42*, 864-890.

200. Saragovi, H. U., Greene, M. I., Chrusciel, R. A., and Kahn, M. (1992) Loops and secondary structure mimetics: development and applications in basic science and rational drug design, *Biotechnology 10*, 773-778.

201. Vasudevan, S. V., and Balaji, P. V. (2001) Dynamics of Ganglioside Headgroup in Lipid Environment: Molecular Dynamics Simulations of GM1 Embedded in Dodecylphosphocholine Micelle, *Journal of Physical Chemistry B 105*, 7033-7041.

202. Yan, J., Kline, A. D., Mo, H., Shapiro, M. J., and Zartler, E. R. (2003) The effect of relaxation on the epitope mapping by saturation transfer difference NMR, *J Magn Reson 163*, 270-276.

203. Ji, Z., Yao, Z., and Liu, M. (2009) Saturation transfer difference nuclear magnetic resonance study on the specific binding of ligand to protein, *Anal Biochem 385*, 380-382.

204. Sonnino, S., Cantˇ, L., Corti, M., Acquotti, D., and Venerando, B. (1994) Aggregative properties of gangliosides in solution, *Chemistry & Physics of Lipids 71*, 21-45.

205. Kabsch, W., and Sander, C. (1983) Dictionary of protein secondary structure: pattern recognition of hydrogen-bonded and geometrical features, *Biopolymers 22*, 2577-2637.

206. Palacios, E. H., and Weiss, A. (2004) Function of the Src-family kinases, Lck and Fyn, in T-cell development and activation, *Oncogene 23*, 7990-8000.

207. Bernatchez, S., Szymanski, C. M., Ishiyama, N., Li, J., Jarrell, H. C., Lau, P. C., Berghuis, A. M., Young, N. M., and Wakarchuk, W. W. (2005) A Single Bifunctional UDP-GlcNAc/Glc 4-Epimerase Supports the Synthesis of Three Cell Surface Glycoconjugates in Campylobacter jejuni, *J. Biol. Chem. 280*, 4792-4802.

208. Cheung, N.-K. V., Saarinen, U. M., Neely, J. E., Landmeier, B., Donovan, D., and Coccia, P. F. (1985) Monoclonal Antibodies to a Glycolipid Antigen on Human Neuroblastoma Cells, *Cancer Res 45*, 2642-2649.

209. Delaglio F, G. S., Vuister GW, Zhu G, Pfeifer J & Bax A. (1995) NMRpipe: a multidimensional spectral processing system based on UNIX pipes. , *J Biomol NMR 6*, 277-293.

210. Mayer, M., and Meyer, B. (2001) Group Epitope Mapping by Saturation Transfer Difference NMR To Identify Segments of a Ligand in Direct Contact with a Protein Receptor, *J. Am. Chem. Soc. 123*, 6108-6117.

211. Case, D. A., Cheatham, T. E., 3rd, Darden, T., Gohlke, H., Luo, R., Merz, K. M., Jr., Onufriev, A., Simmerling, C., Wang, B., and Woods, R. J. (2005) The Amber biomolecular simulation programs, *J Comput Chem 26*, 1668-1688.

212. Woods, R. J., Dwek, R. A., Edge, C. J., and Fraser-Reid, B. (1995) Molecular Mechanical and Molecular Dynamic Simulations of Glycoproteins and Oligosaccharides. 1. GLYCAM_93 Parameter Development, *Journal of Physical Chemistry 99*, 3832-3846.

213. Wang, J., Wolf, R. M., Caldwell, J. W., Kollman, P. A., and Case, D. A. (2004) Development and testing of a general amber force field, *J Comput Chem 25*, 1157-1174.

214. Wang, J., Wang, W., Kollman, P. A., and Case, D. A. (2006) Automatic atom type and bond type perception in molecular mechanical calculations, *Journal of Molecular Graphics and Modelling 25*, 247-260.

215. Rieping, W., Habeck, M., Bardiaux, B., Bernard, A., Malliavin, T. E., and Nilges, M. (2007) ARIA2: Automated NOE assignment and data integration in NMR structure calculation, *Bioinformatics 23*, 381-382.

216. Feig, M., Karanicolas, J., and Brooks, C. L. (2004) MMTSB Tool Set: enhanced sampling and multiscale modeling methods for applications in structural biology, *Journal of Molecular Graphics and Modelling 22*, 377-395.

217. Coley, A. M., Parisi, K., Masciantonio, R., Hoeck, J., Casey, J. L., Murphy, V. J., Harris, K. S., Batchelor, A. H., Anders, R. F., and Foley, M. (2006) The Most Polymorphic Residue on Plasmodium falciparum Apical Membrane Antigen 1 Determines Binding of an Invasion-Inhibitory Antibody, *Infect. Immun. 74*, 2628-2636.

218. Muller, R., Debler, E. W., Steinmann, M., Seebeck, F. P., Wilson, I. A., and Hilvert, D. (2007) Bifunctional Catalysis of Proton Transfer at an Antibody Active Site, *J. Am. Chem. Soc. 129*, 460-461.

219. Jakalian, A., Jack, D. B., and Bayly, C. I. (2002) Fast, efficient generation of high-quality atomic charges. AM1-BCC model: II. Parameterization and validation, *J Comput Chem 23*, 1623-1641.

220. Naim, M., Bhat, S., Rankin, K. N., Dennis, S., Chowdhury, S. F., Siddiqi, I., Drabik, P., Sulea, T., Bayly, C. I., Jakalian, A., and Purisima, E. O. (2007) Solvated Interaction Energy (SIE) for Scoring Protein−Ligand Binding Affinities. 1. Exploring the

Parameter Space, *Journal of Chemical Information and Modeling 47*, 122-133.

221. Jayalakshmi, V., and Krishna, N. R. (2002) Complete Relaxation and Conformational Exchange Matrix (CORCEMA) Analysis of Intermolecular Saturation Transfer Effects in Reversibly Forming Ligand-Receptor Complexes, *Journal of Magnetic Resonance 155*, 106-118.

222. Imberty, A., Chabre, Y. M., and Roy, R. (2008) Glycomimetics and glycodendrimers as high affinity microbial anti-adhesins, *Chemistry 14*, 7490-7499.

223. Chabre, Y. M., and Roy, R. (2008) Recent trends in glycodendrimer syntheses and applications, *Curr Top Med Chem 8*, 1237-1285.

224. Lindhorst, T. K., and Kieburg, C. (1996) Glycocoating of Oligovalent Amines: Synthesis of Thiourea-Bridged Cluster Glycosides from Glycosyl Isothiocyanates, *Angew Chem Int Ed 35*, 1953-1956.

225. Esfand, R., and Tomalia, D. A. (2001) Poly(amidoamine) (PAMAM) dendrimers: from biomimicry to drug delivery and biomedical applications, *Drug Discov Today 6*, 427-436.

226. Liu, X., Lee, C. K., Granek, J. A., Clarke, N. D., and Lieb, J. D. (2006) Whole-genome comparison of Leu3 binding in vitro and in vivo reveals the importance of nucleosome occupancy in target site selection, *Genome Res 16*, 1517-1528.

227. Saragovi, H. U., Bhandoola, A., Lemercier, M. M., Akbar, G. K., and Greene, M. I. (1995) A receptor that subserves reovirus binding can inhibit lymphocyte proliferation triggered by mitogenic signals, *DNA Cell Biol 14*, 653-664.

228. Kasahara, K., Watanabe, Y., Yamamoto, T., and Sanai, Y. (1997) Association of Src Family Tyrosine Kinase Lyn with Ganglioside GD3 in Rat Brain. POSSIBLE REGULATION OF Lyn BY GLYCOSPHINGOLIPID IN CAVEOLAE-LIKE DOMAINS, *J. Biol. Chem. 272*, 29947-29953.

229. Yu, A. L., Uttenreuther-Fischer, M. M., Huang, C. S., Tsui, C. C., Gillies, S. D., Reisfeld, R. A., and Kung, F. H. (1998) Phase I trial of a human-mouse chimeric anti-disialoganglioside monoclonal antibody ch14.18 in patients with refractory neuroblastoma and osteosarcoma, *Journal of Clinical Oncology 16*, 2169-2180.

230. Slart, R., Yu, A. L., Yaksh, T. L., and Sorkin, L. S. (1997) An animal model of pain produced by systemic administration of an immunotherapeutic anti-ganglioside antibody, *Pain 69*, 119-125.

231. Wallace, M. S., Lee, J., Sorkin, L., Dunn, J. S., Yaksh, T., and Yu, A. (1997) Intravenous lidocaine: effects on controlling pain after anti-GD2 antibody therapy in children with neuroblastoma--a report of a series, *Anesth Analg 85*, 794-796.

232. Xiao, W. H., Yu, A. L., and Sorkin, L. S. (1997) Electrophysiological characteristics of primary afferent fibers after systemic administration of anti-GD2 ganglioside antibody, *Pain 69*, 145-151.

233. Petrenko, A. B., Yamakura, T., Baba, H., and Shimoji, K. (2003) The role of N-methyl-D-aspartate (NMDA) receptors in pain: a review, *Anesth Analg 97*, 1108-1116.

234. Salter, M. W., and Kalia, L. V. (2004) Src kinases: a hub for NMDA receptor regulation, *Nat Rev Neurosci 5*, 317-328.

235. Lin, S. Y., Wu, K., Levine, E. S., Mount, H. T., Suen, P. C., and Black, I. B. (1998) BDNF acutely increases tyrosine phosphorylation of the NMDA receptor subunit 2B in cortical and hippocampal postsynaptic densities, *Brain Research Molecular Brain Research 55*, 20-27.

236. Sicheri, F., Moarefi, I., and Kuriyan, J. (1997) Crystal structure of the Src family tyrosine kinase Hck, *Nature 385*, 602-609.

237. Xu, W., Harrison, S. C., and Eck, M. J. (1997) Three-dimensional structure of the tyrosine kinase c-Src, *Nature 385*, 595-602.

238. Cunha, C., Brambilla, R., and Thomas, K. L. (2010) A simple role for BDNF in learning and memory?, *Frontiers in Molecular Neuroscience 3*, 1.

239. Huang, Y. Z., and McNamara, J. O. (2010) Mutual regulation of Src family kinases and the neurotrophin receptor TrkB, *J. Biol. Chem. 285*, 8207-8217.

240. Blum, R., and Konnerth, A. (2005) Neurotrophin-mediated rapid signaling in the central nervous system: mechanisms and functions, *Physiology (Bethesda, Md) 20*, 70-78.

241. Lee, F. S., and Chao, M. V. (2001) Activation of Trk neurotrophin receptors in the absence of neurotrophins, *Proc Natl Acad Sci U S A 98*, 3555-3560.

242. Rajagopal, R., Chen, Z. Y., Lee, F. S., and Chao, M. V. (2004) Transactivation of Trk neurotrophin receptors by G-protein-coupled receptor ligands occurs on intracellular membranes, *Journal of Neuroscience 24*, 6650-6658.

243. Meyer-Franke, A., Wilkinson, G. A., Kruttgen, A., Hu, M., Munro, E., Hanson, M. G., Jr., Reichardt, L. F., and Barres, B. A. (1998) Depolarization and cAMP elevation rapidly recruit TrkB to the plasma membrane of CNS neurons, *Neuron 21*, 681-693.

244. Gillin, S., and Sorkin, L. S. (1998) Gabapentin reverses the allodynia produced by the administration of anti-GD2 ganglioside, an immunotherapeutic drug, *Anesth Analg 86*, 111-116.

245. Eroglu, C., Allen, N. J., Susman, M. W., O'Rourke, N. A., Park, C. Y., Ozkan, E., Chakraborty, C., Mulinyawe, S. B., Annis, D. S., Huberman, A. D., Green, E. M., Lawler, J., Dolmetsch, R., Garcia, K. C., Smith, S. J., Luo, Z. D., Rosenthal, A., Mosher, D. F., and Barres, B. A. (2009) Gabapentin receptor alpha2delta-1 is a

neuronal thrombospondin receptor responsible for excitatory CNS synaptogenesis, *Cell 139*, 380-392.

246. Hendrich, J., Van Minh, A. T., Heblich, F., Nieto-Rostro, M., Watschinger, K., Striessnig, J., Wratten, J., Davies, A., and Dolphin, A. C. (2008) Pharmacological disruption of calcium channel trafficking by the alpha2delta ligand gabapentin, *Proc Natl Acad Sci U S A 105*, 3628-3633.

247. Davies, A., Hendrich, J., Van Minh, A. T., Wratten, J., Douglas, L., and Dolphin, A. C. (2007) Functional biology of the alpha(2)delta subunits of voltage-gated calcium channels, *Trends in Pharmacological Sciences 28*, 220-228.

248. Stanfa, L. C., Singh, L., Williams, R. G., and Dickenson, A. H. (1997) Gabapentin, ineffective in normal rats, markedly reduces C-fibre evoked responses after inflammation, *Neuroreport 8*, 587-590.

249. Liu, X. J., Gingrich, J. R., Vargas-Caballero, M., Dong, Y. N., Sengar, A., Beggs, S., Wang, S.-H., Ding, H. K., Frankland, P. W., and Salter, M. W. (2008) Treatment of inflammatory and neuropathic pain by uncoupling Src from the NMDA receptor complex, *Nat Med 14*, 1325-1332.

250. Li, S., Cao, J., Yang, X., Suo, Z. W., Shi, L., Liu, Y. N., Yang, H. B., and Hu, X. D. (2011) NR2B phosphorylation at tyrosine 1472 in spinal dorsal horn contributed to N-methyl-D-aspartate-induced pain hypersensitivity in mice, *J Neurosci Res 89*, 1869-1876.

251. Williams, D. H., Sharman, G. J., Try, A. C., Dancer, R. J., Cho, Y. R., Staroske, T., Bardsley, B., Maguire, A. J., Cooper, M. A., and O'Brien, D. P. (1997) The roles of dimerization and membrane anchoring in activity of glycopeptide antibiotics against vancomycin-resistant bacteria, *J. Am. Chem. Soc. 119*, 12041-12047.

252. Chen, D., Brahimi, F., Angell, Y., Li, Y. C., Moscowicz, J., Saragovi, H. U., and Burgess, K. (2009) Bivalent peptidomimetic ligands of TrkC are biased agonists and selectively induce neuritogenesis or potentiate neurotrophin-3 trophic signals, *ACS Chem Biol 4*, 769-781.

253. Wormald, M. R., Petrescu, A. J., Pao, Y. L., Glithero, A., Elliott, T., and Dwek, R. A. (2002) Conformational studies of oligosaccharides and glycopeptides: complementarity of NMR, X-ray crystallography, and molecular modelling, *Chem Rev 102*, 371-386.

254. Suzuki, Y., Yanagisawa, M., Ariga, T., and Yu, R. K. (2011) Histone acetylation-mediated glycosyltransferase gene regulation in mouse brain during development, *J Neurochem 116*, 874-880.

255. Raman, R., Raguram, S., Venkataraman, G., Paulson, J. C., and Sasisekharan, R. (2005) Glycomics: an integrated systems approach to structure-function relationships of glycans, *Nat Methods 2*, 817-824.

256. Roche, K. W., Standley, S., McCallum, J., Dune Ly, C., Ehlers, M. D., and Wenthold, R. J. (2001) Molecular determinants of NMDA receptor internalization, *Nature Neuroscience 4*, 794-802.

257. Kudryashov, V., Ragupathi, G., Kim, I. J., Breimer, M. E., Danishefsky, S. J., Livingston, P. O., and Lloyd, K. O. (1998) Characterization of a mouse monoclonal IgG3 antibody to the tumor-associated globo H structure produced by immunization with a synthetic glycoconjugate, *Glycoconjugate Journal 15*, 243-249.

258. Retter, M. W., Johnson, J. C., Peckham, D. W., Bannink, J. E., Bangur, C. S., Dresser, K., Cai, F., Foy, T. M., Fanger, N. A., Fanger, G. R., Woda, B., and Rock, K. L. (2005) Characterization of a proapoptotic antiganglioside GM2 monoclonal antibody and evaluation of its therapeutic effect on melanoma and small cell lung carcinoma xenografts, *Cancer Research 65*, 6425-6434.

259. Brocca, P., Acquotti, D., and Sonnino, S. (1996) Nuclear Overhauser effect investigation on GM1 ganglioside containing N-glycolyl-neuraminic acid (II3Neu5GcGgOse4Cer), *Glycoconj Journal 13*, 57-62.

260. Pichla, S. L., Murali, R., and Burnett, R. M. (1997) The Crystal Structure of a Fab Fragment to the Melanoma-Associated GD2 Ganglioside, *Journal of Structural Biology 119*, 6-16.

261. Cornell, W. D., Cieplak, P., Bayly, C. I., Gould, I. R., Merz, K. M., Ferguson, D. M., Spellmeyer, D. C., Fox, T., Caldwell, J. W., and

Kollman, P. A. (2002) A Second Generation Force Field for the Simulation of Proteins, Nucleic Acids, and Organic Molecules, *J. Am. Chem. Soc. 117*, 5179-5197.

262. William, L. J., Jayaraman, C., Jeffry, D. M., Roger, W. I., and Michael, L. K. (1983) Comparison of simple potential functions for simulating liquid water, *The Journal of Chemical Physics 79*, 926-935.

263. Tom, D., Darrin, Y., and Lee, P. (1993) Particle mesh Ewald: An N [center-dot] log(N) method for Ewald sums in large systems, *The Journal of Chemical Physics 98*, 10089-10092.

264. Ryckaert, J.-P., Ciccotti, G., and Berendsen, H. J. C. (1977) Numerical integration of the cartesian equations of motion of a system with constraints: molecular dynamics of n-alkanes, *Journal of Computational Physics 23*, 327-341.

265. Laskowski, R. A., MacArthur, M. W., Moss, D. S., and Thornton, J. M. (1993) PROCHECK: a program to check the stereochemical quality of protein structures, *Journal of Applied Crystallography 26*, 283-291.

266. Pellecchia, M., Bertini, I., Cowburn, D., Dalvit, C., Giralt, E., Jahnke, W., James, T. L., Homans, S. W., Kessler, H., Luchinat, C., Meyer, B., Oschkinat, H., Peng, J., Schwalbe, H., and Siegal, G. (2008) Perspectives on NMR in drug discovery: a technique comes of age, *Nat Rev Drug Discov 7*, 738-745.

267. Markwick, P. R., Malliavin, T., and Nilges, M. (2008) Structural biology by NMR: structure, dynamics, and interactions, *PLoS computational biology 4*, e1000168.